Cellular and Molecular Mechanisms of Actin Bundling in Epithelial Microvilli

By

Edwin Angelo Morales Obregon

Dissertation

Submitted to the Faculty of the

Graduate School of Vanderbilt University

in partial fulfillment of the requirements

for the degree of

DOCTOR OF PHILOSOPHY

In

Cell and Developmental Biology

August 11th, 2023

Nashville, Tennessee

Approved:

William P. Tansey, Ph.D.

Ken S. Lau, Ph.D.

James R. Goldenring, Ph.D., M.D.

Matthew J. Lang, Ph.D.

Matthew J. Tyska, Ph.D.

To the people whose foundational work have contributed to and inspired this research

ACKNOLEDGEMENTS

There will never be enough words to express all my deep gratitude to my mentor Dr. Matthew Tyska. Throughout these years, Matt has been an endless source of support, encouragement, and exciting ideas. Whenever I faced academic and personal obstacles, heading to Matt's office felt like going into a therapy session as I always left feeling less concerned and more confident. As I approach the end of this journey, I feel incredibly fortunate to have had Matt as a mentor. He has undoubtedly set a high bar for what it means to be an exceptional mentor and an admirable human being, and I feel privileged to have learned and benefitted from both facets.

As a member of the Tyska laboratory, I was also very fortunate to have had the opportunity to work with such a talented and good-hearted group of people: Suli, Leslie, Meredith, Meagan, Bella, Colbie, Bo, Caroline, Deanna, Gill, Jen, Julissa, Olivia, Kianna, Rocio, Leah and Aaron. I am grateful for their valuable feedback and support, which have greatly enriched my academic and personal experience in the lab.

I am also deeply grateful to the members of my dissertation committee: Dr. William Tansey, Dr. Ken Lau, Dr. James Goldenring and Dr. Matthew Lang, for their time and effort in providing feedback that helped shaped this work. I would also like to thank Dr. Marija Zanic for her valuable assistance and advice in the later stages of my graduate career. I am also indebted to my other long-time mentors: Dr. Abel Alcazar, who made possible the idea of a career in science; Dr. Charles Sindelar and Dr. Rong Li, who generously gave me the opportunity to explore the fascinating world of cytoskeletal

research in their laboratories; and Dr. Kexi Yi and Dr. Hung-Ji Tsai, who patiently shared with me all their expertise as scientists, which has greatly benefitted me all these years.

I am also immensely grateful to all the friends I made in Nashville: Andrea, Cayetana, Daniel, Ela, Jorge, Gaby, Li, Linh, Mindy, and Oscar. Their presence and support always brought joy and laughter in all the moments we shared, and I am grateful for the memories we created these years.

I also want to thank my wonderful family Julieta, Wilder, and Deysi for their love and support throughout these years. Even though I was away from home, the countless conversations we had always brought me closer to them. I am also incredibly thankful to have had Lilia by my side, a marvelous woman I admire for enriching various aspects of my daily with a perfect balance of thought-provoking and lighthearted conversations.

Finally, I also want to acknowledge to the countless people I came across throughout these years, who have contributed not only to my scientific journey, but also to my personal life. Even though their names are not explicitly listed in these pages, their actions or words have taught me to embrace adversity and uncertainty in life.

TABLE OF CONTENTS

Page

LIST OF FIGURES

LIST OF ABBREVIATIONS

°C	degrees Celsius
aa	amino acids
AB	actin-binding fragment
ADP	adenosine diphosphate
AMP-PNP	adenylyl-imidodiphosphate
ANKS4B	Ankyrin repeat and SAM domain-containing protein 4B
Arp2/3	Actin-related protein 2/3 complex
ATP	adenosine triphosphate
BA	barbed end
BB	brush border
BAIAP2L1	Brain-specific angiogenesis inhibitor 1-associated protein 2-like protein 1
BSA	bovine serum albumin
CL4	LLC-PK1-CL4 cells
CDHR2	Cadherin-related family member 2, a.k.a. protocadherin-24, protocadherin LKC
CDHR5	Cadherin-related family member 5, a.k.a. m-protocadherin, MUPCDH, MLPCDH
COBL	Cordon bleu, a.k.a. KIAA0633
CO_2	carbon dioxide
C-terminal	carboxy-terminal

DMSO	dimethyl sulfoxide
DSS	dextran sodium sulfate
EGFP	enhanced green fluorescent protein
EM	electron microscopy
Ena/VASP	Enabled/vasodilator-stimulated phosphoprotein
ERM	Ezrin, radixin, moesin protein family
Espin	Ectoplasmic specialization protein, a.k.a. small espin
EPS8	Epidermal growth factor receptor kinase substrate 8
F-actin	filamentous actin
FBS	fetal bovine serum
Fimbrin	Plastin-1, a.k.a. I (intestine specific)-plastin
FL	full-length
FRAP	fluorescence recovery after photobleaching
G-actin	monomeric actin
GAPDH	Glyceraldehyde 3-phosphate dehydrogenase
H&E	hematoxylin and eosin staining
Hs	Homo sapiens
IMAC	intermicrovillar adhesion complex
IBD	inflammatory bowel disease
KD	knockdown
K_D	equilibrium dissociation constant
kDa	kilodaltons
KO	knockout

Max I.P.	maximum intensity projection
mCh	mCherry
min	minute
MBP	maltose-binding protein
MISP	Mitotic spindle positioning, a.k.a. C19ORF21
MV	microvilli
N-terminal	amino-terminal
NIH	National Institutes of Health
NPF	nucleation promoting factors
ns	not significant
N-WASP	Neural Wiskott–Aldrich Syndrome protein
OEx	overexpression
PACSIN2	Protein kinase C and casein kinase substrate in neurons protein 2
PBS	phosphate buffered saline
PCR	polymerase chain reaction
PFA	paraformaldehyde
Phall	phalloidin
PIP(3,4)P2	phosphatidylinositol (3,4)-bisphosphate
PIP(4,5)P2	phosphatidylinositol (4,5)-bisphosphate
PIP(3,4,5)P3	phosphatidylinositol (3,4,5)-triphosphate
Pi	inorganic phosphate
PE	pointed end

PRMT2	Protein arginine N-methyltransferase 2
ROI	region of interest
S1	myosin subfragment-1
SD	standard deviation
SDCM	spinning disk confocal microscopy
SIM	structured illumination microscopy
sec	second
SH3	SRC homology 3
shRNA	short hairpin ribonucleic acid
t	time
TEM	transmission electron microscopy
TIRF	total internal reflection fluorescence
Tmod3	Tropomodulin-3
TRIOBP-4	TRIO and F-actin-binding protein 4
UtrCH	Utrophin calponin homology domain
USH1C	Usher syndrome type-1C
Villin	Villin-1
W4	Ls174T- W4 cells
WGA	wheat germ agglutin
WH2	Wiskott-Aldrich homology 2
WT	wild type

CHAPTER I

INTRODUCTION

What is actin?

Accounting for ~20% of the total protein in a eukaryotic cell, actin is one of the most abundant proteins on earth that was originally discovered as an activator of the motor protein myosin by Straub and Szent-Gyorgyi during investigations on muscle contraction (Bugyi & Kellermayer, 2020). A monomeric actin consists of 375 amino acids (~42 kDa), which fold into four subdomains arranged in a U-shaped flat configuration (Kabsch et al., 1990) (Figure 1-1 A). As a result, the structure of actin is asymmetric, with subdomains 1 and 3 creating a small "target-binding cleft", which is the site where multiple actin-associated proteins bind; and subdomains 2 and 4 creating a large "nucleotide-binding cleft" that can harbor a single nucleotide (primarily ATP) (Dominguez & Holmes, 2011; Kabsch et al., 1990) (Figure 1-1 B). The association of ATP with the nucleotide-binding cleft can be further stabilized by divalent cations such as Ca^{2+} and Mg^{2+} (Kitazawa et al., 1982).

Early biochemical studies found that actin monomers (G-actin) can assemble into fibrous conformations (F-actin) (Oda et al., 2009). Later X-ray studies showed that such fibrous actin networks consisted of filaments arranged in a helical manner (Holmes et al., 1990). Computer simulation analysis suggests that the asymmetry nature of a monomer allows it to polymerize into filaments in a unidirectional fashion, which is primarily driven by more electrostatic interactions available at one side relative to the other side of a

monomer (Sept et al., 1999). Actin polymerization is a complex process that involves multiple steps including nucleation, elongation, hydrolysis, and treadmilling.

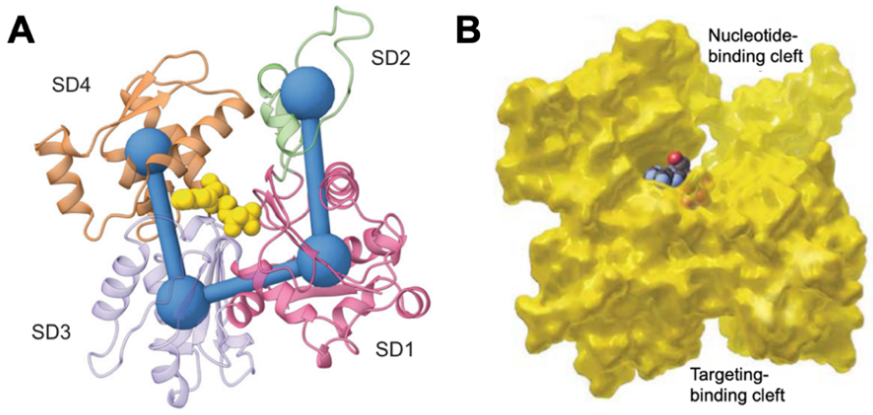

Figure 1-1. Structural conformation of actin
(A) Ribbon diagram of actin showing subdomains SD1 (purple), SD2 (green), SD3 (gray), and SD4 (orange) folded into a U-shaped flat configuration harboring a nucleotide (yellow) at the "nucleotide binding pocket" between subdomains 2 and 4. Adapted from (Sun & Alushin, 2022).
(B) Space-filling model (yellow) of actin highlighting the "nucleotide binding cleft" harboring an ATP molecule; and the "targeting binding cleft". Adapted from (Pollard, 2016).

How does actin assemble into a polymer?

Nucleation

The transition from G-actin to F-actin demands the formation of an intermediate actin "nuclei" consisting of two or three monomers that will serve as a template for polymerization (Pollard & Cooper, 1986). However, the assembly of an actin "nuclei" is highly unfavorable, which makes nucleation the rate-limiting step for actin polymerization (Pollard, 1986), specifically due to the high dissociation rate of monomers comprising dimers and trimers (Pollard, 2016) (Figure 1-2). The incorporation of a fourth monomer

into a trimer creates a more stable actin “nuclei”, likely as a result of maximizing the intermolecular interactions between monomers (Pollard et al., 2000). At this intermediate stage, the incorporation of additional monomers is more favorable, and a proper filament can begin to assemble (Figure 1-2).

Although nucleation is kinetically unfavorable, the incorporation of ATP-Mg^{2+} over ATP-Ca^{2+} seems to promote a more favorable and stable nucleus (Pollard & Cooper, 1986). Thus, once G-actin is coupled with ATP and Mg^{2+}, it can assemble more efficiently (fast polymerization) into dimers and trimers (Cooper et al., 1983). The stability of an actin “nuclei” can be dependent on multiple factors including the concentration of monomer in solution, and the presence of accessory proteins (Pollard et al., 2000).

The high concentration of actin in a typical eukaryotic cell (~ 200 μM) (Korn et al., 1987) is sufficient to trigger spontaneous nucleation in minimal reconstitution assays. However, in physiological conditions, actin monomers are usually associated with “sequestrators” such as profilin and thymosin ß4 (Courtemanche & Pollard, 2013; Safer et al., 1991). Both factors have a strong affinity for monomers, decreasing their ability to spontaneously assemble into dimers and trimers. Thus, despite the large amount of actin in the cytosol, the nucleation of monomers is still rate-limiting due to the activity of actin sequestrators (Pollard et al., 2000).

How do cells overcome the rate-limiting step of nucleation?

As the assembly of an actin “nuclei” is highly unfavorable, some factors known as “nucleators” aid in speeding up this process by simultaneously binding multiple monomers (Firat-Karalar & Welch, 2011). A prerequisite for a protein to function as a nucleator is to

have multiple binding sites for actin monomers (Dominguez, 2016). Formins are well-studied nucleators, which dimerize and bring together monomers via their FH2 domains (Higgs, 2005; Zigmond, 2004). In contrast to other nucleators, formins retain their ability to associate with the fast-growing ends of filaments following nucleation (Breitsprecher & Goode, 2013). Another widely known nucleator is the Arp2/3 complex that binds to pre-existing filaments to activate its nucleating potential, thus giving rise to “branches” of newly polymerizing actin filaments (Svitkina, 2018). However, the Arp2/3 can bypass the necessity of a pre-existing filament when associated with other regulatory factors, which may be required to trigger branching biogenesis (Wagner et al., 2013). While both nucleators can create different types of actin networks, their nucleation activity bringing monomers together reduces the kinetical barrier for new actin monomer incorporation, and thus helps to overcome the rate-limiting step of nucleation.

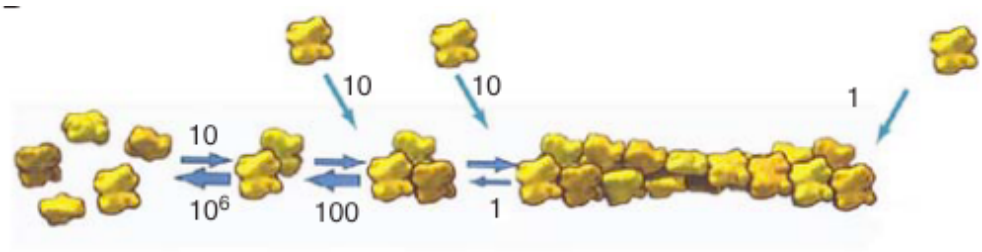

Figure 1-2. Nucleation of actin monomers
Cartoon schematic showing the steps leading to the formation of a stable actin “nuclei” containing three monomers. Right arrows denote the association rates; left arrows indicate disassociation rates. Note that once an actin “nuclei” containing more than three monomers is assembled, the incorporation of an additional subunit is more favorable that the disassembly of one of its subunits. Adapted from (Pollard, 2016).

Elongation

Once the kinetical barrier for nucleation has been overcome, a stable actin "nuclei" can serve as a template for the incorporation of additional monomers at both ends, a process known as "elongation" (Chesarone & Goode, 2009). Although the diameter of each monomer is ~5 nm, the incorporation of a single monomer to the resulting length of a filament is ~2.7 nm (Schaus et al., 2007). For instance, a 100-nm filament segment will consist of approximately 40 monomers (see scale bar in Figure 1-3 A). As alluded to earlier, due to the intrinsic asymmetry of actin monomers, their incorporation into filaments takes place in an oriented fashion (Sept et al., 1999). One way to determine such polarity is to label filaments with the myosin subfragment-1 (S1) (Hirokawa et al., 1982). This results in a filament decorated with arrowheads exposing the intrinsic filament polarity: the nucleotide-binding cleft resides at the "pointed end", and the targeting-binding cleft resides at the "barbed end" (Figure 1-3 A). Notably, these structural differences at both ends of the filament create two kinetically distinct ends with the "barbed end" as the site for fast monomer incorporation, and the "pointed end" as the site for much slower monomer incorporation (Pollard & Cooper, 1986; Welch & Mullins, 2002) (Figure 1-3 B).

A classic study reported the rates of actin polymerization at the barbed and pointed ends growing out of the actin-based acrosomal process of horseshow crab sperm (Pollard, 1986). Specifically, this study estimated the association rate constants (k_{on}; μM^{-1} s^{-1}) and dissociation rate constants (k_{off}; s^{-1}) of ATP- and ADP-bound monomers to/from filament ends (Figure 1-3 B). Using those rates, the resulting K_{off}/K_{on} ratio gives rise to the dissociation equilibrium constant (K_D; μM), also known as the "critical concentration" (Cc) because it refers to the minimal monomer concentration required to elongate a

filament. Thus, in the case of ATP-bound actin, the critical concentration ends up being 0.12 μM for the barbed ends; and 0.6 μM for the pointed ends (Pollard, 1986).

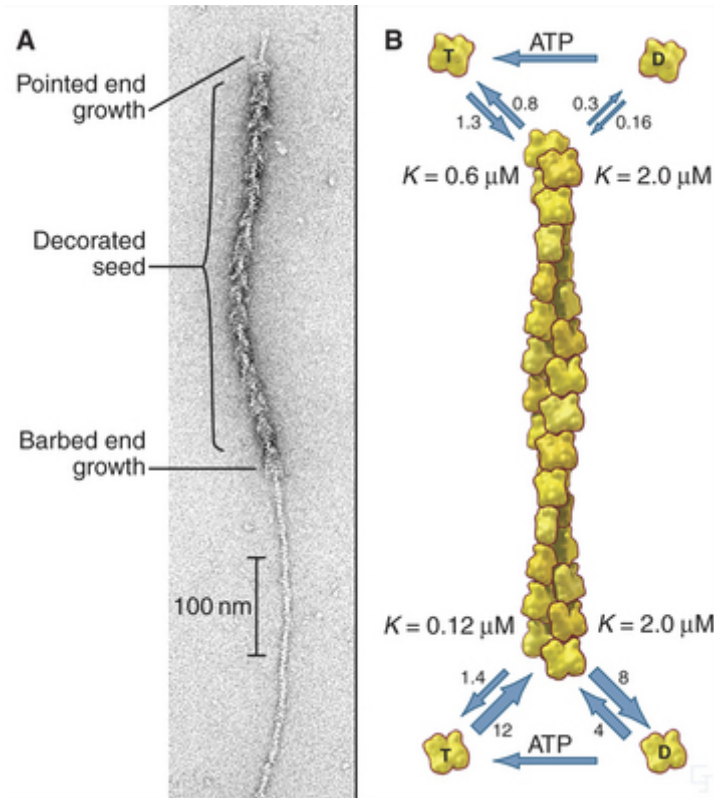

Figure 1-3. Elongation, polarity, and rate constants of F-actin
(A) Negative staining EM image of an actin filament decorated with myosin sub-fragment S1 showing a faster polymerization at the "barbed end" than the "pointed end" as evidenced by the undecorated filament segments.
(B) Cartoon schematic of F-actin showing the different rate constants for ATP and ADP at both the pointed ends and barbed ends. The smaller number denotes the on and off rates (k), and the large numbers show the resulting dissociation constant (or critical concentration) k_{off}/k_{on}.
Adapted from (Pollard, 2016).

How do cells control actin elongation?

Although the critical concentration of monomers in solution controls the elongation rates at both ends of an actin filament, cells employ other accessory proteins or elongation factors to speed up polymerization. In addition to their nucleation role, formins can also serve as actin elongation factors (Chesarone & Goode, 2009). While formins still use their dimeric FH2 domain to engage with the barbed during filament elongation, they also contain structurally disordered FH1 domains harboring polyproline regions with a strong affinity for actin-bound profilin (Higgs, 2005). Such affinity for profilin-monomers allows formin to elongate filaments from the barbed ends using the large pool of profilin-actin monomers found in solution. Another well-studied elongation factor is Enabled/Vasodilator-Stimulated Phosphoprotein (Ena/VASP), which can multimerize into a tetramer (Krause et al., 2003). Recent reconstitution assays determine that as a tetramer, Ena/VASP can simultaneously associate to barbed ends of four filaments, thus promoting their bundling and elongation (Winkelman et al., 2014). Similar to formins, Ena/VASP harbors a poly-proline motif within its EVH2 domain that binds to profilin-actin (Krause et al., 2003). While both formins and Ena/VASP are elongation factors that can increase the elongation rates of the barbed ends, their function can be antagonized by other barbed end-specific factors such as capping protein (Higgs, 2005; Krause et al., 2003), which can cease polymerization from barbed ends.

Traditionally, elongation factors were thought to be exclusive at the barbed ends. However, a very recent study showed that the *Vibrio* proteins VoF and VopL can promote faster elongation from the pointed ends (Kudryashova et al., 2022). Whether host proteins can also promote pointed end elongation remains an open question.

Hydrolysis and treadmilling

As an ATPase, monomeric actin is very inefficient at hydrolyzing ATP (McCullagh et al., 2014). However, the incorporation of G-actin into F-actin triggers structural rearrangements that flatten even more the monomer, which stimulates the hydrolysis of ATP within the nucleotide-binding cleft (Oda et al., 2009). The hydrolysis of ATP actin into ADP-Pi actin takes place within ~2 seconds (Blanchoin & Pollard, 2002). This is followed by the phosphate release within the next ~350 seconds leaving ADP actin alone (Carlier & Pantaloni, 1986) (Figure 1-4). Although ATP is not required for polymerization, the hydrolysis of ATP functions as a molecular timer for filament aging and remodeling (Bugyi & Carlier, 2010).

These three different nucleotide conformations (ATP-actin, ADP-Pi-actin, ADP-actin) create structural differences along the length of the filament from the barbed end to the pointed end. Recent structural studies indicate that such differences may be subtle, as there are no major structural differences along the three filament conformations (Reynolds et al., 2022). Yet, the ADP actin conformation creates more flexible filaments compared to the more rigid filament segments created by ATP/ADP-P_i actin (McCullough et al., 2008; Reynolds et al., 2022).

Early in filament polymerization, the availability of actin monomers promotes the elongation of both the barbed ends and the pointed ends. However, as filaments get longer, the availability of monomers will drop to a stationary concentration (Cs), which will only favor the incorporation of monomers to the barbed ends, with the simultaneous removal of an equal number of monomers from the pointed ends (Figure 1-5). This process is also known as steady-state treadmilling, which is fueled by the hydrolysis of

ATP, and is required for many cellular functions including cell migration, adhesion, and cytokinesis, among others (Bugyi & Carlier, 2010).

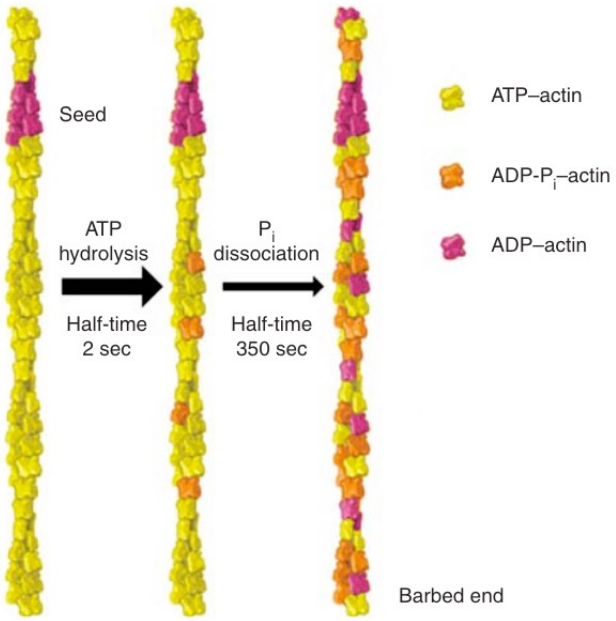

Figure 1-4. Hydrolysis of F-actin ("filament aging")
Cartoon schematic showing an actin filament oriented with its barbed end towards the bottom. ATP-actin hydrolysis rapidly takes place (~2 seconds), while the dissociation of P_i is slightly slower (~350 seconds). Adapted from (Pollard, 2016).

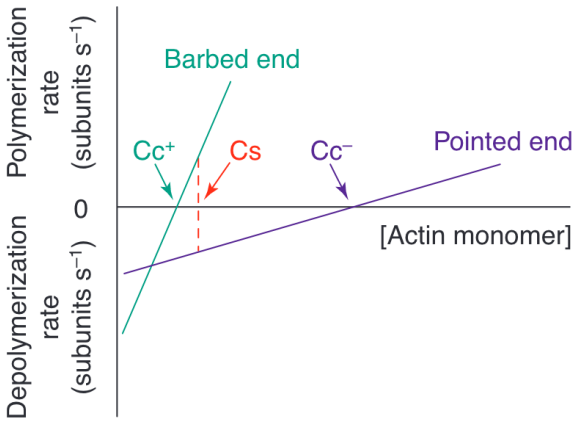

Figure 1-5. Elongation rates of F-actin as a function of G-actin concentration
The critical concentration of the barbed ends (Cc^+) is ~0.12 μM; while the critical concentration at the pointed ends (Cc^-) is ~0.6 μM. Monomer concentrations below Cc^+ favor disassembly at both ends. Monomer concentrations above Cc^- favor assembly at both ends. Monomer concentrations between Cc^+ and Cc^- (~Cs) favor steady-state treadmilling. Adapted from (Chen et al., 2000).

How does actin assemble into higher-order structures?

As a highly dynamic polymer, actin can be harnessed by cellular systems to create complex cytoskeletal structures consisting of multiple filaments arranged in specific configurations. Depending on the type of accessory proteins, the resulting higher-order actin structures can be classified as branched actin networks and linear actin bundles.

Branched actin networks

Branched actin networks, also known as “dendritic networks”, are found predominantly at the leading edge of migrating cells (Svitkina & Borisy, 1999). Although branched actin networks may appear as a meshwork of randomly oriented filaments in electron micrographs, they are highly organized with all their barbed ends uniformly oriented towards the leading edge of cells (Svitkina et al., 1997). Such ultrastructural organization is assembled by the Arp2/3 complex, which crosslinks filaments (Blanchoin et al., 2014). To function as a crosslinker, the Arp2/3 complex needs to be activated by nucleation promoting factors (NPF), which enables Arp2/3 binding to the side of a “mother” filament (Mullins et al., 1998). In this configuration, the Arp2/3 complex can promote the nucleation of “daughter” filaments exhibiting a characteristic angle of ~70° relative to the “mother” filament (Mullins et al., 1998). Subsequent generations of “daughter” filaments will give rise to the resulting branched actin network (Svitkina & Borisy, 1999) (Figure 1-6 A). Remarkably, the tree-like architecture of branched networks has been recapitulated using *in vitro* reconstitution TIRF assays (Amann & Pollard, 2001). The simultaneous assembly of Arp2/3 complex-driven branched actin networks combined with actin treadmilling can

generate forces across the leading edge of cells to push the membrane boundary forward and promote cell motility (Wang, 1985).

As the availability of actin monomers is limited, monomers comprising branched actin networks must be recycled and reincorporated at the barbed ends to continue pushing the leading edge (Pollard & Borisy, 2003). This can be orchestrated by severing and depolymerization factors such as cofilin (Bamburg, 1999). Cofilin preferentially severs aged filaments (i.e., ADP F-actin) (Blanchoin & Pollard, 1999), and depolymerizes monomers from pointed ends (Shekhar & Carlier, 2017; Wioland et al., 2017). Given that aged "mother" filaments comprising a branched actin network are located at the rear back of cells, cofilin may be responsible for their disassembly at those ends (Blanchoin et al., 2014). Moreover, cofilin binding to aged filaments reduces the affinity of Arp2/3 complex to the side of filaments in reconstitution assays, which suggests that cofilin may also promote debranching of these actin networks, thus facilitating its turnover (Chan et al., 2009).

Linear actin bundles

Actin filaments comprising linear bundles can be found in arrangements of mixed polarity (i.e., antiparallel) or uniform polarity (i.e., parallel). In all those cases, actin-bundling proteins are responsible for crosslinking filaments laterally into a compact core bundle.

Actin bundling proteins

The minimal requirement for a protein to function as an actin bundler is to have at least two actin-binding domains (ABD), which can bridge two adjacent filaments together (Otto,

1994). However, having a single ABD may be enough for a bundler with the ability to assemble into a dimer or oligomer (Matsudaira, 1991). Although not an exclusive feature, ABDs usually consist of two calponin homology domains in tandem (Sjöblom et al., 2008). Interestingly, the separation between ABDs in a functional bundling protein defines the resulting inter-spacing between actin filaments (Matsudaira, 1994; Pollard, 2016) (Figure 1-6 B-C). Recent studies show that these differences in filament spacing generated by bundlers function as a sorting mechanism to favor the recruitment of other actin-binding proteins (Winkelman et al., 2016). Other common features that can be found in actin bundling proteins are regulatory modules (i.e., Ca^{2+} sensing motifs) or membrane binding motifs (Matsudaira, 1991).

In addition to their ability to crosslink adjacent actin filaments, bundling proteins can also conduct other functions. One classic example is the bundler villin, which can also sever actin filaments in response to high Ca^{2+} concentrations, thus promoting the remodeling of actin bundles (Bretscher & Weber, 1980a; Ferrary et al., 1999; Revenu et al., 2007). Interestingly, purified villin also displays capping activity of barbed ends, as well as nucleation activity (Glenney Jr. et al., 1981). These various functions of villin can be regulated by phosphorylation (Zhai et al., 2001). The case of villin highlights the functional versatility of actin bundling proteins in addition to their crosslinking activity, which could be regulated in response to specific stimuli.

Antiparallel actin bundles

This type of bundle consists of filaments of mixed polarity with barbed and pointed ends facing either orientation (Figure 1-6 B). Such antiparallel organization is particularly

beneficial for myosin-driven force generation that allows essential cellular processes such as cytokinesis and cell adhesion (Blanchoin et al., 2014; Burridge & Wittchen, 2013; Reymann et al., 2012). In the case of cytokinesis, antiparallel bundles and myosin assemble an actomyosin contractile ring underneath the membrane boundary of the cell, which provides mechanical force to drive cell division in eukaryotes (Barr & Gruneberg, 2007). Although myosins are crucial players that drive contractility, the cytokinetic ring still exerts constriction when myosins are inhibited, which suggests that cytokinesis can still take place in a myosin-independent manner (Davies et al., 2014; Xue & Sokac, 2016). A recent study found that the actin bundling protein anillin can assemble actin bundles in a ring-like pattern, and are sufficient to promote the constriction of these rings *in vitro* (Kučera et al., 2021). Thus, actin bundling proteins may be contributing to the contractile forces exerted during cell division. Other types of antiparallel bundles are those comprising the ventral stress fibers. These bundles are tethered to focal adhesions, serving as an anchoring point for myosin-driven cell adhesion and migration (Cramer et al., 1997; Hotulainen & Lappalainen, 2006).

In antiparallel bundles comprising the contractile ring and stress fibers, α-actinin is a common bundler responsible for conferring these bundles with the characteristic mixed polarity conformation (Cramer et al., 1997; Li et al., 2016). As a monomer with a single ABD, α-actinin dimerizes into a large structure, creating a ~45 nm inter-spacing between the actin filaments it crosslinks (Hampton et al., 2007) (Figure 1-6 B). Such long inter-filament spacing driven by α-actinin has been shown to inhibit binding and bundling of other factors that create much smaller inter-spacings between filaments such as fascin (~8 nm) (Winkelman et al., 2016).

Parallel actin bundles

Bundles of uniform polarity consist of filaments with their barbed ends pointing toward the same direction, usually against the plasma membrane (Chhabra & Higgs, 2007). As the barbed ends are the site of fast monomer incorporation, these can be harnessed to generate a pushing force to deform the plasma membrane into finger-like protrusions (Atilgan et al., 2006) (Figure 1-6 C). Depending on the cell type, a parallel bundle can support membrane protrusions to explore the surrounding environment as in the case of filopodia (Svitkina et al., 2003); to increase the surface area for maximizing nutrient absorption or reabsorption as in the case of microvilli (Mooseker & Tilney, 1975); or to function as mechanosensory structures on the surface of inner hair cells as in the case of stereocilia (Barr-Gillespie, 2015).

While branched actin networks and antiparallel linear bundles are essential for conducting multiple cellular processes, in the following sections we will focus on how polarized parallel bundles are built. Although multiple accessory proteins are responsible for maintaining this type of linear bundles, we will highlight the role of crosslinking proteins that are responsible for interconnecting filaments next to each other, which give rise to the filopodium, stereocilium, and microvillus.

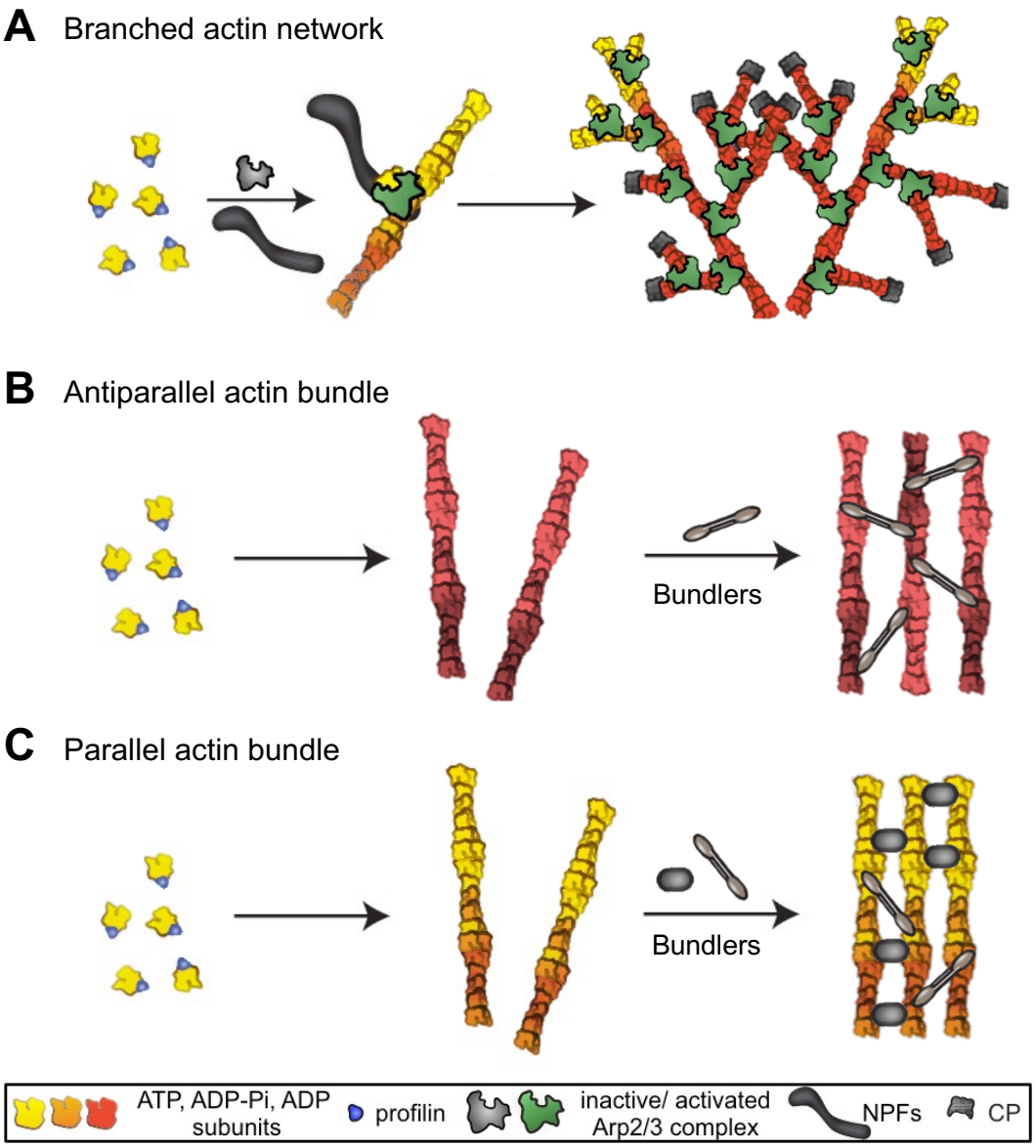

Figure 1-6. Higher-order actin structures
Cartoon schematic showing the various actin arrays assembled by crosslinking proteins. Examples include branched actin network assembled by Arp2/3 complex **(A)**; and linear actin bundles of mixed polarity (parallel and antiparallel bundles) assembled by bundlers **(B-C)**. NPF: Nucleation Promoting Factor; CP: Capping Protein. Adapted from (Blanchoin et al., 2014).

What is a filopodium?

About a century ago, a filopodium was first described as an “extremely fine filamentous pseudopodia” growing out of the surface of nerve cells (Harrison, 1910). We now know that a filopodium is a membrane protrusion supported by a polarized linear bundle consisting of ~10 – 30 actin filaments, which have their barbed ends oriented towards the distal protruding tips (Mattila & Lappalainen, 2008; Mellor, 2010). A single filopodium exhibits an average diameter of ~0.1 – 0.3 μm, and a more variable length that can range from ~10 μm in fibroblasts up to ~150 μm in mesenchymal cells of chick embryos (Sanders et al., 2013; Welch & Mullins, 2002). Although filopodia display a short lifespan (< 60 min), they are highly dynamic structures that undergo cycles of extension and retraction at a rate of ~ 10 μm/min (Özel et al., 2015; Wood & Martin, 2002). These features allow filopodia to carry out diverse functions including cell migration, wound healing, chemoattractant guidance, and extracellular matrix adhesion in various cell types across species (Mattila & Lappalainen, 2008). The ubiquitous nature and availability of filopodia have allowed researchers to understand their composition and propose models for their assembly.

How are filopodia assembled?

Two models have been proposed to explain how a filopodium is assembled: “tip-nucleation” and “convergent elongation” models, although they may not be mutually exclusive (Mattila & Lappalainen, 2008) (Figure 1-7). The “convergent elongation” model postulates that cells harness the uniform polarity of pre-existing branched actin networks to converge multiple filaments into a reduced area underneath the plasma membrane,

which will create enough force to generate a filopodium (Svitkina et al., 2003). Although this model acknowledges the role of a tip complex (i.e., formins, Ena/VASP) organizing the convergent filaments, it highlights the Arp2/3 complex and the branched actin network as main precursors of a filopodium (Yang & Svitkina, 2011). Conversely, the "tip-nucleation" model proposes that filaments are assembled *de novo* at focal points near the plasma membrane, primarily driven by formins (Mattila & Lappalainen, 2008). As such, this model argues that core bundles supporting filopodia are generated independent of Arp2/3-driven branched actin networks (Mattila & Lappalainen, 2008; Yang & Svitkina, 2011). Evidence supporting this model comes from electron micrographs showing an apparent discontinuity between the underlying branched actin networks and the basal end of core bundles, which seem to end as an unbranched "terminal cone" in the case of the amoeba *Dictyostelium discoideum* (Mattila & Lappalainen, 2008). Interestingly, this same organism assembles filopodia in an Arp2/3-independent fashion, further supporting the "tip-nucleation" model (Steffen et al., 2006).

Despite the controversy between the "convergent elongation" and "tip-nucleation" models, both models propose that filaments are elongated by Ena/VASP or formins accompanied by their bundling by fascin. Although Ena/VASP or formins may contribute to the initiation of bundle formation, bundling by fascin will provide enough flexural rigidity to deform the plasma membrane (Atilgan et al., 2006; Blanchoin et al., 2014). Thus far, fascin has been documented as the only bundling protein responsible for crosslinking filaments that make up the core bundles of filopodia (Vignjevic et al., 2006). Interestingly, reconstitution studies suggest that fascin exclusively assembles parallel actin bundles *in vitro* (Breitsprecher et al., 2011; Jansen et al., 2011). This feature presumably allows

fascin to help orchestrate the polarity of the resulting core bundles that support filopodial protrusions. Although force generation to deform the plasma membrane has been proposed to be driven by monomer incorporation to the barbed ends (Theriot, 2000), a recent study highlights the role of barbed-end directed myosins in contributing to generating the force needed to elongate protrusions (Fitz et al., 2023).

As filopodia are ubiquitous on multiple cell types, these protrusions have served as a classical model to study the assembly and dynamics of actin-based protrusions. Moreover, filopodia have also been used as a heterologous model system to investigate the function of factors specific to other actin-based protrusions such as stereocilia and microvilli (He et al., 2019; Weck et al., 2020).

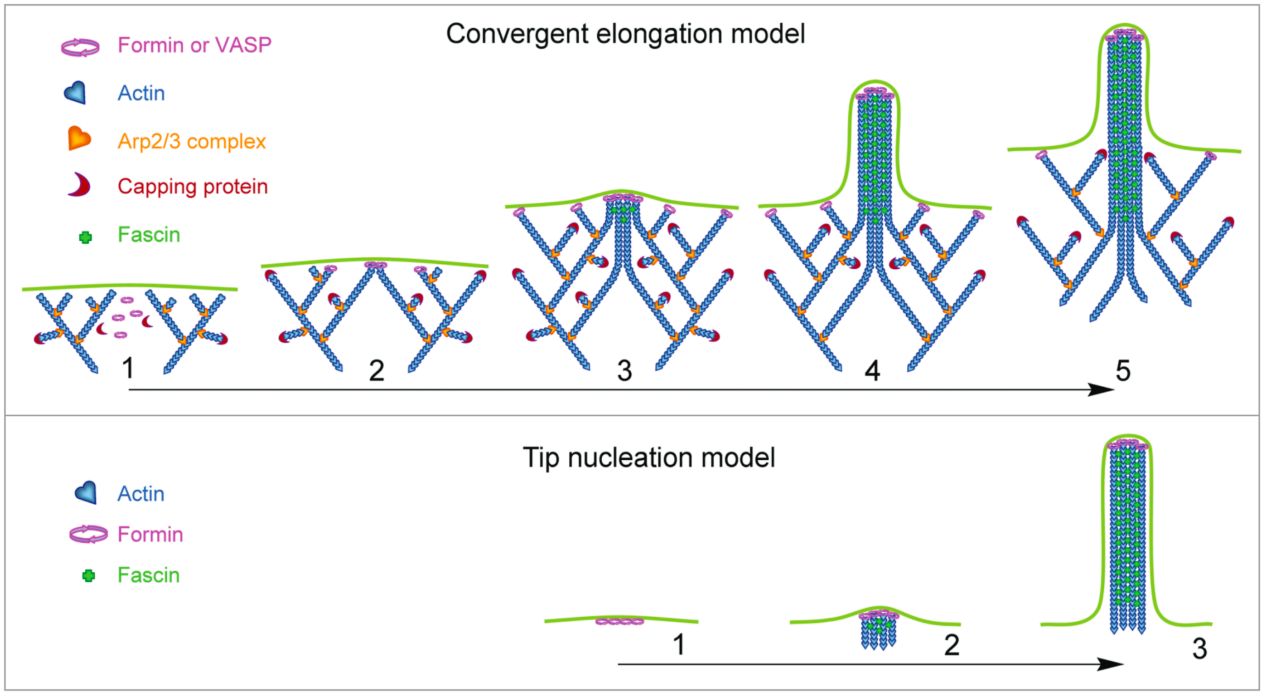

Figure 1-7. Models of filopodia biogenesis
(A) Convergent elongation model. A pre-existing Arp2/3-nucleated branched actin network along with other accessory factors converge multiple filaments onto the plasma membrane to give rise a core actin bundled by fascin, which will generate enough force to push the membrane boundary (1-5).

(B) Tip-nucleation model. A tip complex primarily consisting of formins assemble at focal points below the plasma membrane (1), which drives *de novo* polymerization of multiple actin filaments (2) that will generate the resulting core actin bundled by fascin (3). Adapted from (Yang & Svitkina, 2011).

What is a stereocilium?

Stereocilia are actin-based protrusions arranged in rows of increasing height, which give rise to a staircase-shaped structure known as the "hair bundle" (Schwander et al., 2010). Stereocilia protrusions comprising each row are interconnected with their neighboring stereocilia of adjacent rows through cadherin tip-links (Kazmierczak et al., 2007). As a result of this unique architectural organization, a stereocilia hair bundle functions as a mechanosensory structure that converts mechanical stimuli (i.e., sound waves) into electrical currents, which ultimately translates into hearing (Schwander et al., 2010). Although stereocilia maintain their staircase pattern on the surface of each hair cell, their length is variable depending on their localization within the inner ear (Tilney et al., 1992). This length variability allows hair bundle stereocilia to detect different sound frequencies (Manor & Kachar, 2008).

Thus, the length of a stereocilium can range from ~1 μm up to 120 μm (Manor & Kachar, 2008); while their width can vary between 0.12 and 0.2 μm (Tilney & Saunders, 1983). Thus, the number of constituent actin filaments can also be highly variable with hundreds of them supporting a protrusion (Schwander et al., 2010). In all cases, filaments extend their barbed ends towards the distal tips, and their pointed ends are anchored into an actin meshwork known as the cuticular plate (Tilney et al., 1980). Interestingly, stereocilia protrusions taper at their base, which is accompanied by a decrease in the

number of filaments at the rootlets (McGrath et al., 2017). This narrowing of the stereocilia diameter at their base enhances their sensitivity to sound waves by allowing them to pivot (McGrath et al., 2017).

How are stereocilia assembled?

Early in development, the apical surface of hair cells is populated by short actin-based microvilli-like protrusions, and a single microtubule-based protrusion known as kinocilium (McGrath et al., 2017). Importantly, the kinocilium contributes to the growth and positioning of the hair bundle, presumably by remodeling the existent microvilli-like protrusions (Barr-Gillespie, 2015; McGrath et al., 2017) (Figure 1-8). Although some studies invoked formins as nucleators that may be involved in the assembly of stereocilia (Drummond et al., 2012), there is no evidence showing that formins are present in stereocilia. Thus, our understanding of how actin is nucleated early in stereocilia biogenesis remains unknown. However, some early factors that may orchestrate the assembly of actin in stereocilia include EPS8, which specifically localizes at the tip of stereocilia protrusions, promoting their elongation (Manor et al., 2011). Moreover, EPS8 seems to form a tripartite complex with myosin-15a and whirlin, all of which cooperate to regulate stereocilia elongation (Manor et al., 2011; McGrath et al., 2017). Filaments comprising stereocilia are crosslinked by isoforms of the bundlers espin (Sekerková et al., 2006; Zheng et al., 2000), plastin (Taylor et al., 2015), and fascin (Chou et al., 2011). Interestingly, TRIOBP-4 was identified as another bundler that selectively targets the rootlet of stereocilia (Kitajiri et al., 2010). Interestingly, TRIOBP-deficient mice exhibited deafness, failure to grow rootlets, and less rigid stereocilia (Kitajiri et al., 2010),

presumably as a result of the tight packing of actin filaments that TRIOBP confers *in vitro*. Among all bundling proteins, espin is present early in development suggesting that it may be an early bundler that initiates the bundling and packing of loose filaments, followed by plastin-1, and fascin (Frolenkov et al., 2004; Shin et al., 2010; Taylor et al., 2015; Zheng et al., 2000).

The core bundles supporting stereocilia were initially reported to undergo treadmilling (Rzadzinska et al., 2004). Nevertheless, more recent studies indicate that only a very small segment of the distal end of core bundle stereocilia undergoes treadmilling, while a much larger segment of these core bundles is stable and does not turn over (Drummond et al., 2015; Narayanan et al., 2015).

Although multiple factors of stereocilia hair bundle have been identified, it remains elusive how they are temporally and spatially controlled during all the various phases of stereocilia. One major challenge to studying this is the lack of cell culture models to recapitulate these events. Yet the recent development of organoid models that mimic inner hair cell biology may provide new insights into these mechanisms (Liu et al., 2016).

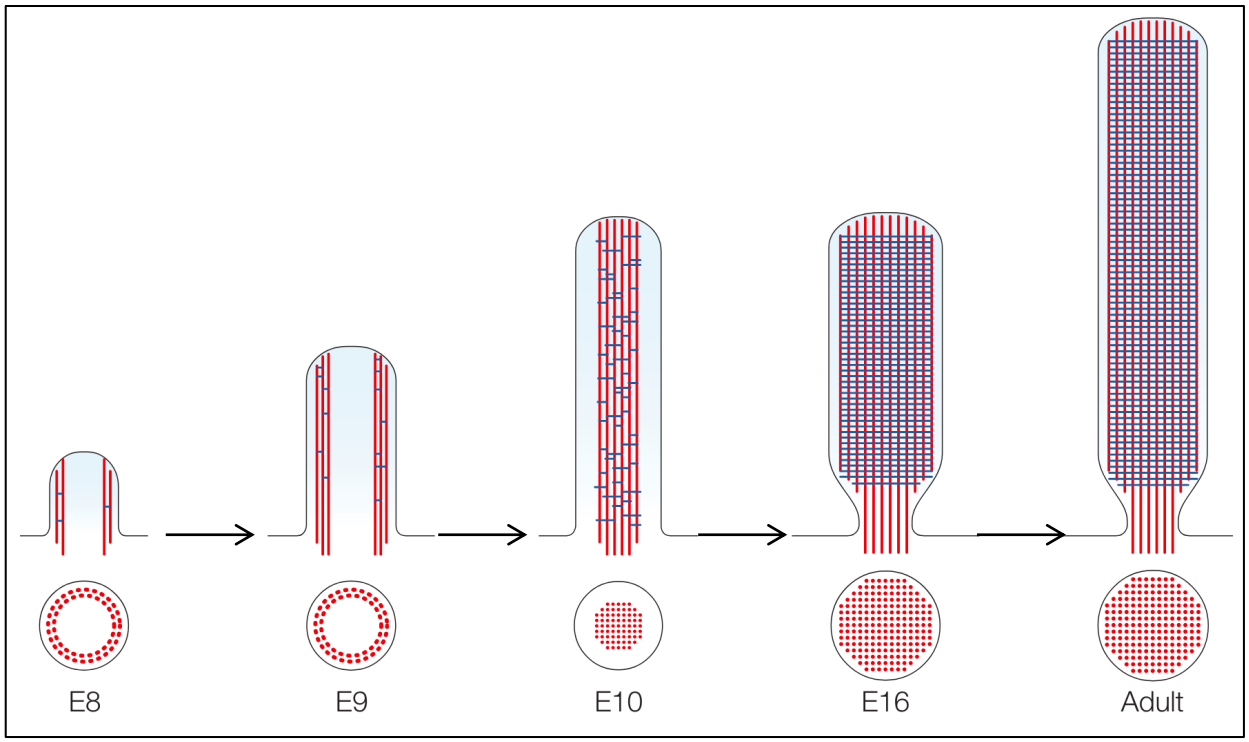

Figure 1-8. Model of stereocilia biogenesis
Cartoon schematic displaying actin remodeling during various stages (E8-Adult) of stereocilia differentiation in chicks' hair bundle. The upper rows show lateral views of a stereocilium, while the bottom row shows cross-sections. Note that actin filaments (red) are loosely packed early in stereocilia differentiation, and become more packed upon the arrival of bundling proteins (blue).
Adapted from (Frolenkov et al., 2004).

The following section on the assembly of microvilli was originally published as:
Morales, E. A., Gaeta, I., & Tyska, M. J. (2023). Building the brush border, one microvillus at a time. Current Opinion in Cell Biology, 80, 102153.

What is a microvillus?

Epithelial monolayers lining the lumens of hollow organs consist of polarized cells that build large numbers of microvilli on their apical surface, which maximize the potential for interacting with lumenal contents (Helander & Fändriks, 2014). In the specific case of nutrient absorbing enterocytes, the dominant cell type in the intestinal monolayer, a single cell builds several thousand microvilli on its apical surface during differentiation. The result is a unique array - referred to as the “brush border” - defined by its striking morphological order and uniformity (Crawley, Mooseker, et al., 2014a; Delacour et al., 2016; Sauvanet et al., 2015) (Figure 1-9 A-B). Given that the vertebrate gut epithelium is an abundant source of brush border material, enterocyte microvilli have been the focus of ultrastructural and biochemical investigations for many years. Indeed, our understanding of the cytoskeletal composition and structure of microvilli is in large part based on decades of investigation in this system, which began with Mooseker and Tilney’s discovery of actin as a highly abundant protein in isolated brush border fractions (Tilney & Mooseker, 1971).

Moving forward ~50 years to present day, we now know that microvilli exhibit a simple architecture consisting of a supporting core bundle of 20-40 actin filaments encapsulated by plasma membrane (Mooseker & Tilney, 1975; Ohta et al., 2012) (Figure 1-9 C-D). Filaments in this bundle are packed together by a complement of bundling proteins including villin (Bretscher & Weber, 1979), espin (Bartles et al., 1998), fimbrin (Bretscher & Weber, 1980b), and MISP (Morales et al., 2022). The core bundle is laterally

tethered to the enveloping plasma membrane by membrane-actin linking proteins, including ERM family protein ezrin (Gould et al., 1986), and class 1 myosins such as myosin-1a (Conzelman & Mooseker, 1987; Tyska et al., 2005), and myosin-1d (Benesh et al., 2010). The resulting structure is a cylindrical membrane protrusion ~1-2 μm in length and ~100 nm in diameter. Importantly, individual actin filaments in a core bundle are polarized, with all barbed ends - the favored site of actin monomer incorporation – at the distal tip (Mooseker et al., 1982; Mooseker & Tilney, 1975; Pollard & Mooseker, 1981). Conversely, all pointed ends extend down into the sub-apical cytoplasm, where they are embedded in a cytoskeletal meshwork referred to as the “terminal web” (Hirokawa et al., 1982; Hirokawa & Heuser, 1981; Palay & Karlin, 1959a, 1959b). Most but not all these filaments appear to run continuously from the distal tip down to the proximal (Ohta et al., 2012). The two ends of the core bundle are also defined by the enrichment of specific factors; all barbed ends at the distal tip are strongly decorated with EPS8 and BAIAP2L1 end (Croce et al., 2004; Postema et al., 2018), which both contain structural motifs with the potential to link plasma membrane to the actin cytoskeleton. The basal ends of core bundles are associated with distinct factors including COBL (a putative actin nucleator) (Ahuja et al., 2007; Beer et al., 2020; Grega-Larson et al., 2015), Tmod3 (a pointed end capper) (A. Weber et al., 1994; K. L. Weber et al., 2007), and non-muscle myosin-2 (a force generator and potential actin disassembly factor) (Chinowsky et al., 2020). Finally, in a mature brush border, microvillar packing is driven and organized by tip-tip adhesion links that consist of a heterophilic complex of two protocadherins, CDHR2 and CDHR5 . These adhesive factors are positioned at microvillar tips by the barbed end directed motor myosin-7b (Chen et al., 2001; Weck et al., 2016) via interactions that are mediated by

the two scaffolding proteins, ANKS4B and USH1C (Crawley et al., 2016; Crawley, et al., 2014; Li et al., 2016, 2017; Weck et al., 2020; Yu et al., 2017) (Figure 1-10). A similar complex links the distal tips of stereocilia on the surface of mechanosensory hair cells (He et al., 2019; Li et al., 2016, 2017; Yu et al., 2017) and inactivating mutations in those factors or their binding partners result in sensory disorders, including Usher syndrome (Géléoc & El-Amraoui, 2020).

When and where do cells build microvilli?

As microvilli are defining features of the functionally mature epithelial cells, they are assembled in large numbers during differentiation. In the context of the intestinal epithelium, this process takes place on the surface of nascent enterocytes as they migrate out of stem cell-containing crypts on to the villus surface. Although the precise timing of this transition remains unclear, in mice the entire ~500 μm voyage from crypt to villus tip takes ~5 days (van der Flier & Clevers, 2009). Differentiation takes place over the course of only a few cell diameters (< 25 μm) along this axis as they pass through the crypt-villus transition. These spatial and temporal points of reference allow us to estimate that the 2000-3000 microvilli that ultimately comprise a mature brush border are assembled over a time scale of hours. Thus, timely control of the factors that regulate the growth of microvilli is essential for completing differentiation.

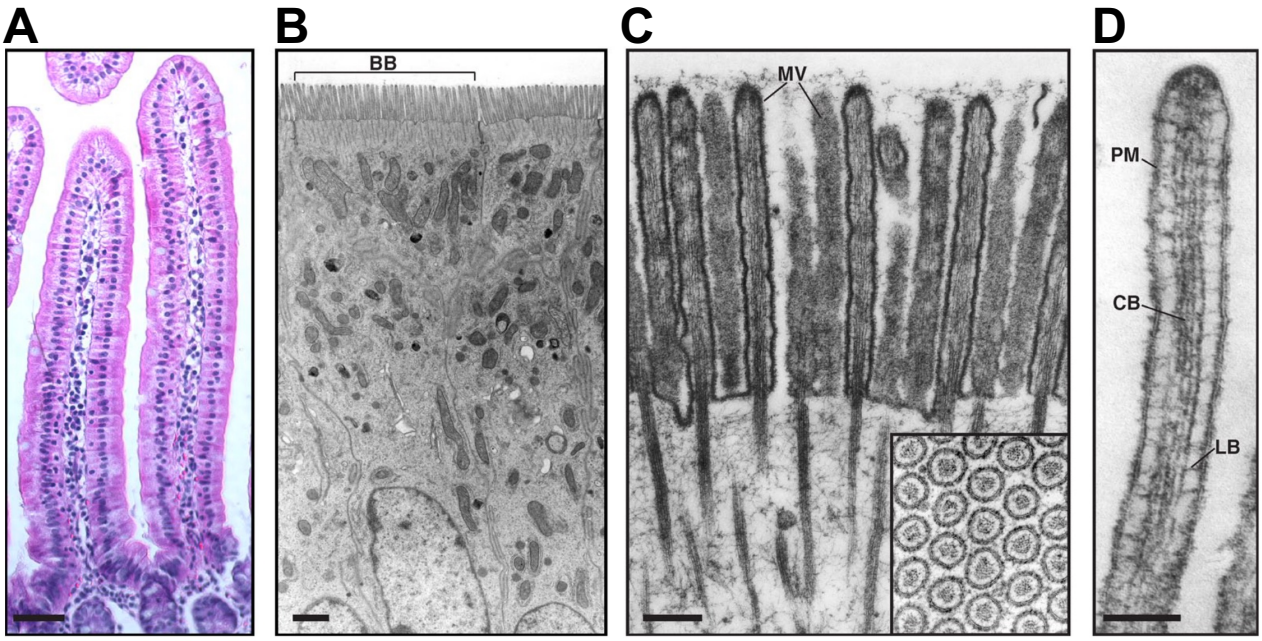

Figure 1-9. Structural organization of the brush border microvilli
(A) H&E staining of a section of the small intestine displaying the villus domain as a large finger-like protrusion, and the crypt domain as an invagination in between two villus. Scale bar = 50 μm.
(B) TEM image of a section of an enterocyte displaying a uniform brush border on their apical surface. Scale bar = 1 μm.
(C) TEM image of the apical section of an enterocyte showing the microvilli protrusions comprising the brush border. Scale bar. = 0.2 μm.
(D) Zoom-in of a single microvillus showing the core actin bundles supporting the encapsulating membrane protrusion. Scale bar = 0.1 μm.
Adapted from (Crawley, et al., 2014b).

How are microvilli assembled?

Given that microvilli are actin bundle-supported structures, understanding how constituent actin filaments are polymerized and bundled to create these core cytoskeletal units are key goals. To build a core bundle, actin polymerization must first be initiated at the proper sites, immediately subjacent to the apical plasma membrane. The resulting nascent filaments must also be elongated to the required length, aligned, and bundled in

a polarized manner such that all their growing barbed ends are situated directly against the membrane. In this arrangement, they can work together to generate the mechanical force needed to produce the outward membrane curvature that is characteristic of microvilli (Footer et al., 2007; Theriot, 2000). Importantly, approximately 30 filaments must be polymerized, such that the collective force generated at the distal end of a bundle will exceed the threshold bending stiffness of the plasma membrane without buckling (Atilgan et al., 2006; Mogilner & Rubinstein, 2005; Orly et al., 2014). Moreover, recent live cell imaging studies demonstrate that not all core bundles are assembled in a de novo fashion, as a subset are templated from the bundles in pre-existing microvilli (Gaeta et al., 2021). How microvillar actin polymerization is initiated or templated, and how filaments are elongated, oriented, and bundled in parallel are all fundamental open questions, but recent studies are offering exciting mechanistic hints, which are discussed in more detail below.

How are core bundle actin filaments generated?

As an individual immature epithelial cell migrates through the crypt-villus transition, a sparse lawn of nascent microvilli transforms into a densely packed array consisting of thousands of microvilli (Pothier & Hugon, 1980). Because an individual microvillus contains thousands of actin monomers, building an entire brush border demands 10s of millions of subunits. Interestingly, high levels of G-actin accumulate in the sub-apical region of both immature and differentiated enterocytes (Faust et al., 2019), and incorporation of these subunits into filaments might be regulated by the monomer binding protein, profilin (Rotty et al., 2015; Suarez et al., 2015), which is also enriched sub-apically

(Faust et al., 2019). Recent high resolution live-cell imaging also revealed that “clouds” of G-actin accumulate at the plasma membrane in the minutes preceding protrusion growth (Gaeta et al., 2021). Actin monomer availability, which can impact the growth of specific actin networks (Burke et al., 2014; Rotty et al., 2015; Suarez et al., 2015) is limiting during the assembly of microvilli, as increasing the supply of G-actin (e.g. by inhibiting the ubiquitous nucleation activity of Arp2/3) increases the actin content and length of microvilli (Faust et al., 2019).

Beyond the availability of cytoskeletal building blocks, assembling a microvillus also requires molecular machinery for controlling actin monomer-monomer interactions and forming polymerization competent “nuclei” in space and time. Proteomic studies of brush border enriched fractions have identified some interesting candidates (McConnell et al., 2011; Revenu et al., 2012). One such factor is Cordon bleu (COBL), which harbors three actin monomer-binding WH2 domains arranged in tandem near its C-terminus. COBL might promote filament nucleation by stabilizing three monomers configured in a short pitch helix (Chen et al., 2013; Husson et al., 2011). Although such nucleation activity is predicted to be weak (Dominguez, 2016), studies have indicated that it may be enhanced by Ca^{2+} and calmodulin (Hou et al., 2015), and potentially by PRMT2-driven methylation at the arginine residue within its second WH2 domain, which promotes strong G-actin binding in the context of neuronal branching (Hou et al., 2018). *In vitro* studies of COBL fragments have also revealed other diverse activities including filament severing and monomer sequestration (Husson et al., 2011; Jiao et al., 2014). Importantly, loss- and gain-of-function studies in epithelial cell culture models implicate COBL in the control of microvillar growth and length control, although the details appear model dependent

(Grega-Larson et al., 2015; Wayt & Bretscher, 2014). Mice lacking COBL exhibit structural perturbations in the brush border terminal web, consistent with a role in organizing the cytoskeleton in this compartment (Beer et al., 2020). Intestinal tissue in these animals appear grossly normal, but this is expected given the high capacity for functional compensation noted in previous studies of mice lacking key brush border structural components (Ferrary et al., 1999; Revenu et al., 2012; Tyska et al., 2005). COBL also contains an N-terminal polyproline rich domain that associates with the SH3 domain of PACSIN2, an F-BAR protein that drives enrichment of this factor on the apical membrane (Grega-Larson et al., 2015; Schwintzer et al., 2011; Wayt & Bretscher, 2014). To date, aside from COBL, no other factors with actin nucleation potential have been identified in microvilli. Moreover, a contribution from the ubiquitous Arp2/3 nucleation complex, which generates branched actin filament networks, has also been ruled out (Faust et al., 2019; Grega-Larson et al., 2015). Thus, despite persistent confusion in the literature, COBL must remain a candidate for generating the actin filaments that comprise the microvillar core bundle.

How are core bundle actin filaments elongated?

Once actin monomers are brought together to form a stable nucleus, subsequent elongation of its barbed end to produce a filament of functional length is likely driven by one or more factors that prevent barbed end capping. Formins hold filament elongation potential (Kovar & Pollard, 2004) and were identified as brush border components in two proteomic studies (McConnell et al., 2011; Revenu et al., 2012). Although SMIFH2 inhibition of formins failed to impair microvillar growth in cell culture models (Grega-

Larson et al., 2015), those results are difficult to interpret in light of this compound's off target effects on myosin motors (Nishimura et al., 2021), which have also implicated in microvillar length control (Chinowsky et al., 2020). Other leading candidate elongation factors are EPS8 and its binding partner, BAIAP2L1, which target to the distal ends of microvilli where filament barbed ends reside. EPS8 contains N-terminal motifs that may support membrane association, a central SH3 domain capable of dimerization, and C-terminal actin binding motifs, and was originally suggested to function in filament capping and bundling (Hertzog et al., 2010). Through polyproline motifs, EPS8 interacts with the SH3 domain found in BAIAP2L1. BAIAP2L1 in turn contains an I-BAR domain that drives localization to regions of outward membrane curvature (like that found at microvillar tips) and may promote dimerization; a poorly conserved C-terminal WH2 domain also provides additional actin binding potential. Indeed, overexpression of BAIAP2L1 is sufficient to rescue the microvillus length defect in cells lacking EPS8, while a mutant of BAIAP2L1 lacking the WH2 domain does not (Postema et al., 2018). Based on experiments in intestinal epithelial cell culture models, EPS8 and BAIAP2L1 work together to promote core bundle elongation (Postema et al., 2018). Although EPS8 and BAIAP2L1 colocalize, EPS8 in particular demonstrates exquisitely specific enrichment in puncta at the distal ends of microvilli (Postema et al., 2018), and related structures including the filopodia found at the edge of motile cells and stereocilia that extend from the apex of mechanosensory cells (Croce et al., 2004; Manor et al., 2011). As one might expect based on its unique localization, EPS8 has been implicated in protrusion length control in these different contexts (Croce et al., 2004; Disanza et al., 2006; Manor et al., 2011; Postema et al., 2018).

Recent live imaging studies revealed that EPS8 puncta target to the apical surface and mark future sites of microvillar growth minutes before core bundle assembly begins, further suggesting that this factor may be involved in initiation as well as elongation (Gaeta et al., 2021). Moreover, after a core bundle forms, the initiating EPS8 punctum persists at its distal end, and loss of this punctum is followed immediately by core bundle disassembly (Gaeta et al., 2021). Notably, the core bundles that support nascent microvilli exhibit robust treadmilling (Loomis et al., 2003; Tyska & Mooseker, 2002), an activity that drives the movement of these protrusion across the apical surface (Meenderink et al., 2019). Such dynamics are also regulated by EPS8 and BAIAP2L1 and are hypothesized to play a key role in organizing microvillar packing as protrusion density increases (Meenderink et al., 2019). Whether the EPS8/BAIAP2L1 complex exerts definitive anti-capping activity, which one might expect for factors that promote elongation, remains to be determined.

In addition to the *de novo* polymerization of core bundle actin filaments, which would necessarily require an actin nucleator, newer live imaging data also points to a second distinct pathway for growing core bundles, which takes advantage of filaments in pre-existing core bundles, rather than growing new polymers de novo. Indeed, a subset of nascent microvilli emerge from a process whereby a “mother” microvillus gives rise to a “daughter”, which typically grow from the base of the pre-existing protrusion (Gaeta et al., 2021). Notably, classic ultrastructural studies attempting to capture microvillus re-growth events in tissue explants perturbed with hydrostatic pressure, were the first to document evidence of “forked” microvilli that were consistent with a mother/daughter growth mechanism (Tilney & Cardell, 1970). Evidence of daughter growth was also

recently captured *in vivo* in the *C. elegans* intestine (Zhu et al., 2022), suggesting this mode of microvilli growth may be widespread. How might a daughter microvillus grow from the base of a mother? Although EPS8 and BAIAP2L1 are tip specific factors, they occasionally travel in a retrograde fashion to the base of a treadmilling mother microvillus and eventually appear to template daughter growth laterally from the pre-existing core bundle (Gaeta et al., 2021; Meenderink et al., 2019). One possibility is that retrograde movement of these factors represents a subset of filaments that fall behind in terms of elongation relative to other filaments in the treadmilling core, and then - with the help of EPS8 and BAIAP2L1 - restart elongation near the base of mother microvillus where monomer concentrations are expected to be higher.

How are actin filaments bundled with uniform polarity?

Classic ultrastructural studies used S1 labeling to establish that all actin filaments in the core bundle extend their barbed ends toward the distal tip (Hirokawa & Heuser, 1981). Such “barbed end out” orientation is a common feature of actin-supported surface protrusions, which makes physical sense considering that barbed end elongation potentially generates pushing force for creating outward membrane curvature. How this orientation is created during microvillar assembly remains unclear, although one possibility is that nascent filaments are oriented as they are brought together during filament bundling, which is driven by multiple enterocyte-expressed factors including villin, espin and fimbrin (Bartles et al., 1998; Bretscher & Weber, 1979, 1980b). Intriguingly, triple KO mice lacking all three of these molecules (VEP KO) still assembled microvilli suggesting the existence of other bundling proteins (Revenu et al., 2012). Although EPS8

was initially invoked as a bundling protein that might compensate, its specific localization to the distal tips of protrusions argues against a conventional bundling activity throughout the length of the core bundle (Gaeta et al., 2021). More recently, Mitotic Spindle Positioning (MISP) was identified as a new unconventional bundling protein that selectively bundles the rootlet ends of microvilli (Kumeta et al., 2014; Morales et al., 2022). Whether MISP or other yet-to-be-identified bundlers compensate bundling activity in VEP KO mice remains an open question.

Are any of these bundling factors sufficient for driving uniform filament polarity? Intriguingly, fimbrin-actin bundles assembled *in vitro* exhibit polarized S1 labeling, suggesting that this factor may be capable driving uniform polarity in cells (Glenney et al., 1981). In enterocyte brush borders, fimbrin appears to accumulate closer to the pointed ends of core bundle filaments (Grimm-Günter et al., 2009). MISP also exhibits highly preferential localization near the basal/pointed ends of microvillar actin filaments (Morales et al., 2022), and can recruit fimbrin to bundled actin in cells, suggesting their preferential binding to one end could provide a mechanism for orienting filament polarity. Binding near filaments ends might not be essential, however, as espin is generally found along the length of the actin core and its overexpression in cultured cells appears to be sufficient for assembling exaggerated bundles consisting of filaments of uniform polarity (Loomis et al., 2006). The filopodial bundler, fascin, also localizes uniformly along the length of bundles it creates and is sufficient for driving uniform filament polarity in these structures (Jansen et al., 2011; Vignjevic et al., 2006).

Whereas actin bundling proteins generally exhibit filament side binding potential, another possible non-mutually exclusive mechanism for orienting actin filaments involves

barbed end binding factors such as EPS8, which as alluded to above, marks sites of microvillar growth and remains persistently attached to the core bundle distal end through its lifetime (Gaeta et al., 2021). Given that EPS8 also associates with the apical plasma membrane - either directly or through binding partner, BAIAP2L1 - it is well positioned to orient filament barbed ends against the membrane during core bundle assembly. The proposal that specific membrane-associated protein machinery organize core bundle growth dates back to classic ultrastructural studies, which collectively revealed that the distal ends of core bundles in newly forming and fully formed microvilli make contact with the plasma membrane at electron dense patches (Mooseker & Tilney, 1975; Tilney & Cardell, 1970). Such sites were hypothesized to be enriched in factors that control actin assembly. Although EPS8 is a reasonable candidate constituent of these electron dense regions, this remains to be confirmed experimentally at the ultrastructural level.

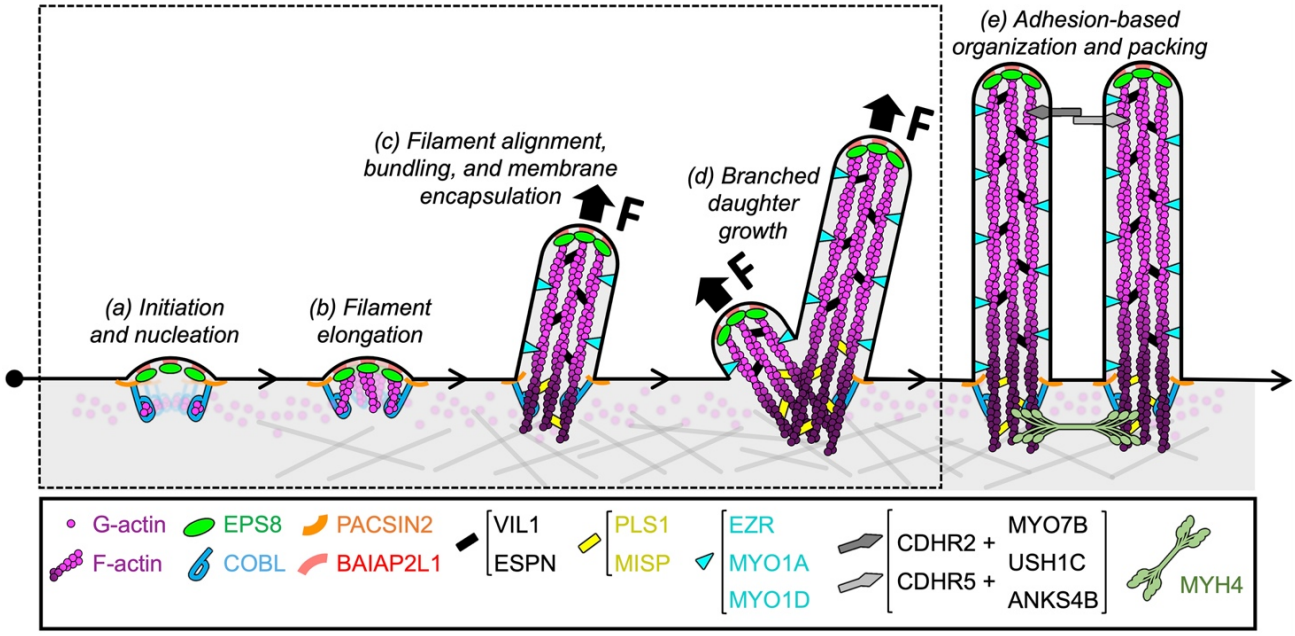

Figure 1-10. Model of microvilli biogenesis

(A) Sites of microvillus growth are marked by discrete puncta containing EPS8 and BAIAPP2L1. As the only actin nucleator identified in microvilli thus far, COBL might play a role in generating actin filaments *de novo*.

(B) A complex of EPS8/BAIAP2L1 drives the elongation of core bundle filaments.

(C) Filament alignment could be promoted by EPS8 together with bundling activities of MISP, fimbrin (PLS1), villin (VIL1), and espin (ESPN). Membrane encapsulation of the core actin bundle is orchestrated by the membrane-cytoskeleton linking factors ezrin (EZR), myosin-1a (MYO1A), and myosin-1d (MYO1D), and this coincides with core bundle elongation.

(D) In addition to de novo growth, a nascent microvillus can also give rise to a daughter microvillus laterally in a process that takes advantage of recycled EPS8 and BAIAP2L1.

(E) Microvilli packing is driven by the intermicrovillar adhesion complex, which consists of protocadherins CDHR2 and CDHR5, the actin-based motor, myosin-7b (MYO7B) and scaffold proteins, USH1C and ANKS4B. Microvillar rootlet ends are interconnected by non-muscle myosin-2 (MYH4). Steps highlighted by the dashed box denote events that have being less explored microvilli assembly. Adapted from (Morales et al., 2023).

MISP: The elusive actin-binding factor in microvilli

C19orf21, a 75 kDa protein, was originally discovered in a proteomic study using nuclear matrix fractions (Hirano et al., 2009; Ishii et al., 2008). Functional characterization studies later revealed that C19orf21 is an actin-binding protein that localizes to the cell cortex and promotes spindle/chromosome orientation during cell division, and thus was named Mitotic Spindle Positioning (Maier et al., 2013; Zhu et al., 2013). In this context, MISP orients the mitotic spindle by stabilizing its astral microtubules, which are projected toward the cell cortex. MISP indirectly engages with astral microtubules, presumably as a result of its ability to directly interact with end-specific factors of microtubules (i.e., EB1, $p150^{glued}$ and the dynamin/dynactin complex) (Zhu et al., 2013). Moreover, MISP has been also found to directly interact with the active form of ezrin *in vitro*, yet they do not seem to fully overlap on the surface of epithelial and non-epithelial cells (Kschonsak & Hoffmann, 2018). Although some studies reported MISP being uniformly distributed at the cell cortex (Maier et al., 2013; Zhu et al., 2013), MISP has also been found at the base of filopodia of growth cones, and in stereocilia of hair cells (Kumeta et al., 2014).

Structural predictions show that MISP is largely disordered (Figure 1-11), which may explain the insolubility of its full-length version in previous purification attempts (Kumeta et al., 2014). Interestingly, biochemical studies found that MISP functions as an actin-bundling protein (Kumeta et al., 2014), harboring at least three actin-binding fragments within its amino acid sequence (169-351 aa; 352-524 aa; 525-680 aa) (Figure 5-5). Furthermore, MISP also harbors multiple phosphorylation sites within its amino acid sequence, some of which are required for MISP function in promoting mitotic progression

(Zhu et al., 2013). Recently, it was found that phosphorylation may also control the ability of MISP to bind and bundle actin filaments *in vitro* (Maarof et al., 2021).

Recent studies have implicated the role of MISP in disease. Using DSS-induced colitis models, one study showed MISP KO mice exhibit loss of intestinal crypts, presumably as a result of reduced proliferation (Hiura et al., 2023). Such phenotype was accompanied by significant weight loss compared to wild-type mice, which was indicative of abnormal brush border function. Another study found that MISP expression levels were upregulated in pancreatic cancer cells, which promoted increased migration and invasion of these cell models *in vitro* (Huang et al., 2022).

In a proteomic analysis of native brush border microvilli, we found peptides corresponding to an “uncharacterized” protein referred to as C19orf21, which coincided with a similar hit our lab obtained in a previous proteomic analysis (McConnell et al., 2011). Human Protein Atlas confirmed that C19orf21/MISP exhibited a strong localization to brush border microvilli in H&E staining (Uhlén et al., 2015), which motivated us to explore its role as an actin-binding factor in brush border microvilli.

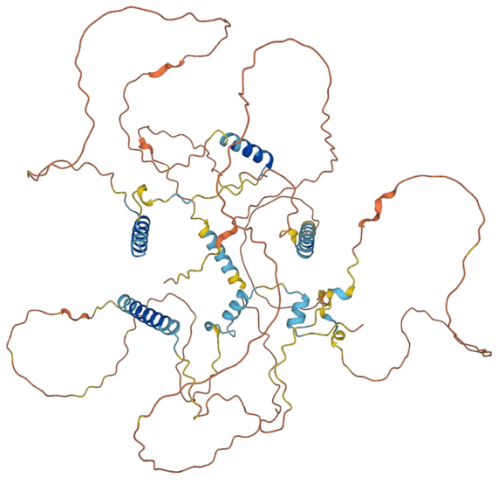

Figure 1-11. Predicted structure of human MISP
Source: AlphaFold (https://alphafold.ebi.ac.uk/entry/Q8IVT2)

Summary

The ability of actin monomers to assemble into polymers allows cells to create architectural networks essential for specific cellular functions. The assembly, maintenance, and recycling of such diverse actin networks are tightly regulated by multiple actin-binding proteins. Among those accessory factors, actin bundlers provide the mechanical stability that shapes these actin networks while maintaining their dynamic nature.

Some remarkable examples of these actin networks are the polarized linear bundles that shape the membrane protrusions that make up filopodia, stereocilia, and microvilli. In the case of microvilli, a study found that triple KO mice for three known actin bundlers were still able to assemble microvilli protrusions (Revenu et al., 2012), invoking the existence of yet-to-be-identify actin bundlers, which may carry out compensatory functions. In this work, we identify Mitotic Spindle Positioning (MISP) as a fourth actin bundling protein of microvilli.

MISP was originally described as an actin-binding protein functioning in the context of cell division (Maier et al., 2013; Zhu et al., 2013). One biochemical study exploring the actin binding function of MISP found that it had bundling potential (Kumeta et al., 2014). Motivated by finding peptides corresponding to MISP in a proteomic analysis of native brush border, we sought to characterize the actin-binding role of MISP at a tissue-, cellular- and single-molecule level.

In Chapter III, we characterized the function and localization of MISP in native intestinal tissue and cell culture models using confocal and structured illumination microscopy. Here, we identified MISP as a new resident of brush border microvilli,

functioning as a bundling protein. Unlike other bundlers, we found that MISP exhibits a selective decoration of the rootlets of microvilli. Moreover, this selective localization of MISP is required for rootlet maintenance and brush border assembly. At the end of this chapter. we showed that the cytoskeleton-membrane crosslinker ezrin is partially responsible for MISP restriction to rootlets.

In Chapter IV, we characterized the biochemical properties of MISP binding to F-actin. Using *in vitro* reconstitution assays and TIRF microscopy, we revealed that MISP displays a preferential association to the pointed ends of aged actin filaments (i.e., ADP F-actin), which are highly enriched in microvillar rootlets. We next found that MISP can assemble multi-filament arrays of antiparallel and parallel bundles. The assembly of such higher-order parallel bundles likely reflects the specific binding of MISP to the pointed ends of filaments.

Taken together, our findings reveal that MISP is confined to rootlets by extrinsic and intrinsic mechanisms, which likely contribute to the assembly and maintenance of the brush border microvilli. Moreover, MISP's selective binding to the pointed ends, along with its bundling capacity sheds light on a potential mechanism to establish the polarity of core actin bundles at early stages of their assembly.

CHAPTER II

MATERIAL AND METHODS

Cell culture

Ls174T-W4 cells (W4; human colon epithelial cancer cells), CACO-2BBE cells (human colorectal adenocarcinoma epithelial cell line), LLC-PK1-Cl4 cells (CL4; pig kidney epithelial cells), HeLa cells (human cervical cancer cell line), and HEK293T cells were cultured in Dulbecco's modified Eagle's (DMEM) medium with high glucose and 2 mM L-glutamine (Corning; 25-005-CI). Ls174T-W4 cells (a generous gift from Dr. Hans Clevers) were grown in media supplemented with 10% tetracyclin-free fetal bovine serum (Atlanta Biological, S10350), 1 mg/ml G418 (Gold Biotechnology; G-418), 10 µg/ml blasticidin (Gold Biotechnology; B-800), and 20 µg/ml phleomycin (InvivoGen; ant-ph-1). For CACO-2BBE cells, the media was supplemented with 20% fetal bovine serum. For LLC-PK1-Cl4, HeLa, and HEK293T cells, the media was supplemented with 10% fetal bovine serum. All cultured cells were grown at 37 °C and 5% CO2.

Cloning and constructs

The full length human MISP sequence harbored in a pCMV-SPORT plasmid (Harvard PlasmID Database; HsCD00326629) was subcloned by PCR and TOPO-cloned into a pCR™8 Gateway entry vector (Invitrogen; 46-0899). In-frame sequence insertion was confirmed by sequencing. MISP was then shuttled into Gateway-adapted plasmids: pEGFP-C1, pmCherry-C1, and pHALO-C1. Similarly, the human beta-actin and UtrCH

sequences were cloned and shuttled into a Gateway adapted HALO-C1 plasmid. To create lentiviral expression vectors, the human MISP sequence was subcloned by PCR and inserted into a puromycin-resistant pLVX1-EGFP backbone by restriction enzyme digestion using XhoI and BamHI. The human fimbrin and villin sequences were cloned into a pEGFP-C1 plasmid (Clontech; 6084-1). The pEGFP-N1 construct harboring the human ezrin sequence was purchased from Addgene, plasmid# 20680. The pEGFP-C1-espin (rat small espin) was a generous gift from Dr. Jim Bartles. To create baculovirus expression vectors, the MISP and EGFP-MISP sequences were subcloned into modified pFastBac-6xHis-MBP LIC expression vector (Addgene; plasmid #30116). All constructs were confirmed by sequencing.

Transfection and lentivirus production

For overexpression experiments except in Figure 3-4 G, cells were transfected using Lipofectamine2000 (Invitrogen; 11668019) according to the manufacturer's instructions. For stable overexpression experiments in Figure 3-4 G, cells were transduced with lentiviral particles expressing pLVX-EGFP or pLVX-EGFP-MISP. For KD experiments, cells were transduced with lentiviral particles expressing PLKO.1 scramble control and MISP-targeted shRNA plasmids (Sigma-Aldrich; TRCN0000422523, TRCN0000116527). For both stable overexpression and KD experiments, lentiviral particles were generated by transfecting HEK293T cells with 6 μg of the corresponding lentiviral expression vector alluded to above, 4 μg psPAX2 packing plasmid (Addgene, 12260), and 0.8 μg pMD2.G envelope plasmid (Addgene; #12259) using FuGENE 6 (Promega; E2691). Lentiviral particles were harvested and concentrated using a Lenti-X

Concentrator (Clontech; 631231). Concentrated lentiviral particles were supplemented with polybrene (Sigma-Aldrich; H9268) and incubated with W4 cells at 80% confluency. After 24 hours, the media was replaced with fresh media containing puromycin (Gold Biotechnology; P-600-100) for selection. Selection was applied for 14 days, replacing with fresh selection media every other day. For KD experiments, rescue assays were conducted using an EGFP-MISP construct designed to be refractory to shRNA KD.

Tissue immunostaining

Frozen tissue sections were washed with 1X PBS and blocked with 5% Normal Goat Serum (Abcam; ab7481) for 2h at room temperature. Sections were washed and incubated with primary antibodies overnight at 4 °C. Primary antibodies used were rabbit anti-MISP (Thermo Scientific; PA5-61995), or rabbit anti-Cofilin (Sigma; C8736). Tissue sections were then washed with 1X PBS and incubated with Alexa-Fluor-568 Phalloidin (Invitrogen; A12380), Wheat German Agglutinin (WGA) 405M (Biotium; 29028-1), and F(ab')2-goat ant-rabbit IgG Alexa-Fluor-488 (Molecular probes; A11070) for 2 h at room temperature. Tissue sections were washed with 1X PBS and mounted in ProLong Gold (Invitrogen; P36930).

Cell immunostaining

Cells grown on a glass coverlips were fixed with 4% paraformaldehyde (EMS; 15710) in 1X PBS for 15 minutes at 37 °C. Fixed cells were washed with 1X PBS, and permeabilized with 0.1% Triton X-100 in 1X PBS for 15 minutes at room temperature. Cells were washed with 1X PBS and blocked with 5% Bovine Serum Albumin (BSA) in 1X PBS for 2 hours

at room temperature. Cells were washed and incubated with primary antibodies overnight at 4 °C. Primary antibodies used were anti-MISP (Thermo Scientific; PA5-61995), anti-villin (Santa Cruz; sc-66022), anti-ezrin (CST; 3145). Cells were washed with 1X PBS four times for 5 minutes and incubate with secondary antibodies. Goat anti-rabbit Alexa Fluor 488 F(ab')2 Fragment (Molecular Probes; A11070), goat anti-mouse Alexa Fluor 568 F(ab')2 Fragment (Molecular Probes; A11019), Alexa Fluor 568-phalloidin (Invitrogen; A12380), Wheat Germ Agglutinin 405M (WGA) (Biotium; 29028-1), DRAQ5 (Thermo Scientific; 62251). Cells were washed again with 1X PBS and mounted on glass slides using ProLong Gold (Invitrogen; P36930).

Western blot analysis

Cell lysates were prepared using RIPA buffer (Sigma-Aldrich; R0278) supplemented with protease inhibitors (Roche; 04693124001). Samples were centrifuged at 20,000 x g for 15 minutes to remove cell debris. The resulting supernatant was boiled with Laemmli sample buffer for 5 minutes. Samples were then loaded on a 4-12% NuPAGE gradient gel (Invitrogen; NP0322BOX). Gels were transferred onto a nitrocellulose membrane at 30V for 18 hours. Membranes were blocked with 5% dry milk diluted in 1X PBS containing 0.1% Tween-20 (PBS-T) for 2 hours at room temperature. The membranes were incubated with primary antibody diluted in 1X PBS-T containing 1% BSA overnight at 4°C. Primary antibodies used were anti-MISP (Thermo Scientific; PA5-61995), anti-villin (Santa Cruz; sc-66022), anti-GAPDH (Cell Signaling; 2118), anti-β-actin (Sigma-Aldrich; A5316). Membranes were then washed with 1X PBS-T and incubated with secondary antibodies for 1 hour at room temperature. Secondary antibodies used were IRdye 800

donkey anti-rabbit (LI-COR; 926-32213) or donkey anti-mouse (LI-COR; 926-32212). Membranes were washed with 1X PBS-T and imaged using the Odyssey CLx infrared scanner (LI-COR). Images were processed using the FIJI software (NIH). Protein expression levels were normalized to GAPDH.

Confocal and super-resolution microscopy, and image processing

Laser scanning confocal imaging was conducted using Nikon A1 Microscope equipped with 405, 488, 561 and 645 nm LASERs, Apo TIRF 100x/1.45 NA, Plan Apo 60x/1.4 NA, Plan Fluor ELWD 40x/0.6 NA objectives. Live-cell imaging was conducted using a Nikon Ti2 Eclipse equipped with 488, 561 and 645 nm excitation LASERs, Apo TIRF 100x/1.49 NA and Plan Fluor 40x/1.3 NA objectives, a Hamamatsu X1 spinning disk, and Photometrics Prime 95B sCMOS or Hamamatsu Orca-Fusion BT sCMOS cameras. FRAP was also conducted using a Bruker mini-scanner module capable of producing ROI specific 405 nm photo-stimulation. Images were deconvolved and/or denoised using Nikon Elements software. Super-resolution imaging was performed using a Nikon Structured Illumination Microscope (N-SIM) equipped with 405, 488, 561 and 640 nm LASERs, an SR Apo TIRF 100x/1.49 NA objective, and an Andor iXon Ultra DU-897 EMCCD camera. Images were reconstructed using Nikon Elements software. For imaging in all microscope modalities, gain was matched between samples during image acquisition.

TIRF microscopy and image processing

Total Internal Reflection Fluorescence (TIRF) and Laser Scanning Confocal microscopy imaging were conducted using the Nikon A1 Microscope equipped with 405, 488, 561 nm LASERs, Apo TIRF 100x/1.45 NA objective, and an Evolve EMCCD camera for the TIRF modality (Photometrics Technology). Images were denoised using Nikon Elements software for images shown in Figures 4-3, 4-4, 4-5, 4-7. During imaging acquisition, the gain was matched between samples for comparison.

Transmission electron microscopy

To prepare MISP/F-actin mixtures for electron microscopy (EM), F-actin was prepared as previously described. Phalloidin-stabilized F-actin was incubated with or without purified MISP at a 5:1 molar ratio overnight at 4 °C. Carbon-coated copper grids (EMS; cat# CF300-Cu) were glow discharged and coated with 0.1% poly-lysine solution for 15 min and washed 2 times with ddH2O to remove free poly-lysine. Samples were incubated with the grids for 15 min, briefly washed with ddH2O, and negative stained with 2% uranyl acetate. Images were collected on a FEI Tecnai T-12 transmission electron microscope operating at 100 kV using an AMT CMOS camera.

Protein purification

6xHis-MBP-MISP and 6xHis-EGFP-MBP-MISP constructs were expressed in Sf9 insect cells. Insect cell pellets were resuspended in lysis buffer (20 mM Tris HCl, 0.3 M KCl, 10 mM imidazole, 10% glycerol, 2 mM DTT, pH 7.5) supplemented with protease inhibitors (Roche, 5892953001). Resuspended samples were lysed using a Dounce homogenizer

and passed through an 18-gauge needle to shear DNA. The resultant lysate was then centrifuged at 35,000 rpm in a Ti 50.2 rotor (Beckman) for 30 minutes at 4 °C. Clarified lysates were then filtered using a 0.45 µm syringe filter. Samples were then loaded into a HisTrap column according to the manufacturer protocol and eluted with a 50-500 mM linear imidazole gradient (pH 7.5). Protein purity was assessed by SDS-PAGE. Eluted protein was concentrated using a centrifugal filter (Millipore; UFC803024). For *in vitro* EM experiments, the 6xHis-MBP tag was cleaved from 6xHis-MBP-MISP using a TEV protease (NEB; P8112) for 1 hour at room temperature. The cleaved 6xHis-MBP tag was removed by incubating the solution with Ni-NTA magnetic beads (NEB; S1423) for 1 hour at 4 °C. The solution was then placed in a magnetic rack to separate the bead-bound 6xHis-MBP fraction from MISP. The purified full length MISP was run in an SDS-PAGE gel to confirm successful cleavage.

Actin co-sedimentation assays

Rabbit skeletal G-actin (Cytoskeleton Inc., AKL99) was resuspended according to manufacturer instructions. Resuspended G-actin were centrifuged at 100,000 x g to remove aggregated monomers. G-actin was then polymerized according to the manufacturer instruction. For low-speed sedimentation assays, F-actin was stabilized with phalloidin (Sigma-Aldrich, A22287), and centrifuged at 20,000 x g to precipitate nonspecific aggregates. F-actin (5 µM) was incubated with increasing concentrations of 6xHis-MBP-MISP (0–5 µM) for 15 minutes at room temperature. Subsequently, all MISP/F-actin sample series were centrifuged at 10,000 x g for 20 minutes at room temperature. For high-speed sedimentation assays, MBP-MISP (0.5 µM) was incubated

with increasing concentrations of non-stabilized F-actin (0 - 10 μM) for 2 hours at 4 °C. Subsequently, all MISP/F-actin sample series were centrifuge at 100,000 x g for 30 minutes at 4 °C. In low- and high-sedimentation assays, the supernatant was carefully removed without disrupting the pellet. Both supernatant and pellet fractions were boiled with samples buffer and run into a 4-12% NuPAGE gradient gel (Invitrogen, NP0322BOX). Gels were stained with Coomassie blue (Bio-Rad, 1610786) and imaged in a gel imaging system (Bio-Rad, Gel Doc™ EZ System).

In vitro reconstitution assays

Coverslip functionalization. Coverslips (Thorlabs, CG15KH) were placed into a glass jar, bathed in acetone for 30 minutes, incubated in ethanol for 15 minutes, and washed in MiliQ water three times. Subsequently, the coverslips were sonicated in 2% Hellmanex or 2% Micro90 for 2 hours at room temperature in a water bath sonicator, followed by series of washes in MiliQ water. Coverslips were then transferred into a 0.1 M KOH bath, incubated for 30 minutes, washed in MiliQ water and dried with clean nitrogen gas. For functionalization, coverslips were submerged in a glass jar containing mPEG-Silane (Laysan Bio Inc, MPEG-SIL-5000) or Biotin-mPEG-Silane (Laysan Bio inc, Biotin-PEG-SIL-5K) solution, and protected from light for 18 hours. The next day, coverslips were washed with clean ethanol and MiliQ water. Finally, coverslips were dried once again with clean nitrogen gas and stored at 4 °C for up to two weeks.

TIRF flow channel preparation. Strips of double-sided tape were placed along the length of the functionalized side of a coverslip leaving a gap of approximately 2-3 mm

between each strip. Flow channels were made by placing the coverslip/tape strips on a clean glass slide. The flow channels were subsequently sealed by gently pressing the areas with tape in between glass sides, and stored at 4°C. Before each experiment, the flow channels were washed with high salt (50 mM Tris-HCl pH 7.5, 600 mM KCl, 1% BSA) and low salt (50 mM Tris-HCl pH 7.5, 150 mM KCl, 1% BSA) buffers, blocked with 1X TBSA (50 mM Tris-HCl pH 7.5, 50 mM KCl, 1% BSA) for 5 minutes, and coated with 0.1 – 1 µg/ml streptavidin (SIGMA, 189730) for 5 minutes.

Actin preparation. Rhodamine-actin (Cytoskeleton, AR05), biotin-actin (Cytoskeleton, AB07), and black actin (Cytoskeleton, AKL99) were resuspended in G-actin buffer (5 mM Tris-HCl, pH 8.0; 0.2 mM $CaCl_2$) supplemented with 0.2 mM ATP (SIGMA, 10519979001) and mixed at a final ratio of 20:1:79, respectively. Alternatively, G-buffer was supplemented with 0.2 mM AMP-PNP (SIGMA, A2647) to prepare non-hydrolysable ATP-bound filaments. Subsequently, the resulting G-actin mix was ultracentrifuged at 90K rpm for 30 minutes at 4°C in an ultracentrifuge (Beckman, Optima TL 100) to remove actin oligomers and/or aggregates.

MISP binding on immobilized F-actin*.* G-actin was mixed with TIRF polymerization buffer (50 mM KCl, 1 mM $MgCl_2$, 1 mM EGTA, 10 mM Imidazole pH 7.0, 50 mM DTT, 0.2 mM ATP, 15 mM Glucose, 0.5% Methylcellulose, 1X Oxyrase, 0.1% BSA), and flowed in through a streptavidin-coated flow channel at a final concentration of 500 nM. At this concentration, actin is expected to polymerize exclusively from the barbed ends while the pointed ends depolymerize very slowly. Once the polarity of filaments was determined as

evidenced by the exclusive and rapid elongation from barbed ends, EGFP-MISP molecules were flowed in at a final concentration of 12.5 nM, and its binding position relative to the filament was monitored over time.

MISP-driven anchoring of F-actin. Biotin-anti-6xHis antibodies (SIGMA, MA1-21315-BTIN) were flowed in through a streptavidin-coated flow channel. Subsequently, EGFP-MISP molecules (harboring a 6xHis tag at the N-terminus) were flowed in at a final concentration of 12.5 nM, incubated for 5 minutes to allow for their immobilization. To monitor short filament capturing events, G-actin (500 nM) was mixed with TIRF polymerization buffer and polymerize for approximately 5 minutes before flowing in the reaction through the MISP-immobilized flow channel.

Preparation of ADP, ADP-Pi, and ATP-like F-actin

F-Actin was generated as described earlier but was stabilized with unlabeled phalloidin (ThermoFisher, P3457) to allow for dilution below the critical concentration (< 100 nM). Phalloidin was also added at different time points of polymerization to generate F-actin in the ADP and ADP-Pi state as previously described (Zimmermann et al., 2015). To note, phalloidin was included in all buffers throughout these assays to maintain the nucleotide state of filaments, especially in the case of the ADP-Pi condition.

ADP F-actin phalloidin stabilized. Rhodamine-biotin G-actin (1 µM) was polymerized at room temperature, and phalloidin (2 µM) was added at a 2:1 molar ratio. F-actin was further aged for 24 hours before conducting assays.

ADP-Pi F-actin phalloidin stabilized. Rhodamine-biotin G-actin (1 μM) was polymerized at room temperature in the presence of phalloidin (2 μM) at a 2:1 molar ratio, and used within the next 24 hours of preparation.

AMP-PNP F-actin phalloidin stabilized. Rhodamine-biotin G-actin (1 μM) was polymerized at room temperature in the presence of the nucleotide analog AMP-PNP (0.2 mM) and phalloidin (2 μM) at a 2:1 molar ratio, and used within the next 48 hours of preparation.

In all experiments, all different versions of actin filaments were flowed in into the TIRF channel, washed with TIRF buffer. Subsequently, EGFP-MISP in TIRF buffer was flowed in into the TIRF channel as imaging was in progress to determine dwell times.

Quantification

All images were process and analyzed using Nikon Elements software or FIJI software package (https://fiji.sc). Time series volumes from live imaging experiments were registered using the StackReg plugin in FIJI as needed.

***Analysis of signal intensity in intestinal tissue samples*.** To measure signal intensities along microvilli, a 1-pixel-wide line scans were drawn along the base-tip axis of BB. To measure signal intensities in the BB along the crypt-villus axis, an ROI containing the BB was drawn and straightened using the Straighten plugin in FIJI; average intensities were

calculated across the resulting rectangle. All intensity values were normalized from 0 (base) to 1 (tip) and fit to a Gaussian curve using PRISM v. 9.0.

***Analysis of BB assembly in W4 cells*.** To quantify the percentage of W4 cells capable of forming BBs, cells exhibiting a single polarized cap of F-actin (representing a BB) were counted manually. For rescue experiments, only W4 cells expressing an EGFP-MISP refractory construct were scored. To quantify the overall actin intensity in W4 cells, multiple ROIs containing single cells were generated using Nikon Elements software, and F-actin intensities measured in each ROI.

***Measuring the lengths of microvilli and rootlets in W4 cells*.** For the purposes of quantification throughout the paper, we define a microvillus as the segment of a core bundle that is wrapped in plasma membrane, and 'rootlet' as the segment that is free of membrane wrapping. Microvilli and rootlet lengths were measured separately using a membrane marker to delineate the boundary of these regions. To calculate membrane coverage (i.e. fraction of the core bundle wrapped in membrane), we summed the average lengths of microvilli and rootlets per cell to obtain a total core bundle length. We then calculated membrane coverage as the ratio of average microvilli length to total core bundle length.

***Inter-filament spacing*.** To quantify the spacing between MISP-bundled actin filaments, EM images were process using the FFT bandpass filter in FIJI. We used image filtering to remove small structures down to 10 pixels (5 nm) and large structures up to 100 pixels (50 nm). Line scans were then drawn perpendicular to tightly packed actin filaments,

signal intensity was plotted, and the distance between peaks was measured. For control conditions, actin bundles with an inter-filament spacing of less than 20 nm were considered for quantification and processed as described above.

***FRAP analysis*.** ROIs of similar area were drawn over the microvilli and rootlets of W4 cells, and bleached using a 405 nm LASER steered with a Bruker mini-scanner. Cells were imaged for 30 seconds before photobleaching, bleached over the course of 5 sec, and then imaged every 10 sec for 30 min to capture signal recovery dynamics. All intensity values for each condition were normalized from 0 to 1 and plotted together to facilitate comparison. Average values for each condition were fit using two-phase association curves.

***Microvilli and rootlet assembly in W4 cells*.** To quantify the intensity of actin turnover in the microvilli and rootlets in W4 cells overexpressing mCherry-MISP, EGFP-fimbrin and HALO-β-actin, we drew ROIs delimiting these domains in the β-actin channel. As cells were not synchronized in their differentiation following doxycycline addition, in each cell we set '0' as the time frame where the β-actin signal in the rootlet domain increased above background.

***Ezrin inhibition in W4 cells*.** To quantify MISP enrichment to the BB upon ezrin inhibition in W4 cells overexpressing mCherry-MISP, ezrin-EGFP, and HALO-UtrCH, we drew ROI containing the BB in the β-actin channel. As the effect of NSC668394 on ezrin inhibition from the BB was not synchronized across cells, we arbitrarily set the time point '0' as 9

frames (22.5 minutes) before ezrin signal dropped below background. All intensity values for each condition were normalized from 0 to 1 and plotted together to facilitate comparison.

***MISP dwell time on phalloidin-stabilized F-actin*.** Line scans were drawn along movies of actin filaments longer than 2 μm and converted into kymographs. From these kymographs, the dwell time of multiple MISP binding events along the filament were measured and plotted in a histogram. Only finite MISP dwell times were considered for fitting purposes.

MISP binding on polymerizing F-actin. The distribution of MISP binding events on filaments were calculated as follows: A single MISP binding event was considered positive if it remained stably bound to a single actin filament longer than 8 frames (i.e., 70 seconds). A line scan was drawn along the corresponding filament in the first frame of MISP binding to determine the filament length. The maximum MISP peak intensity was used as a reference point to determine its “distance from the pointed ends”.

***MISP apparent association rates*.** Rectangular ROIs (2 x 1.2 μm) were drawn along immobilized filaments (50 nM), which were used to measure EGFP-MISP (50 nM) fluorescence intensity over time. Intensity values were plotted and fitted with an exponential curve to estimate the apparent association rates.

***MISP-driven anchoring of single actin filaments*.** Anchoring events refer to events where a single polymerizing filament was immobilized by a single MISP puncta. A “pointed end anchoring event” was considered positive when the captured filament kept polymerizing from the opposite free end. A “barbed end anchoring event” was considered positive when the filament kept polymerizing from the captured end. Events that did not meet these criteria were considered as “side capturing events”.

***MISP-driven bundling of two actin filaments*.** We manually quantified the number of MISP-driven bundling events of two filaments by observing the direction of their growth before or after they overlapped. If filaments were already overlapping, their direction of growth was evident by the increase in the intensity of two filaments compared to one filament. To quantify the intensity of EGFP-MISP, we drew 0.5μm x 2-pixel lines scans along 1- and 2- filaments at multiple time points. Values were then arbitrarily normalized to generate the plot.

Statistical analysis

Statistical significance was performed using the unpaired T-test for pairwise comparison. Statistical correlation was conducted using the Pearson correlation coefficient for colocalization analysis. All statistical analysis was computed in PRISM v. 9.0. (GraphPad).

CHAPTER III

MITOTIC SPINDLE POSITIONING (MISP) IS AN ACTIN BUNDLER THAT SELECTIVELY STABILIZES THE ROOTLETS OF EPITHELIAL MICROVILLI

Originally published as:
Morales, E. A., Arnaiz, C., Krystofiak, E. S., Zanic, M., & Tyska, M. J. (2022). Mitotic Spindle Positioning (MISP) is an actin bundler that selectively stabilizes the rootlets of epithelial microvilli. Cell reports, 39(3), 110692.

Summary

Microvilli are conserved actin-based surface protrusions that have been repurposed throughout evolution to fulfill diverse cell functions. In the case of transporting epithelia, microvilli are supported by a core of actin filaments bundled in parallel by villin, fimbrin, and espin. Remarkably, microvilli biogenesis persists in mice lacking all three of these factors, suggesting the existence of unknown bundlers. We identified Mitotic Spindle Positioning (MISP) as an actin binding factor that localizes specifically to the rootlet end of the microvillus. MISP promotes rootlet elongation in cells, and purified MISP exhibits potent filament bundling activity *in vitro*. MISP-bundled filaments also recruit fimbrin, which further elongates and stabilizes bundles. MISP confinement to the rootlet is enforced by ezrin, which prevents decoration of the membrane-wrapped distal end of the core bundle. These discoveries reveal how epithelial cells optimize apical membrane surface area and offer insight on the remarkable robustness of microvilli biogenesis.

Introduction

Surface protrusions are essential features that enable cells to interact with the external environment in all domains of life. Choanoflagellates, the closest living relatives of animals, are unicellular eukaryotes that developed one of the earliest known polarized feeding systems consisting of long-lived actin-based protrusions, which we now generally refer to as microvilli (Sebé-Pedrós et al., 2013). Multicellular eukaryotes eventually maximized solute transport by compartmentalizing large numbers of microvilli on the surface of specialized hollow organs (Peña et al., 2016). In animals, striking examples of such organization are found on the apical luminal surface of enterocytes in the small intestine, where densely packed arrays of thousands of microvilli extend from the surface of individual cells, collectively forming the brush border (BB) (Crawley, Mooseker, et al., 2014b). In other specialized cases, arrays of microvilli have been repurposed for diverse functions including sperm recognition in oocytes, mechanosensation in inner ear hair cells, and light detection in photoreceptor cells, among others (Lange, 2011).

An individual microvillus extends from the cell surface as a finger-like membrane protrusion, supported by a core of 20-40 actin filaments bundled in parallel (Mooseker & Tilney, 1975; Ohta et al., 2012). Core actin bundles exhibit lengths on the micron scale and flexural rigidities high enough to deform the enveloping plasma membrane (Atilgan et al., 2006). Previous studies established that at least three bundlers assemble the microvillar core bundle: villin, fimbrin (also known as plastin-1), and espin (Bartles et al., 1998; Bretscher & Weber, 1979, 1980b). Villin is the first bundler recruited apically during BB differentiation, followed by fimbrin, and espin (Bartles et al., 1998; Ezzell et al., 1989). Single villin or espin knockout (KO) mice exhibit near-normal microvillar morphology and

organization (Ferrary et al., 1999; Pinson et al., 1998; Revenu et al., 2012). In contrast, fimbrin KO mice exhibit microvilli that are ~15% shorter (Grimm-Günter et al., 2009; Revenu et al., 2012). Remarkably, villin-espin-fimbrin triple KO mice are viable and their enterocytes still assemble apical BBs, although microvillar length is reduced by ~40% (Revenu et al., 2012). This latter finding underscores the remarkable robustness of microvillar growth and further suggests that BB assembly is driven by multiple factors operating in parallel, some of which may remain unidentified.

Within the microvillus, actin filaments that comprise the core bundle are oriented with their barbed ends toward the distal tip and pointed ends extending down into the subapical cytoplasm (Mooseker & Tilney, 1975). The barbed ends are the preferred site of new actin monomer incorporation whereas the pointed ends are the favored site of disassembly (Pollard & Mooseker, 1981). Kinetic differences at the two ends create a system that allows subunits to flux retrograde through the core bundle in a process referred to as ‘treadmilling’ (Kirschner, 1980). Indeed, recent studies with epithelial cell culture models revealed that treadmilling is crucial for microvilli assembly and motility (Gaeta et al., 2021; Meenderink et al., 2019).

While a long segment of the core bundle protrudes from the cell surface enveloped in plasma membrane, a much shorter segment – the ‘rootlet’ – extends down into the subapical cytoplasm. Core bundle rootlets are directly linked to a dense filamentous network called the ‘terminal web’, an organelle-free zone that presumably regulates trafficking to and from the apical plasma membrane (Mooseker et al., 1983). Ultrastructural studies first suggested that rootlets are interconnected with terminal web filaments at least in part by non-muscle myosin-2 and spectrin (Hirokawa et al., 1982).

Deep in the terminal web, rootlets appear to be directly crosslinked with a meshwork of cytokeratins (Hirokawa et al., 1982, 1983). One possible crosslinking factor is the actin bundler fimbrin, which is found along the length of the core bundle with an apparent enrichment on the rootlet (Grimm-Günter et al., 2009). Based on the highly interconnected nature of filaments throughout the terminal web, this network likely serves as a physical platform that offers long-term stability and mechanical support for protruding BB microvilli. Although core bundle rootlets can only interact with the terminal web filaments if they remain free of membrane wrapping, factors that protect the proximal end of the bundle from membrane encapsulation during microvillar growth remain undefined.

Biophysical investigations have also established that the structural stability of microvilli is promoted by tethering core bundles to the surrounding plasma membrane (Nambiar et al., 2010). Core bundles are laterally bridged to their enveloping membrane by myosin-1a and -6, as well as ezrin (Berryman et al., 1993; Hegan et al., 2012; Howe & Mooseker, 1983). Recent studies on the dynamics of growing microvilli revealed that ezrin accumulates in a nascent microvillus in parallel with core bundle elongation, and that loss of ezrin from the protrusion leads to microvillus collapse (Gaeta et al., 2021). Ezrin is a well characterized membrane-cytoskeleton linker that adopts two states: an open ‘active’ state when phosphorylated and a closed ‘inactive’ state when dephosphorylated (Bretscher et al., 1997). Dynamic cycling between these two states allows ezrin to bridge treadmilling actin bundles to the enveloping plasma membrane (Viswanatha et al., 2012), while providing continuous mechanical support for the protrusion. However, mechanisms that constrain ezrin enrichment to the distal segment

of the core bundle and control the extent of membrane wrapping remain poorly understood.

Here we report that Mitotic Spindle Positioning (MISP) is a BB component that targets specifically to the rootlets of microvillar core bundles. Previous studies revealed that MISP is an actin binding and bundling protein that promotes mitotic spindle orientation and mitotic progression (Kumeta et al., 2014; Maier et al., 2013; Zhu et al., 2013), although a role in native tissues has yet to be reported. In intestinal epithelial cells, we found that MISP is enriched in the subapical region beneath the plasma membrane at the base of the BB, where it colocalizes with fimbrin along core bundle rootlets. Loss- and gain-of-function studies revealed that MISP elongates rootlets and limits the extent of membrane wrapping of core bundles. Consistent with these phenotypes, MISP bundles F-actin *in vitro* and in cells, creating structures that are primed for fimbrin recruitment. Overexpression of both factors leads to a striking overgrowth of hyper-stable rootlets from the subapical domain. Further, we found that MISP confinement to microvillar rootlets depends on the presence of active ezrin in the microvillus. Overall, our findings lead to a model for rootlet specification whereby ezrin and MISP exert mutual exclusivity to establish membrane-wrapped vs. unwrapped segments of the core bundle. MISP confinement to rootlets, in turn, recruits fimbrin to further crosslink the proximal ends of core bundles in the terminal web. This work holds important implications for understanding the assembly and stabilization of actin-based protrusions in diverse epithelial systems, and also provides a molecular rationale for the remarkable robustness of BB assembly alluded to in previous multi-gene loss-of-function mouse models (Delacour et al., 2016).

Results

MISP localizes to the rootlets of BB microvilli

In a previous proteomic study, we identified peptides from MISP in BBs isolated from mouse small intestine (McConnell et al., 2011). To validate MISP as a bona fide BB resident and to examine its localization in native tissues at higher resolution, we immunostained paraffin sections of mouse small intestine. Confocal microscopy of stained sections revealed that MISP specifically localizes to the BB along the full length of the crypt-villus axis (Figure 3-1 A). This was consistent with MISP localization to the apical surface of the intestinal epithelium in H&E staining from the Human Protein Atlas (Figure 3-2 A) (Uhlén et al., 2015). Using an anti-villin antibody to label core actin bundles and a membrane marker to delineate the apical surface, we found that MISP is highly enriched in the terminal web and exhibits mutually exclusive labeling with the membrane-wrapped protruding microvilli (Figures 3-1 A and 3-1 B). As previously reported (Dudouet et al., 1987; Robine et al., 1985), we found that villin signal gradually increases along the crypt-villus axis, following the direction of enterocyte migration and differentiation (Figures 3-1 A, 3-1 C and 3-1 D; magenta labels). In contrast, MISP signal remains relatively constant along the crypt-villus axis (Figures 3-1 A, 3-1 C and 3-1 D; green labels), suggesting that this factor is apically targeted independent of differentiation state. We recapitulated this observation in cell culture using CACO-2BBE cells, which differentiate and take on an enterocyte-like phenotype after a prolonged period of confluent culture (Peterson et al., 1993; Peterson & Mooseker, 1993). In this system, MISP was also expressed and localized from early to late stages of microvilli assembly (Figures 3-1 E-G). These staining results are consistent with a previous study showing that MISP targets

apically in 3D CACO-2 cyst cultures (Kschonsak & Hoffmann, 2018). Localization to the actin-rich apical domain is also broadly consistent with staining in non-polarized HeLa cells, where endogenous and overexpressed MISP localize to actin-rich structures (Kumeta et al., 2014; Maier et al., 2013; Zhu et al., 2013). Together, our data indicate MISP is a BB component that is highly enriched in the subapical terminal web throughout the full course of enterocyte differentiation.

Previous work established that MISP holds actin binding and bundling potential (Kumeta et al., 2014). In light of these data and our imaging studies indicating highly specific terminal web enrichment, we next sought to determine if MISP associates with core bundle rootlets at the base of microvilli. To examine this possibility, we turned to LS174T-W4 cells (herein referred to as 'W4 cells'), a human intestinal epithelial cell line engineered to provide switch-like control over BB assembly (Baas et al., 2004). Using super-resolution structural illumination microscopy (SIM), we found that MISP was highly enriched on the rootlet segments of core bundles that extend immediately beneath the apical membrane (Figures 3-1 H and 3-1 I), which was consistent with its localization in mouse intestinal tissue. We also examined the localization of an EGFP-tagged variant of MISP expressed in LLC-PK1-CL4 cells, a pig kidney epithelial cell line that displays individual microvilli extending from the apical surface (Gaeta et al., 2021). In these cultures, we again noted a striking enrichment of MISP on microvillar rootlets, with a signal that was mutually exclusive with the membrane-wrapped protruding microvilli (Figures 3-2 B and 3-2 C). Together, these localization studies in native tissues and cell culture models uniformly indicate that MISP specifically targets to core bundle rootlets and is excluded from the membrane-wrapped segment of the core bundle.

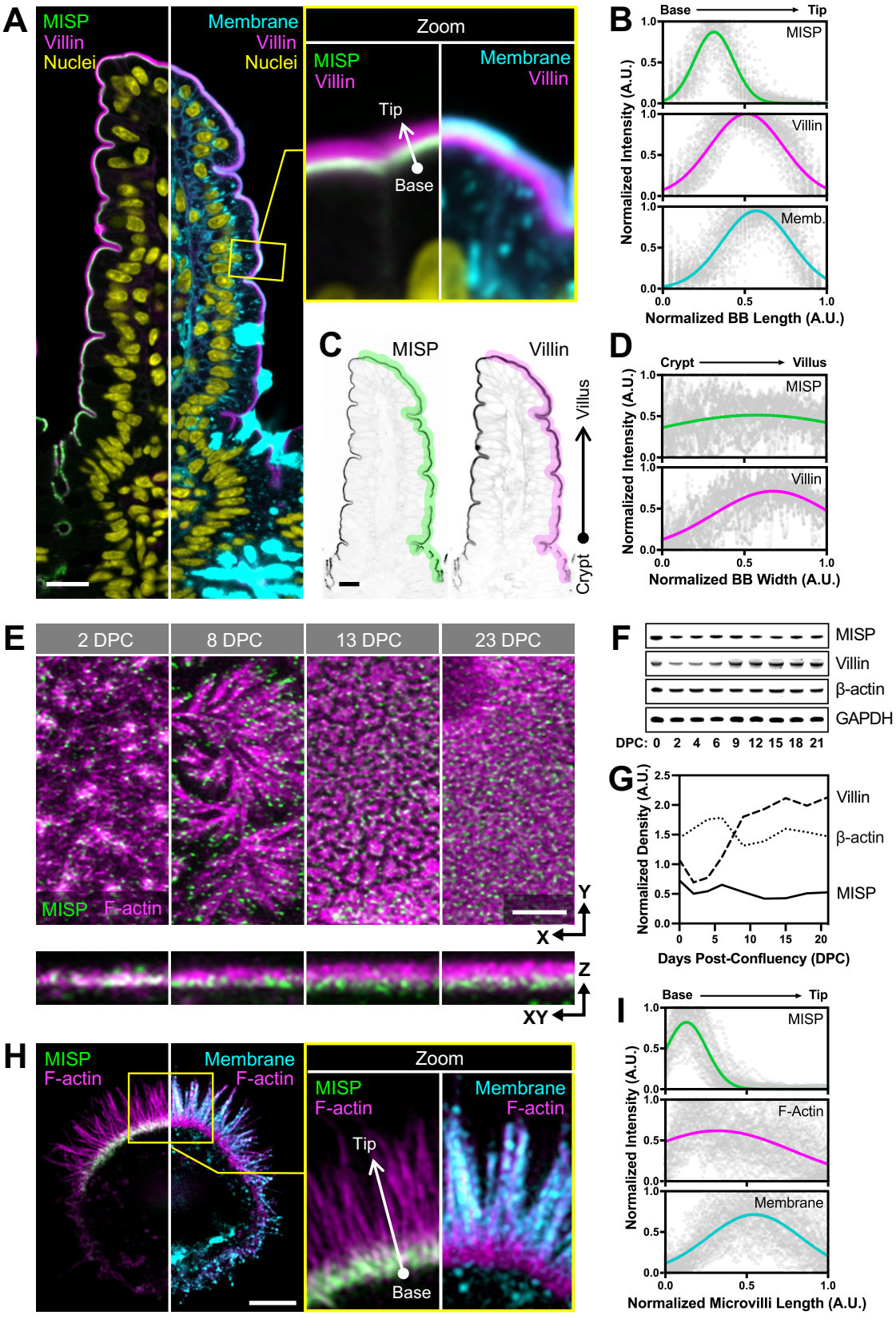
A
MISP
Villin
Nuclei
Membrane
Villin
Nuclei
Zoom
MISP
Villin
Membrane
Villin
Tip
Base
B
Base
Tip
MISP
Villin
Memb.
Normalized Intensity (A.U.)
Normalized BB Length (A.U.)
C
MISP
Villin
Villus
Crypt
D
Crypt
Villus
MISP
Villin
Normalized Intensity (A.U.)
Normalized BB Width (A.U.)
E
2 DPC
8 DPC
13 DPC
23 DPC
MISP
F-actin
Y
X
Z
XY
F
MISP
Villin
β-actin
GAPDH
DPC: 0 2 4 6 9 12 15 18 21
G
Villin
β-actin
MISP
Normalized Density (A.U.)
Days Post-Confluency (DPC)
H
MISP
F-actin
Membrane
F-actin
Zoom
MISP
F-actin
Membrane
F-actin
Tip
Base
I
Base
Tip
MISP
F-Actin
Membrane
Normalized Intensity (A.U.)
Normalized Microvilli Length (A.U.)

Figure 3-1. MISP localizes to microvillar rootlets
(A) Confocal images of small intestinal sections stained for MISP (green), villin (magenta), DNA with DRAQ5 (yellow), and membrane with WGA (cyan). Panel shows a split three-color merge. Scale bar = 15 μm.
(B) Fluorescence intensity distributions of MISP, villin, and apical membrane measured parallel to the microvillar axis as indicated by the white arrow in A; n = 200 line scans measured on five villi.
(C) Inverted MISP and villin channles from A. Scale bar = 15 μm. (D) Fluorescence intensity distribution of MISP and villin measured relative to the crypt-villus axis as indicated by the highlighted area in C; black arrow shows line scan orientation; n = 11 scans of six villi.
(E) Confocal maximum intensity projection (Max IP) of CACO-2BBE cells at different stages of differentiation stained for MISP (green) and F-actin with phalloidin (magenta). Upper panels show XY en face views at the indicated days post-confluency (DPC); bottom panels show resliced XZ views. Scale bar = 3 μm.
(F) Western blot time series of CACO-2BBE cell lysates probed for MISP, villin, β-actin, and GAPDH at the indicated DPC.
(G) Density values of MISP, villin, and β-actin bands from F normalized to GAPDH and plotted as a function of DPC.
(H) SIM Max IP of a W4 cell stained for MISP (green), F-actin with phalloidin (magenta), and membrane with WGA (cyan). Panel shows a split two-color merge. Scale bar = 3 μm.
(I) Fluorescence intensity distributions of MISP, F-actin, and apical membrane from line scans measured parallel to the microvillar axis as indicated by the white arrow in H; n = 58 line scans of single core bundles from 10 cells. All plots B, D and I show Gaussian curve fits of the raw data for each channel.

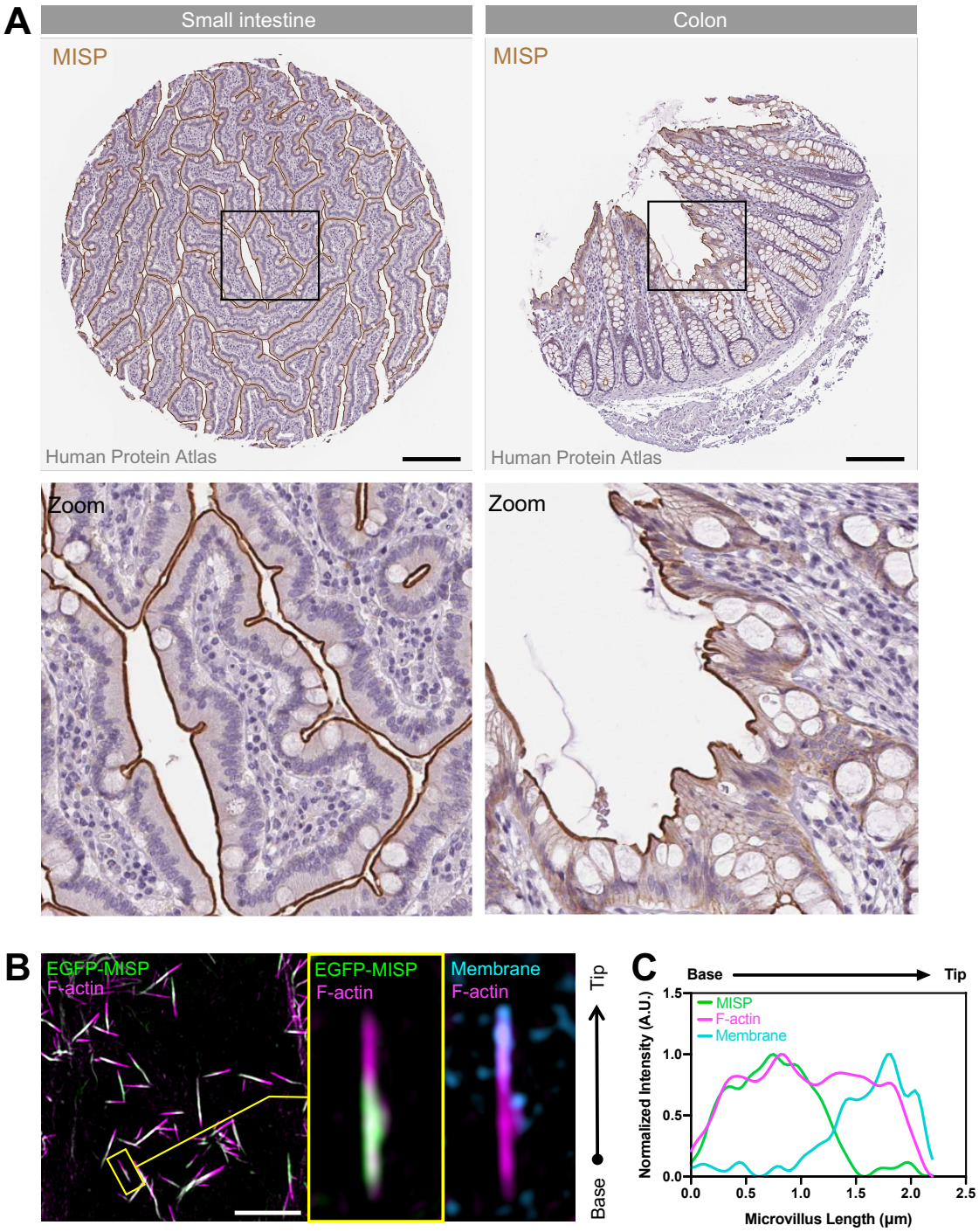

Figure 3-2. MISP localizes to the apical surface of human intestinal tissue and porcine kidney tissue

(A) H&E staining of human small intestine and colon tissue samples stained for MISP (brown) extracted from the Human Protein Atlas. Each panel shows zoomed regions corresponding to the black boxes. Scale bar = 200 μm. Images are available at v21proteinatlas.org and can be found at the following links:

https://images.proteinatlas.org/49511/148888_A_7_2.jpg,
https://images.proteinatlas.org/49511/148888_A_7_3.jpg
(B) SIM maximum intensity projection image of a CL4 overexpressing EGFP-MISP and stained for F-actin with phalloidin (magenta); and membrane with WGA (cyan). The left panel shows merged channels. The right panel shows zoomed images of the yellow box shown in the left panel. Scale bar = 5 μm.
(C) Fluorescence intensity measurements of an individual microvillus shown in the zoomed image from panel B.

MISP is required for maintaining rootlets at the base of microvilli

Core bundle rootlets are anchored in the terminal web, which likely provides mechanical support for BB assembly and long-term stability. To determine if MISP is required for normal BB assembly and microvillar structure, we generated W4 cell lines with stable shRNA-mediated knockdown (KD) of MISP. Loss of MISP was confirmed by Western Blot analysis (Figures 3-3 A and 3-3 B). Using low magnification confocal microscopy, we scored the fraction of cells that were BB positive as indicated by polarized F-actin staining. At a population level, the percentage of W4 cells forming a polarized BB decreased from 82% in the scramble control to 70% in MISP KD cells (Figures 3-4 A and 3-4 B). This modest phenotype was rescued when an EGFP-MISP construct refractory to KD was reintroduced (Figure 3-4 B). However, the overall intensity of F-actin per cell decreased significantly in MISP KD cells (Figure 3-4 C), suggesting a marked perturbation in F-actin network architecture even in cells that still exhibited polarized BB assembly. To further understand the impact of MISP loss-of-function, we look closer at individual MISP KD cells that still formed a polarized BB. Measurements of microvillar dimensions revealed that the overall length of core bundles did not change significantly between scramble control and MISP KD cells (Figure 3-3 C). However, using a membrane marker to

delineate the membrane-wrapped vs. unwrapped segments of the core bundle, we found that the protruding microvillus increased in length (1.96 ± 0.37 μm in controls vs. 2.22 ± 0.39 μm in KD) at the expense of rootlet length, which decreased significantly (0.43 ± 0.09 μm in controls vs. 0.27 ± 0.07 μm in KD; Figures 3-4D and 3-4E). The microvillus/rootlet ratio calculated on a per cell basis increased in MISP KD cells compared to control cells (Figure 3-4 F), and this was consistent with the increased percent membrane coverage measured for MISP KD core bundles (Figure 3-3 D). Thus, rootlet shortening in MISP KD cells is driven by membrane overwrapping of core bundles.

As loss of MISP shortened rootlets and increased membrane wrapping of core bundles, we sought to determine if increasing MISP levels would elongate rootlets at the expense of membrane wrapping. To test this hypothesis, we stably overexpressed EGFP-MISP in W4 cells and examined microvillar structure using SIM. Similar to the localization studies described to above, EGFP-MISP exhibited specific enrichment on microvillar rootlets. Relative to control cells, MISP overexpression promoted a significant elongation of both the membrane-wrapped (2.30 ± 0.48 μm in controls vs. 2.54 ± 0.49 μm in OEx) and rootlet (0.44 ± 0.12 μm in controls vs. 0.61 ± 0.15 μm in OEx) segments of the core bundle (Figures 3-4 G and 3-4 H). These changes together drove a significant increase in the overall length of core bundles, and a slight reduction in percent membrane coverage of total core bundles in MISP-overexpressing cells (Figures 3-3 E and 3-3 F). However, the marked elongation of rootlets decreased the microvillus/rootlet ratio under these conditions (Figure 3-4 I). In combination, these findings show that MISP promotes microvillar rootlet elongation and protects this end of the core bundle from membrane wrapping.

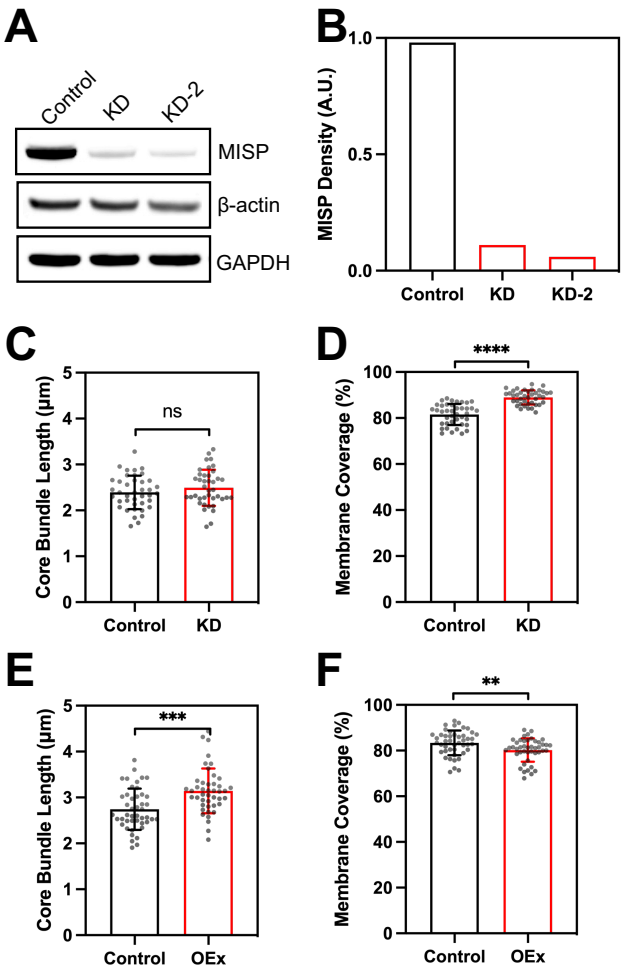

Figure 3-3. MISP KD and OEx regulate the membrane coverage of core actin bundles

(A) Western blot analysis of endogenous MISP in scramble control and MISP KD W4 cells.

(B) Density quantification of MISP bands from western blot shown in A. Densities were normalized to GAPDH.

(C, E) Length measurements of core actin bundles for KD (C) and overexpression (E) conditions described in Figure 3-4 D and 3-4 G, respectively. Each data point represents the average length of > 10 core actin bundles per cell; n ≥ 40 cells per condition. All data points are representative of three independent experiments.

(D, F) Membrane coverage measurements of core actin bundles for KD (D) and overexpression (F) conditions described in Figure 3-4 D and 3-4 G, respectively. Each data point represents the membrane coverage percentage of core actin bundles per cell; n ≥ 40 cells per condition. All data points are representative of three independent experiments. All bar plots and error bars denote mean ± SD. p-values were calculated using the unpaired T-test ('ns': not significant; **: $p < 0.01$; ***: $p < 0.001$; ****: $p < 0.0001$).

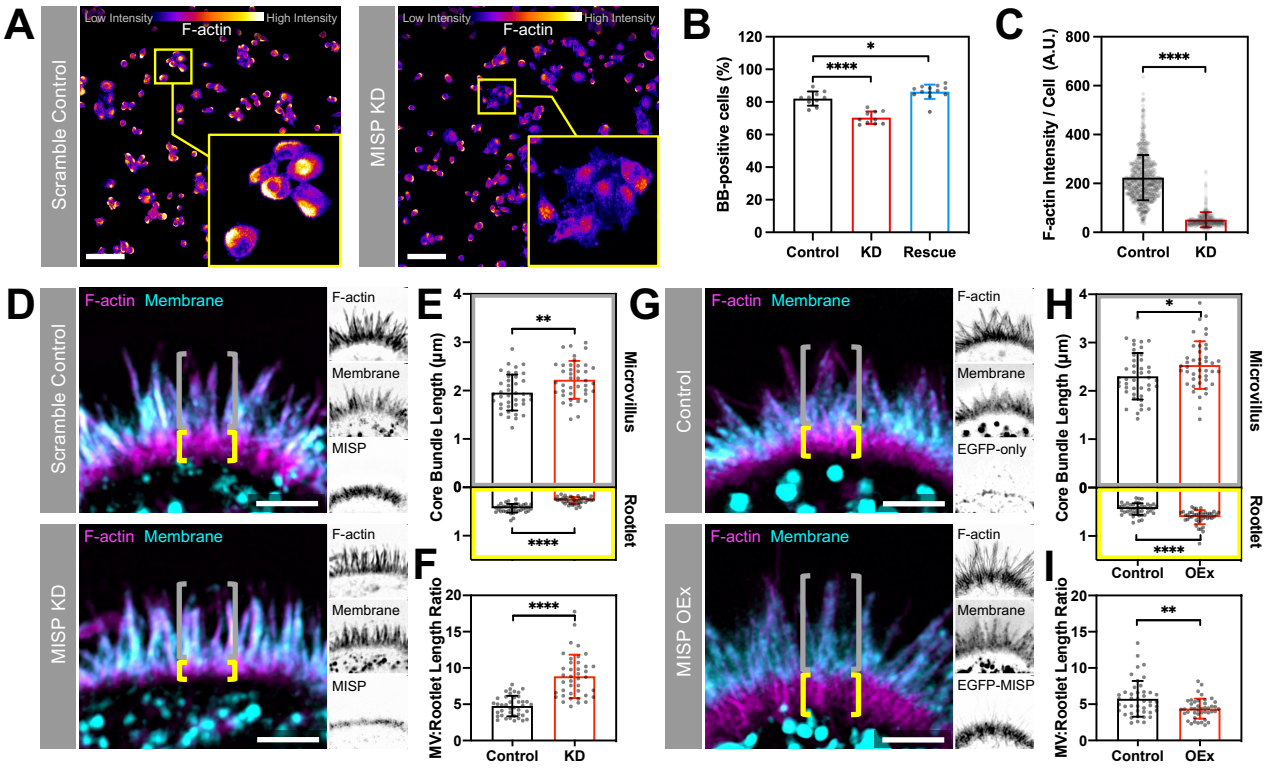

Figure 3-4. MISP is required for maintaining rootlets

(A) Confocal Max IPs of scramble control and MISP knockdown (KD) W4 cells stained for F-actin; intensity color-coded so warmer colors denote higher intensities. Zooms show representative cells for each condition. Scale bar = 100 µm.

(B) Percentage of W4 cells forming BBs (BB-positive cells) from A comparing scramble control, MISP KD, and EGFP-MISP rescue conditions. Each dot represents the percentage of BB-positive cells in a single field of 620 µm2; n ≥ 10 fields per condition.

(C) F-actin intensity values of W4 cells from A. Each dot represents the average F-actin intensity of a single cell; n > 600 cells per condition.

(D) SIM Max IPs of the BB of W4 cells in scramble control (top) and MISP KD (bottom) conditions stained for F-actin (magenta) and membrane (cyan); each panel shows merge with their inverted single channels. Yellow brackets indicate the extension of actin rootlets; gray brackets show the extension of microvilli. Scale bars = 2 µm.

(E) Lengths of microvilli (gray, top plot) and rootlets (yellow, bottom plot) from scramble control and KD cells. Each dot represents the average of > 10 length values per cell; n ≥ 40 cells per condition. All data represent three independent experiments.

(F) Microvillus/rootlet length ratios measured on a per cell basis from E.

(G) SIM Max IPs of the BB of W4 cells in control (top) and MISP overexpressing (bottom) cells stained for F-actin (magenta) and membrane (cyan); each panel shows merge with their inverted single channels. Yellow brackets indicate the extension of actin rootlets; gray brackets show the extension of microvilli.

(H) Lengths of microvilli (gray, top) and rootlets (yellow, bottom) from control and MISP OEx cells. Each dot represents the average of >10 length values per cell; n ≥ 40 cells per condition. All data represent three independent experiments. (I) Microvillus/rootlet length

ratios measured on a per cell basis from H. All bar plots and error bars denote mean ± SD. p-values were calculated using the unpaired T-test (*: $p < 0.05$; **: $p < 0.01$; ****: $p < 0.0001$).

Purified MISP assembles tightly packed linear actin bundles *in vitro*

Based on the terminal web localization of MISP and the impact of MISP perturbation on rootlet length, we sought to determine if purified MISP is sufficient to drive the formation of linear F-actin bundles similar in structure to core bundle rootlets. Full length human MISP was highly insoluble in previous purification attempts and thus far only truncated fragments have been studied *in vitro* (Kumeta et al., 2014). Although MISP's actin binding potential might be distributed throughout the molecule, the C-terminal half of MISP was capable of linking F-actin together in mesh-like networks (Kumeta et al., 2014). To further develop our understanding of MISP's actin binding properties, we sought to express and characterize the activity of full length human MISP. To aid with solubility, we tagged the N-terminus of MISP and EGFP-MISP with maltose-binding protein (MBP) and purified these variants from Sf9 insect cells for further characterization (Figures 3-5 A and 3-5 B). We first confirmed that soluble MBP-MISP was sufficient to sediment F-actin (Figure 3-5 C). Using a low-speed sedimentation assay, we found that MBP-tagged full length MISP robustly bound to and bundled F-actin in a concentration-dependent manner (Figures 3-6 A and 3-6 B). To gain insight on MISP's affinity for actin, we conducted a high-speed sedimentation assay and found that MISP binds to F-actin with a dissociation constant of 0.76 μM (Figures 3-6 C and 3-6 D), which is comparable to other bundlers expressed in epithelial cells (Bartles et al., 1998; Kitajiri et al., 2010). Interestingly, this dissociation constant is also comparable to that reported for the C-terminal half of MISP (a.a. 352-

680), which suggests that this fragment might contribute to most of the binding affinity for F-actin in full length MISP. To directly visualize the impact of MISP on F-actin organization and bundling, we mixed MBP-EGFP-MISP with phalloidin-stabilized F-actin and then examined the resulting structures using confocal microscopy. MISP/F-actin mixtures exhibited extensive bundling and crosslinking of filaments, particularly in regions that were heavily decorated with MBP-EGFP-MISP (Figure 3-6 E; zoom 1). F-actin intensity in bundles was also significantly higher when MISP was present in solution (Figure 3-6 F). Interestingly, MISP accumulated at the ends of some actin bundles where the phalloidin signal was lower (Figures 3-6 E and 3-6 G; red arrowheads in zoom 2). To examine the ultrastructural organization of these samples, we turned to transmission electron microscopy (TEM). We removed the MBP tag using TEV protease to reduce the possibility of functional interference from this moiety before TEM imaging (Figure 3-5 D). In control samples (F-actin alone), TEM images revealed single actin filaments that extended for many microns across the grid surface (Figure 3-6 H; left panels). In contrast, MISP/F-actin mixtures exhibited extensive crosslinking of filaments and the formation of tightly packed linear actin bundles (Figure 3-6 H; right panels). Although the tightly packed, 3D nature of these bundles precluded clear determination of filament polarity in our images, spacing measurements revealed that filaments in these bundles were separated by an average distance of 10.2 ± 2.5 nm (Figure 3-6 I), which is shorter than the distances between filaments bundled by villin or espin (~12 nm), but comparable to the spacing produced by fimbrin (Bartles et al., 1998; Hampton et al., 2008; Matsudaira et al., 1983; Volkmann et al., 2001). Together, these findings demonstrate that MISP is

sufficient to form tightly packed linear actin bundles with an inter-filament spacing similar to that of fimbrin.

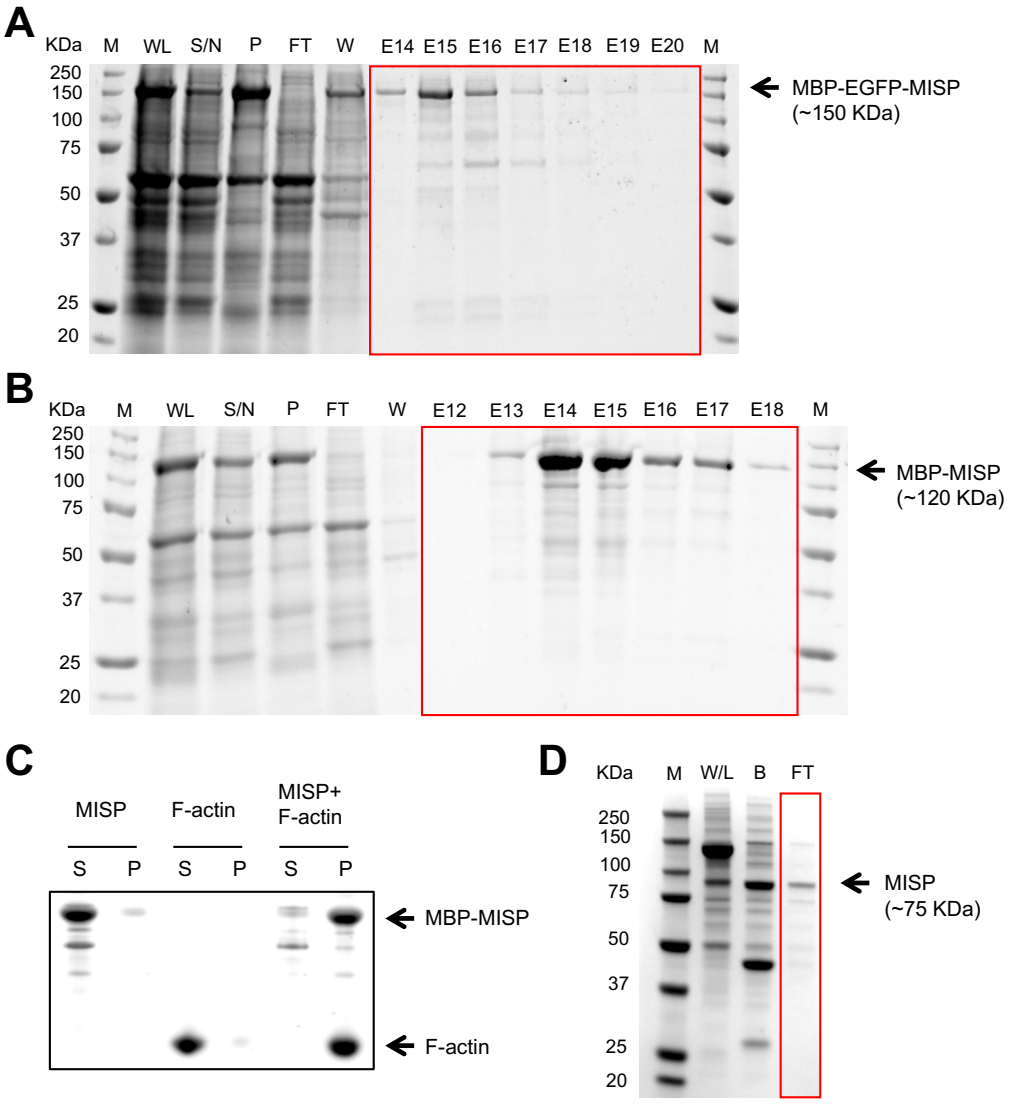

Figure 3-5. MISP purified from Sf9 insect cell lines sediments F-actin
(A-B) Purification of MBP-EGFP-MISP and MBP-MISP from Sf9 insect cells. Coomassie-stained SDS polyacrylamide gel showing all purification steps: whole lysate (WL), supernatant fraction (S/N), pellet fraction (P), flow through (FT), wash (W), and elution (E). 'M' denotes protein ladder marker (10-250 KDa).
(C) Coomassie-stained SDS polyacrylamide gel of low-speed sedimentation of MBP-MISP (1 μM) and F-actin (5 μM) and their corresponding controls.
(D) TEV protease cleavage of purified MBP-MISP. Coomassie-stained SDS polyacrylamide gel showing purification steps: control whole lysate (W/L), fraction bound to beads after TEV cleavage (B), flow through (FT). Purified MISP was recovered from the flow through fraction. 'M' denotes protein ladder marker (10-250 KDa).

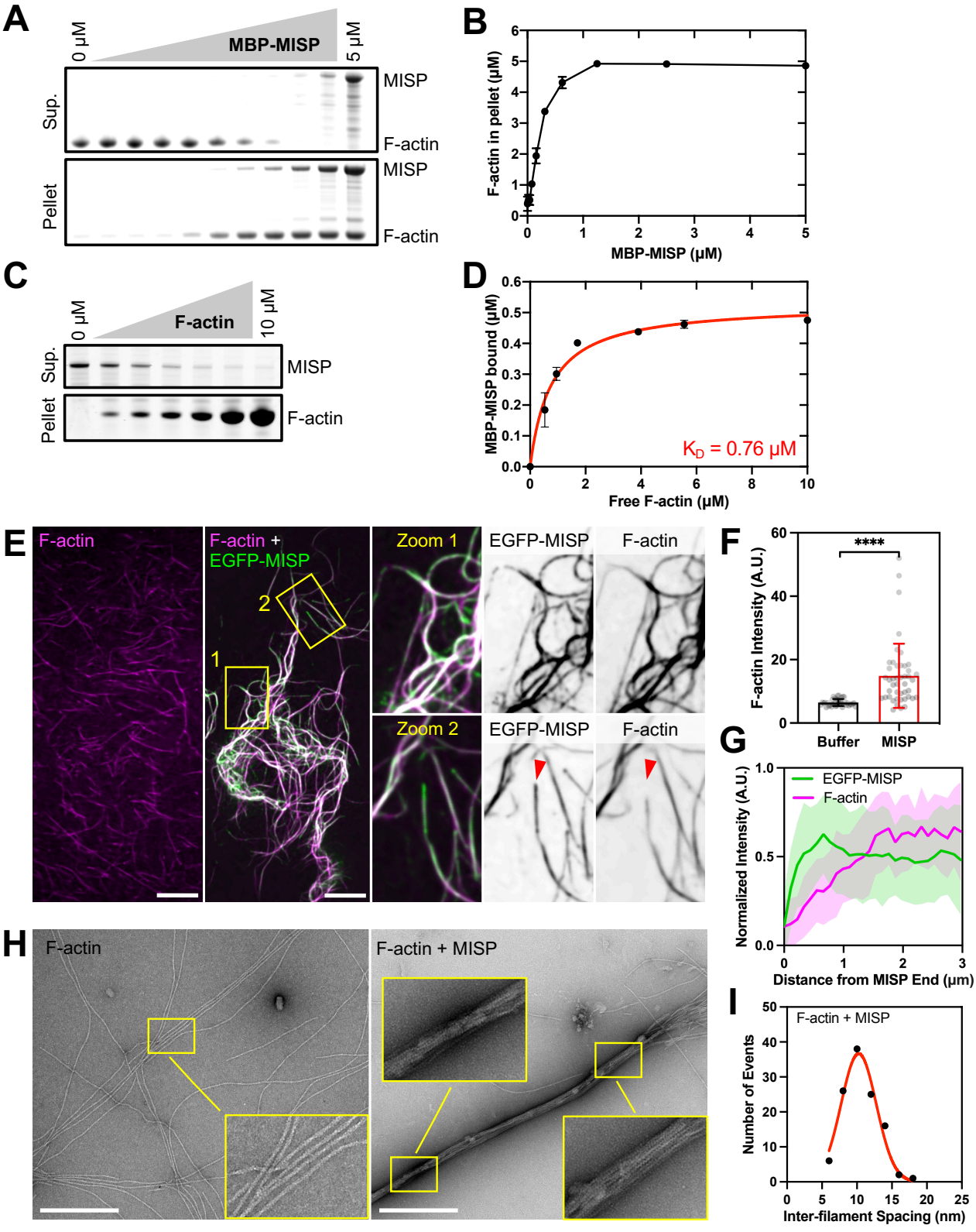
A
0 μM
MBP-MISP
5 μM
Sup.
MISP
F-actin
Pellet
MISP
F-actin
B
F-actin in pellet (μM)
MBP-MISP (μM)
C
0 μM
F-actin
10 μM
Sup.
MISP
Pellet
F-actin
D
MBP-MISP bound (μM)
K_D = 0.76 μM
Free F-actin (μM)
E
F-actin
F-actin + EGFP-MISP
1
2
Zoom 1
EGFP-MISP
F-actin
Zoom 2
EGFP-MISP
F-actin
F
****
F-actin Intensity (A.U.)
Buffer
MISP
G
EGFP-MISP
F-actin
Normalized Intensity (A.U.)
Distance from MISP End (μm)
H
F-actin
F-actin + MISP
I
F-actin + MISP
Number of Events
Inter-filament Spacing (nm)

Figure 3-6. Purified MISP assembles tightly packed linear actin bundles *in vitro*
(A) Low-speed sedimentation assay of phalloidin-stabilized F-actin (5 μM) and increasing concentrations of MBP-MISP (0–5 μM). Coomassie-stained SDS-PAGE shows the supernatant and pellet fractions recovered after centrifugation.
(B) Density quantification of bands shown in A. All data represent three independent experiments. Error bars denote mean ± SD.
(C) High-speed sedimentation assay of MBP-MISP (0.5 μM) and increasing concentrations of non-stabilized F-actin (0–10 μM). Coomassie-stained SDS-PAGE shows the supernatant and pellet fractions recovered after centrifugation.
(D) Density quantification of bands shown in C. All data represent three independent experiments that were fit using a hyperbolic saturation binding model yielding a K_D = 0.76 μM. Error bars denote mean ± SD.
(E) Confocal images of phalloidin-stabilized F-actin (0.5 μM; magenta) alone or pre-mixed with MBP-EGFP-MISP (0.1 μM; green). Zooms correspond to the yellow boxes shown in merge; single channels are shown as inverted images. Red arrowheads indicate the end of MISP-bundled F-actin. Scale bar = 10 μm.
(F) Fluorescence intensities of F-actin in buffer alone or with MISP from E. Each dot represents the integrated intensity value of a 250 μm^2 field; n ≥ 39. Bar plots and error bars denote mean ± SD. p-values were calculated using the unpaired T-test (****: p < 0.0001).
(G) Line scan analysis of EGFP-MISP (green) and F-actin (magenta) intensities measured at bundles ends shown in E.
(H) Transmission electron microscopy images of negatively stained phalloidin-stabilized F-actin (0.2 μM) in buffer alone or pre-mixed with purified MISP (0.04 μM). Scale bar = 400 nm.
(I) Histogram of inter-filament spacing measurements from bundles shown in H. Each dot represents the average of ≥ 110 values; bin size = 2. Average values were fit using a Gaussian curve.

MISP recruits fimbrin to actin bundles

Among the three previously characterized actin bundlers in the BB, fimbrin is the only one that appears to preferentially accumulate on core bundle rootlets, where it might mediate physical interactions with the terminal web cytokeratin network (Grimm-Günter et al., 2009). We therefore sought to determine if MISP binding to F-actin depends on fimbrin, either cooperatively or competitively. To this end, we turned to HeLa cells, which do not typically form microvilli but can assemble a variety of other actin-based networks. Interestingly, mCherry-MISP expression alone promoted the formation of aberrant actin bundles throughout the cytoplasm (Figure 3-7 A; top panel), whereas EGFP-fimbrin expression had little impact on existing actin networks (Figure 3-7 A; middle panel). However, when MISP and fimbrin were co-expressed, fimbrin was robustly recruited to MISP-bundled F-actin (Figure 3-7 A; bottom panel), showing a strong colocalization with MISP (Figure 3-7 B). We conducted similar co-expression experiments using fluorescently tagged versions of villin or espin. Independent of the presence or absence of MISP, villin remained cytosolic (Figure 3-8 A). In contrast, espin promoted the elongation of filopodia-like structures that were reminiscent of microvillar protrusions induced by espin-overexpression in LLC-PK1-CL4 cells (Loomis et al., 2003). Interestingly, in MISP/espin-expressing HeLa cells, MISP enriched at the base of these filopodia-like protrusions, and the aberrant cytosolic bundles observed in MISP only cells were absent (Figure 3-8 B). Overall, these data indicate that MISP promotes the formation of actin bundles, which in turn recruit fimbrin but not villin or espin, and further suggest a hierarchical functioning of these factors during microvillar assembly.

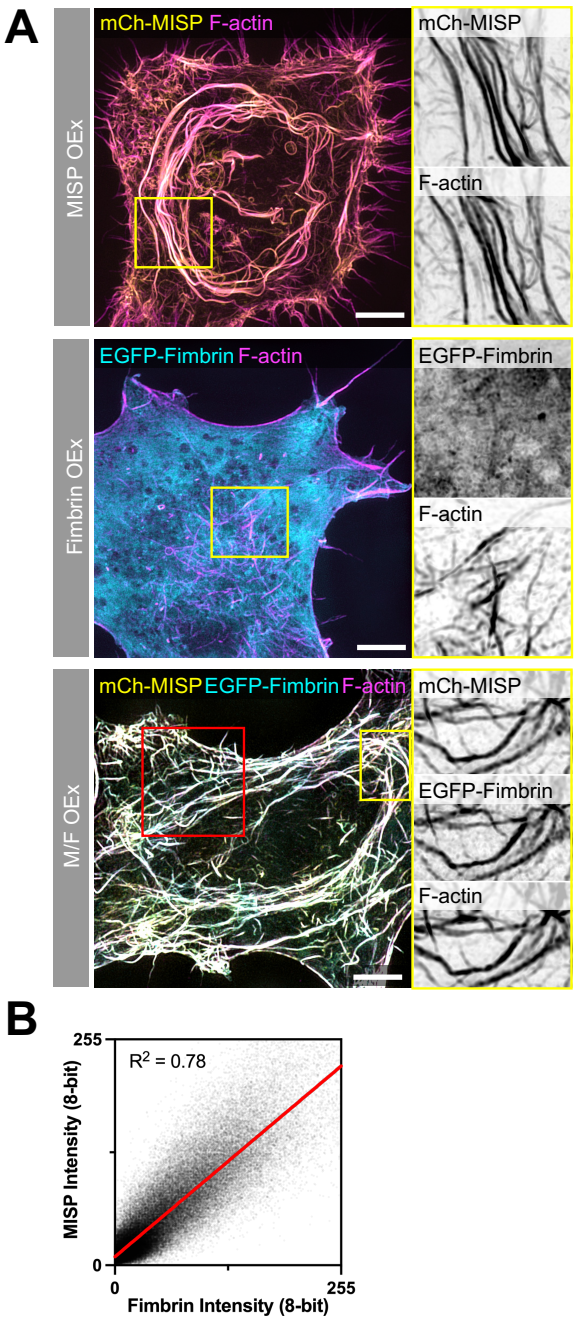

Figure 3-7. MISP recruits fimbrin to actin bundles

(A) SIM Max IPs of HeLa cells overexpressing mCherry-MISP (top panel), EGFP-fimbrin (middle panel), and mCherry-MISP and EGFP-fimbrin (bottom panel). All cells were stained for F-actin with phalloidin (magenta). Each panel shows merge with their zooms as inverted single channels. Scale bar = 5 μm.

(B) Colocalization analysis of mCherry-MISP and EGFP-fimbrin intensities along actin bundles shown in the red box in A; data were fit using linear regression.

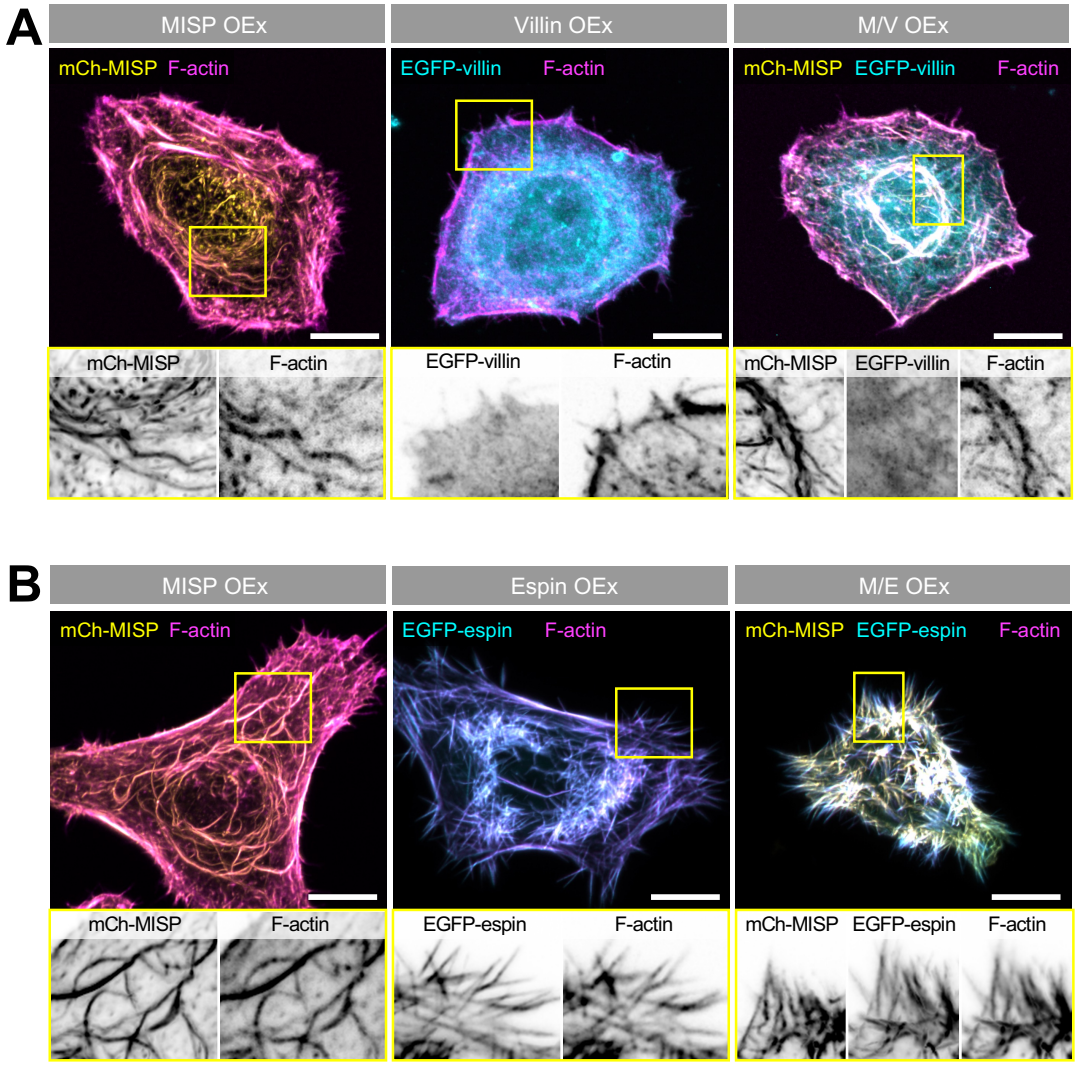

Figure 3-8. MISP does not recruit villin or espin to aberrant cytosolic bundles
(A) Confocal maximum intensity projection images of HeLa cells overexpressing mCherry-MISP (left panel), EGFP-villin (middle panel), and mCherry-MISP and EGFP-villin (right panel). All cells were stained for F-actin with phalloidin (magenta). Each panel shows merged channels on top; inverted single channel images along the bottom show zoomed regions highlighted by the yellow box in the merge images. Scale bar = 10 μm.
(B) Confocal maximum intensity projection images of HeLa cells overexpressing mCherry-MISP (left panel), EGFP-espin (middle panel), and mCherry-MISP and EGFP-espin (right panel). All cells were stained for F-actin with phalloidin (magenta). Each panel shows merged channels on top; inverted single channel images along the bottom show zoomed regions highlighted by the yellow box in the merge images. Scale bar = 10 μm.

MISP and fimbrin cooperate to elongate microvillar rootlets

We next sought to determine if MISP and fimbrin cooperate to elongate rootlets in W4 cells. Indeed, HALO-MISP and EGFP-fimbrin co-expression resulted in a dramatic hyper-elongation of rootlets, which extended deep into the cell (Figure 3-9 A). The tangled nature of these exaggerated rootlets prevented us from measuring the length of individual core bundles in these structures. Instead, we focused on measuring the length of protruding microvilli as well as the maximum distance that rootlets reached into the cytoplasm using a membrane marker as a point of reference. While the length of microvilli increased with moderate significance, the reach of rootlets strikingly increased by ~3-fold in cells co-expressing MISP and fimbrin compared to cells overexpressing either MISP or fimbrin alone, or untransfected control cells (3.01 ± 1.35 μm vs. 0.91 ± 0.41 μm vs. 1.18 ± 0.49 μm vs 0.70 ± 0.16 μm, respectively) (Figures 3-9 A and 3-9 B). We also observed that these exaggerated rootlet networks converged as they grew further from the apical membrane (Figure 3-10 A). Colocalization analysis showed a strong correlation between MISP and fimbrin signals throughout these structures (Figure 3-10 B). To further define the properties of the exaggerated rootlets promoted by MISP and fimbrin co-expression, we conducted Fluorescence Recovery After Photobleaching (FRAP) assays on W4 cells expressing HALO-β-actin alone, or in combination with EGFP-fimbrin and mCherry-MISP. Photobleaching of HALO-β-actin allowed us to directly interrogate actin dynamics in distinct regions of interest (ROIs) in transfected cells. In the microvilli of control cells, β-actin turned over with a thalf of 126.7 s, which likely reflects the treadmilling rate of core bundles in this system (Figures 3-9 C and 3-9 E; green labels). However, in cells co-expressing MISP and fimbrin, we noted two distinct recovery rates: β-actin in protruding

microvilli turned over at a rate that was 4-fold slower than controls (thalf = 529.1 s), whereas recovery in exaggerated rootlets was extremely slow to nonexistent (Figures 3-9 D and 3-9 E; magenta and cyan labels, respectively). Therefore, consistent with their actin bundling activities, MISP and fimbrin co-expression hyper-stabilized core bundles and reduced β-actin flux through both rootlets and protruding microvilli.

To further understand how these hyper-elongated and stable rootlets assemble relative to protruding microvilli, we used live imaging to visualize BB assembly in W4 cells expressing mCherry-MISP, EGFP-fimbrin, and HALO-β-actin. During the first two hours after the addition of doxycycline to promote BB assembly, we observed the assembly of a terminal web actin network immediately beneath the apical cap (Figures 3-9 F and 3-9 G; cyan labels). As this dense network accumulated sub-apically, microvilli began to emerge (Figures 3-9 F and 3-9 G; magenta labels). Consistent with our FRAP analysis, core bundle rootlets elongated from the subapical region below microvillar protrusions with no apparent actin turnover or disassembly from the basal ends (Figure 3-9 F; β-actin channel). These results suggest that the assembly of a terminal web actin network precedes the assembly of microvilli, which is consistent with the proposed role of the terminal web in offering mechanical support for protrusion assembly (Tilney & Cardell, 1970).

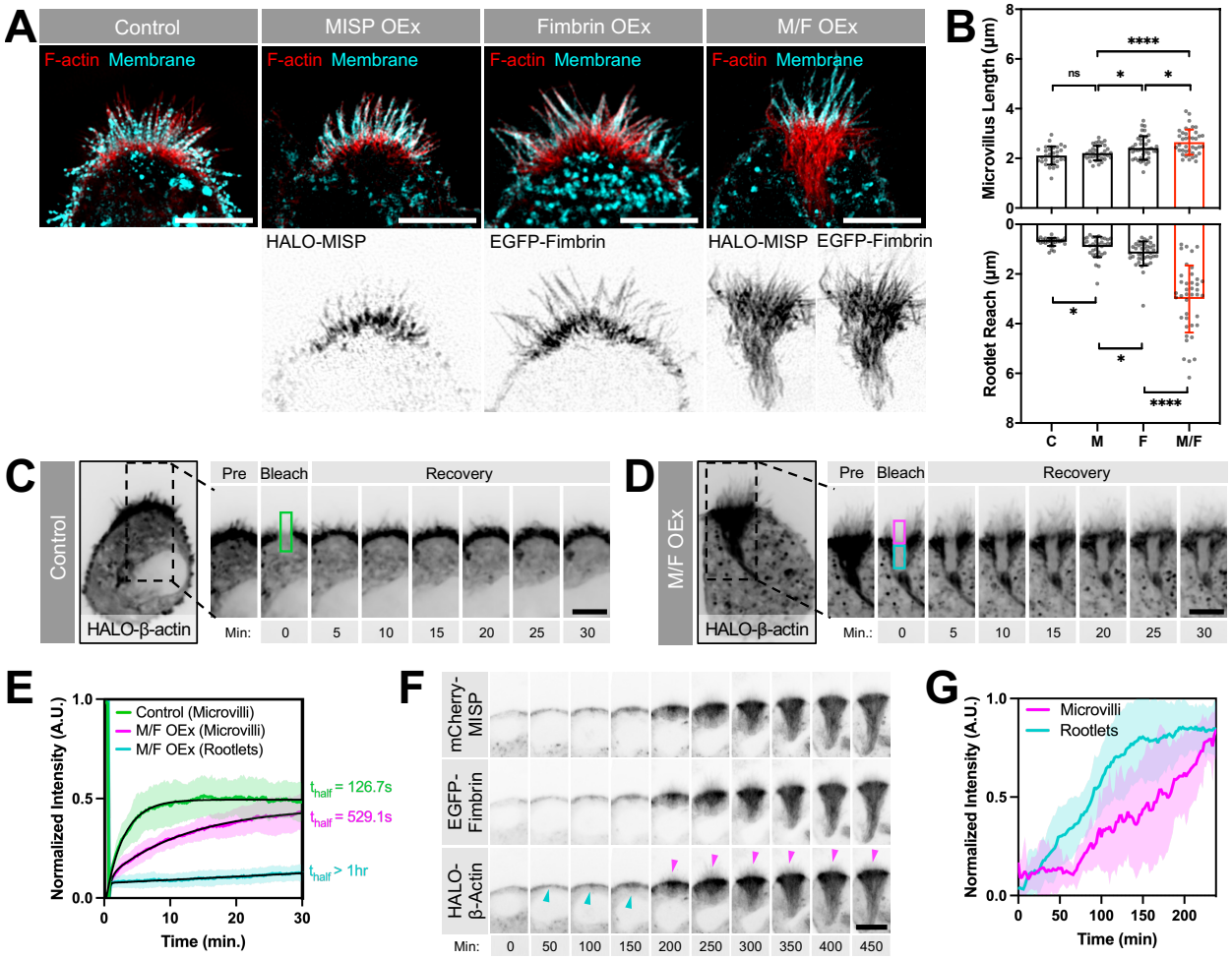

Figure 3-9. MISP and fimbrin cooperate to elongate rootlets

(A) SIM Max IPs of W4 cells no-transfected (Control), and overexpressing HALO-MISP (MISP OEx), EGFP-fimbrin (Fimbrin OEx), or HALO-MISP and EGFP-fimbrin together (M/F OEx). All cells were stained for F-actin with phalloidin (red) and membrane with WGA (cyan). Each panel shows merges on top with inverted single channels along the bottom. Scale bar = 5 µm.

(B) Lengths of microvilli ('Microvillus Length', top plot) vs. distance that rootlets extend into the cytoplasm ('Rootlet Reach', bottom plot) in W4 cells expressing the constructs described in A. Each dot represents the average of > 10 length values per cell; n ≥ 34 cells per condition. All data represent three independent experiments. Bar plots and error bars are mean ± SD. p-values were calculated using the unpaired T-test ('ns': not significant; *: $p < 0.05$; ****: $p < 0.0001$).

(C, D) Photobleaching analysis of W4 cells expressing HALO-β-actin alone (C) or HALO-β-actin with EGFP-fimbrin and mCherry-MISP (D). Although a single ROI was positioned on the BB and bleached in both conditions, the ROI in D was subdivided into two sub-ROIs to quantify differences in the recovery of the apical microvilli (magenta box) vs. subapical rootlets (cyan box). Scale bar = 5 µm.

(E) Fluorescence intensity recovery of HALO-β-actin from the color-coded ROIs described in C and D; n > 14 cells per condition. All intensity values for each condition

are shown as mean ± SD. Average values for each condition were fit using two-phase association curves.
(F) Time series montages of W4 cells expressing HALO-β-actin, EGFP-fimbrin and mCherry-MISP after adding doxycycline to induce BB assembly. Cyan arrowheads denote initiation of terminal web actin network assembly. Magenta arrowheads denote microvilli assembly. Scale bar = 10 μm.
(G) Fluorescence intensity of HALO-β-actin during BB assembly from microvilli and terminal web actin network in F; n = 10 cells.

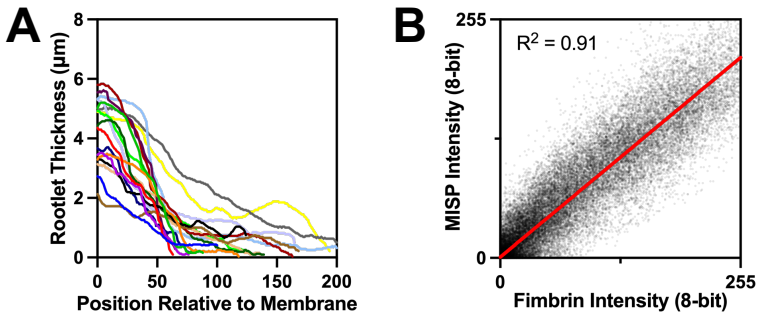

Figure 3-10. Giant rootlets generated by MISP/Fimbrin co-expression converge as a cone-like network
(A) Rootlet width measurements of W4 cells overexpressing HALO- MISP and EGFP-fimbrin from panel A of Figure 3-9 ('M/F OEx'). Width was plotted starting at the membrane boundary (x = 0) extending down into the cell body where rootlet ends converged. Each line represents a measurement from a single cell; n = 10 cells.
(B) Colocalization analysis between HALO-MISP and EGFP-fimbrin intensities measured along rootlets shown in panel A of Figure 3-9 ('M/F OEx'). Values were fit using linear regression.

MISP and ezrin exhibit mutually exclusive targeting along core actin bundles

Our localization studies in native tissues and cell culture models establish that MISP localizes specifically to the rootlet segment of the core bundle, which remains free of plasma membrane wrapping. Although such specific targeting for a BB component has not been described before, one possible explanation is that MISP is normally prevented from occupying the membrane-wrapped segment of the core bundle by other microvillar actin binding factors. One potential competing factor is ezrin, a membrane-actin linker that provides structural stability to microvilli (Casaletto et al., 2011; Saotome et al., 2004). Interestingly, active ezrin was previously identified as a MISP binding partner, and these two proteins also demonstrate partial colocalization at the cortex in dividing HeLa cells and CACO-2 cysts (Kschonsak & Hoffmann, 2018). A close inspection of W4 cells using SIM revealed that endogenous ezrin localizes to the membrane-wrapped ends of microvillar core bundles as expected (Figure 3-11 A), and shows a mutually exclusive signal relative to MISP rootlet labeling (Figure 3-11 A). This is consistent with previous work indicating that knockdown or inactivation of ezrin increases MISP levels at the cell cortex (Kschonsak and Hoffmann, 2018). To determine if MISP is confined to microvillar rootlets by ezrin, we expressed an ezrin-EGFP construct in W4 cells and monitored the localization of endogenous MISP. In control W4 cells, SIM images revealed that MISP signal was uniformly distributed at the base of the BB as expected (Figures 3-12 A and 3-12 B; left panels). However, in W4 cells expressing ezrin-EGFP, we noted that MISP signal was displaced towards the BB periphery; MISP was almost entirely excluded from the center of the apical domain where ezrin levels were highest (Figures 3-12 A and 3-12 B; right panels). 3D rendering of ezrin-overexpressing cells revealed that MISP signal

appeared as a ring-like structure surrounding ezrin signal at the center of the BB. When we stained ezrin-overexpressing cells with phalloidin and WGA to visualize F-actin and the plasma membrane, F-actin signal was reduced in regions lacking MISP signal (Figures 3-12 A and 3-12 B). This was also accompanied by drastic shortening of core bundle rootlets (0.43 ± 0.10 μm in controls vs. 0.28 ± 0.06 μm in OEx) and a significant increase in length of protruding microvilli (2.16 ± 0.36 μm in controls vs. 2.58 ± 0.40 μm in OEx; Figures 3-12 A and 3-12 C), which resulted in an increased microvillus/rootlet ratio in ezrin-overexpressing cells compared to control cells (Figure 3-12 D). Interestingly, the length of membrane-wrapped vs. unwrapped segments of core bundles, as well as their ratio, in ezrin-overexpressing cells are similar to what we observed in MISP KD cells (Figure 3-4). Using differentiated CACO-2BBE monolayers, we recapitulated these experiments and found that MISP levels were also reduced in ezrin-overexpressing conditions with no apparent redistribution to other cellular compartments (Figures 3-11 B-D). Together these findings indicate that normal levels of ezrin are required to maintain MISP targeting to core bundle rootlets, which in turn promotes their elongation.

Within microvillar protrusions, phosphorylated ezrin adopts an open state that bridges the plasma membrane to the underlying actin cytoskeleton (Bretscher et al., 1997). We hypothesized that the open/active state of ezrin within membrane protrusions restricts MISP to core bundle rootlets. To test this idea, we used an ezrin inhibitor (NSC668394), which disrupts its phosphorylation and actin-binding capacity (Bulut et al., 2012). We overexpressed ezrin-EGFP, mCherry-MISP, and HALO-UtrCH (an F-actin binding probe based on the calponin homology domain of utrophin) in W4 cells and monitored their fluorescence intensity over time before and after the addition of 50 μM

NSC668394. Using confocal microscopy, we observed that ezrin enrichment in the BB was lost within a 3-hour window following exposure to NSC668394. Notably, in all these events, the loss of ezrin signal was followed by a striking increase of MISP and UtrCH signal throughout the BB (Figures 3-12 E and 3-12 F). Moreover, overaccumulation of MISP and UtrCH in NSC668394-treated W4 cells also coincided with a dramatic increase in microvillar length (Figure 3-12 E; UtrCH channel). However, these instances of elongation were temporary as protrusions eventually collapsed after 30-60 min of growth without impacting the accumulation of MISP and UtrCH at the base of the BB. To further define the impact of ezrin accumulation on MISP localization and microvillar structure, we used SIM to look closer at the BB of W4 cells fixed after 2 hours of NSC668394 treatment. SIM images revealed a significant increase in the overall length of core bundles in NSC668394-treated cells compared to control cells (3.58 ± 0.83 μm vs. 8.25 ± 2.11 μm) (Figures 3-12 G and 3-12 H). Interestingly, MISP occupancy along core bundles also increased from 38% in DMSO-treated cells to 53% in NSC668394-treated cells (Figure 3-12 I). These findings indicate that ezrin and its associated membrane-actin linking activity confine MISP to the rootlets of microvilli.

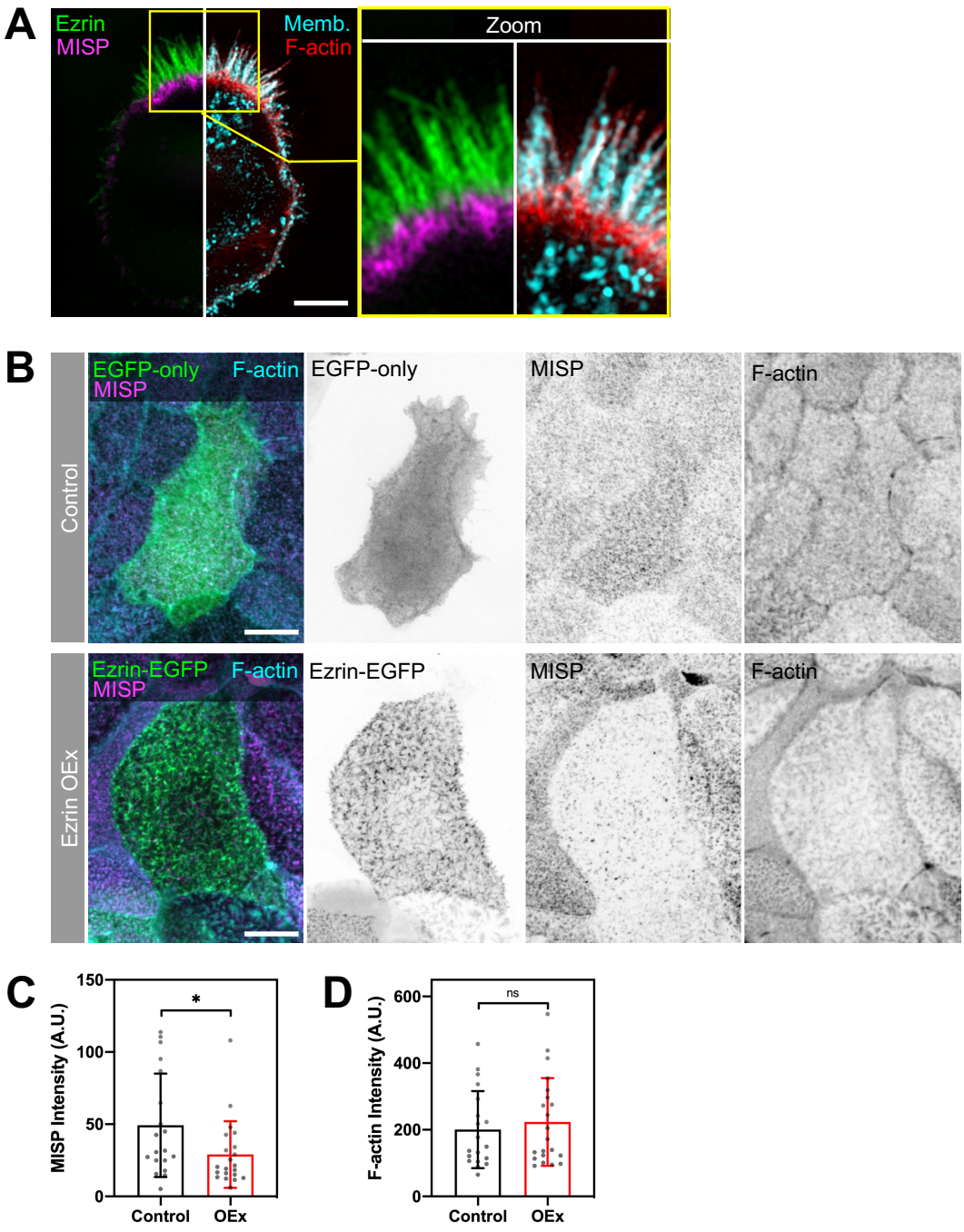

Figure 3-11. Endogenous ezrin levels are required for maintaining MISP on actin rootlets

(A) SIM maximum intensity projection image of a W4 cell stained for: MISP (magenta); ezrin (green); F-actin with phalloidin (red); and membrane with WGA (cyan). The left panel shows the image split into two to display a combination of two-color channels. The right panel shows zoomed images of the yellow box shown in the left panel. Scale bar = 3 μm.

(B) Confocal maximum intensity projection images of CACO-2BBE cells overexpressing EGFP alone ('Control', top panel) or ezrin-EGFP ('Ezrin OEx', bottom panel), and stained for endogenous MISP (magenta), and F-actin with phalloidin (cyan). Each panel shows merged channels with their corresponding inverted single channel images to the right. Scale bar = 10 μm.
(C-D) Fluorescence intensities of MISP (C) or F-actin (D) from panel B comparing control and ezrin-overexpressing cells. Each data point represents the averaged MISP or F-actin intensity of a single cell; n > 15 cells per condition. Bar plots and error bars denote mean ± SD. p-values were calculated using the unpaired T-test ('ns': not significant; *: $p < 0.05$).

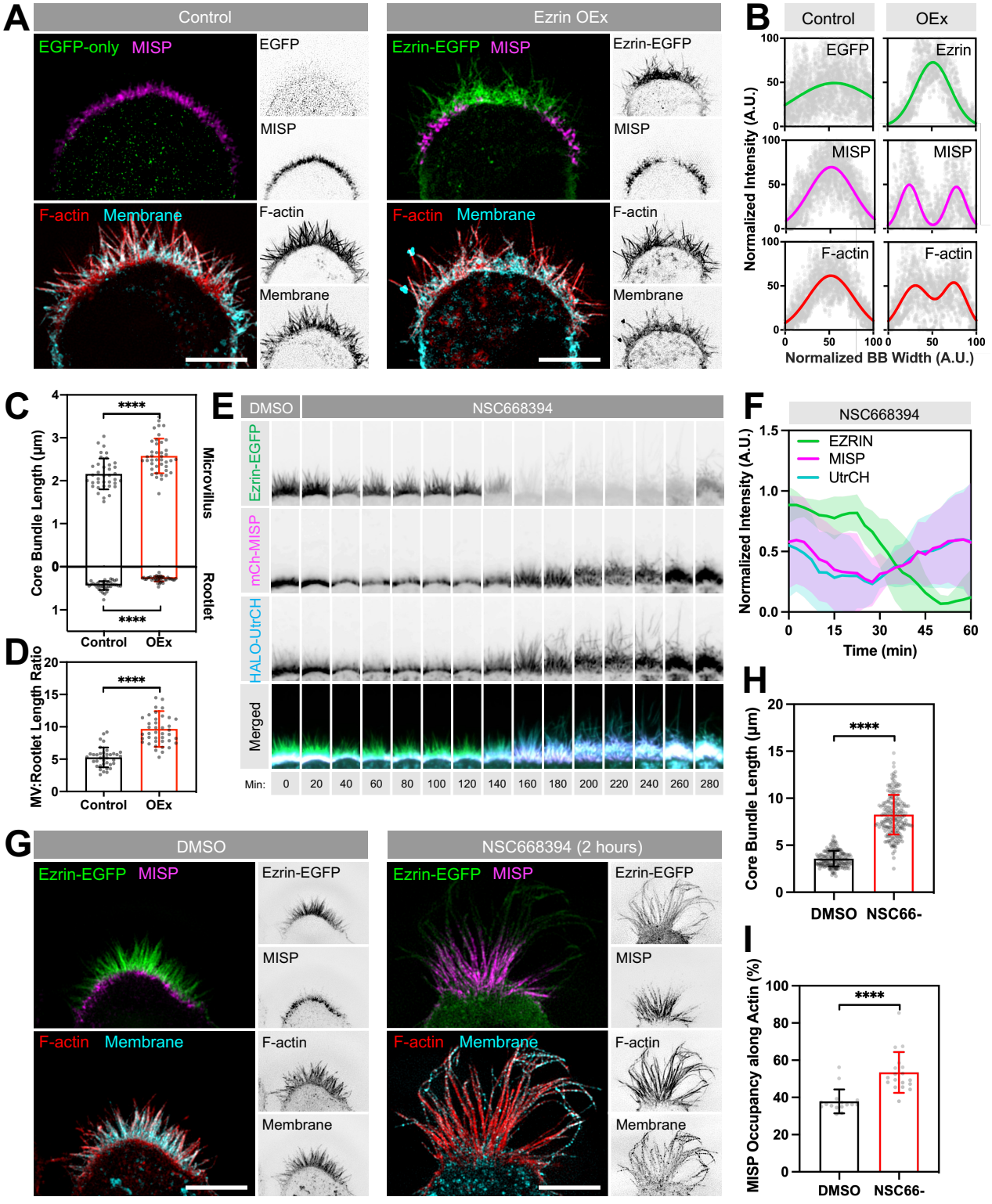
A
Control
Ezrin OEx
EGFP-only MISP
EGFP
MISP
F-actin Membrane
F-actin
Membrane
Ezrin-EGFP MISP
Ezrin-EGFP
MISP
F-actin Membrane
F-actin
Membrane
B
Control
OEx
EGFP
Ezrin
MISP
MISP
F-actin
F-actin
Normalized Intensity (A.U.)
Normalized BB Width (A.U.)
C
Core Bundle Length (μm)
****
****
Microvillus
Rootlet
Control
OEx
D
MV:Rootlet Length Ratio
****
Control
OEx
E
DMSO
NSC668394
Ezrin-EGFP
mCh-MISP
HALO-UtrCH
Merged
Min: 0 20 40 60 80 100 120 140 160 180 200 220 240 260 280
F
NSC668394
EZRIN
MISP
UtrCH
Normalized Intensity (A.U.)
Time (min)
H
Core Bundle Length (μm)
****
DMSO
NSC66-
I
MISP Occupancy along Actin (%)
****
DMSO
NSC66-
G
DMSO
NSC668394 (2 hours)
Ezrin-EGFP MISP
Ezrin-EGFP
MISP
F-actin Membrane
F-actin
Membrane

Figure 3-12. MISP and ezrin exhibit mutually exclusive targeting at opposite ends of core actin bundles

(A) SIM Max IPs of W4 cells overexpressing EGFP alone (green, left panel) or ezrin-EGFP (green, right panel), and stained for endogenous MISP (magenta), F-actin with phalloidin (red), and membrane with WGA (cyan). Each panel shows two-color merges with their inverted single channels. Scale bar = 5 μm.

(B) Intensity distributions across the BB from left to right, measured for each marker described in A. Distributions were fit using single or double Gaussian curves. Number of cells per condition ≥ 8.

(C) Lengths of microvilli (top plot) and rootlets (bottom plot) from W4 cells shown in A. Each dot represents the average of > 10 length values per cell; n ≥ 37. All data represent three independent experiments.

(D) Microvillus/rootlet length ratios measured on a per cell basis from C.

(E) Confocal Max IP time series montages of a W4 cell expressing ezrin-EGFP (green), mCherry-MISP (magenta), HALO-UtrCH (blue) before and after adding NSC668394 (ezrin inhibitor). Width of each box in the montage is 7 μm.

(F) Fluorescence intensity values of markers described in E. Data is shown as mean ± SD.

(G) SIM Max IPs of W4 cells expressing ezrin-EGFP in DMSO (left panel) or NSC668394 (right panel) conditions after 2 hours of exposure. Cells were stained for endogenous MISP (magenta), F-actin with phalloidin (red), and membrane with WGA (cyan). Each panel shows two-color merges with their inverted single channels. Scale bar = 5 μm.

(H) Lengths of core bundles from conditions described in G. Each dot represents the length of a single core bundle; n > 190 length values. (I) Percentages of MISP occupancy along core bundles from the conditions in G. Each dot represents the percentage of the average MISP coverage along core bundles per cell; n > 16 cells per condition; length values per cell > 10. All bar plots and error bars denote mean ± SD. p-values were calculated using the unpaired T-test (****: $p < 0.0001$).

Discussion

The filament crosslinking activity of actin bundlers provides the microvillar core bundle with the flexural rigidity needed to overcome plasma membrane tension and protrude from the cell surface (Atilgan et al., 2006). Although villin, fimbrin, and espin are canonical actin bundlers that have been identified and characterized in the context of the epithelial BB, persistent microvillar growth in mice lacking all three of these factors suggested the existence of as-of-yet unidentified bundlers (Revenu et al., 2012). Epidermal growth factor receptor pathway substrate 8 (EPS8) has been invoked to potentially compensate for crosslinking activity in the absence of other canonical bundlers (Revenu et al., 2012). However, its specific localization to the distal tips of microvilli is at odds with the need for canonical bundlers to be distributed along the length of the core bundle. Additionally, whereas certain cell types employ isoforms of fascin to drive robust parallel bundling of filaments in other related actin-based protrusions such as filopodia and stereocilia (Krey et al., 2016; Roy & Perrin, 2018; T. M. Svitkina et al., 2003), there is no evidence for fascin expression in transporting epithelia of the gut and kidney. Thus, the identity of other functional bundlers in the apical BB has remained an open question.

Here, we identify MISP as a BB resident that holds F-actin bundling potential. Previous studies on MISP focused on its role during mitotic progression (Kschonsak & Hoffmann, 2018; Maier et al., 2013; Zhu et al., 2013). In that context, cortically localized MISP contributes to anchoring the asters of spindle microtubules to cortical actin-rich structures during metaphase (Maier et al., 2013; Zhu et al., 2013). In native intestinal tissues and differentiating epithelial cell culture models, we found that MISP localizes to the base of core bundles that support microvilli. Moreover, confocal and super-resolution

images revealed that MISP is restricted to the rootlet ends of core bundles, which are embedded in the subapical terminal web and thus are not wrapped by plasma membrane. These results also align well with MISP being enriched in the proximal region of neuronal growth cones, where the pointed ends of filopodial actin filaments coalesce (Kumeta et al., 2014). Thus, localization near pointed ends of actin filaments appears to be a conserved property of MISP. Interestingly, MISP labeling is observed not only in the terminal web of enterocytes along the villus, but also in the subapical region of immature/differentiating enterocytes found in the crypt. Therefore, MISP is enriched at the cell apex during the window of differentiation when microvilli are actively growing. Having a rootlet-specific bundler present at early stages of differentiation is consistent with classic ultrastructural studies, which suggested that the growth of new microvilli is supported by a simultaneous maturation of the terminal web immediately beneath the apical membrane (Tilney & Cardell, 1970).

Our data indicate that MISP selectively stabilizes the rootlet ends of core bundles. Indeed, MISP KD in W4 cells led to significant shortening of rootlets when visualized with SIM, whereas overexpression promoted rootlet elongation. The bundle elongation induced by increasing MISP levels aligns well with previous studies on espin, which also drives microvillus elongation when overexpressed (Loomis et al., 2003). Previous MISP overexpression studies in HeLa cells reported a ‘thickening’ of actin structures, which is generally consistent with our observations (Kumeta et al., 2014). However, that study also showed that depletion of MISP led to filopodial overgrowth, which seems to be at odds with our conclusion that MISP promotes the assembly of parallel actin bundle-based protrusions. These phenotypic distinctions are related to the prominent differences in

actin network architecture found in unpolarized HeLa cells vs. the polarized intestinal epithelial cells at the focus of our study.

We propose that the gain- and loss-of-function phenotypes observed in our experiments are explained by MISP's F-actin bundling activity, which we reconstituted *in vitro*. F-actin bundles assembled with purified MISP demonstrate tight packing with an average inter-filament spacing of ~10.2 nm, which is close to that reported for fimbrin (~9-12 nm) (Matsudaira et al., 1983; Volkmann et al., 2001), but slightly shorter to the distance between filaments bundled by villin or espin (~12 nm) (Bartles et al., 1998; Hampton et al., 2008). This suggests that the arrangement of filaments in intact microvilli reflects the collective activity of multiple bundlers, each bringing their own characteristic spacing. Indeed, previous EM studies on filament packing and spacing in stereocilia core bundles, which are occupied by fascin-2, espin-1, and fimbrin (Krey et al., 2016) and TRIOBP-4 and -5 (Kitajiri et al., 2010) are consistent with this general idea.

Intriguingly, co-expression of MISP and fimbrin cooperatively elongated core bundle rootlets deep into the cytoplasm of W4 cells. The exaggerated nature of these rootlets allowed us to capture the temporal details of their formation, which preceded microvilli assembly. Thus, the apical localization of bundlers early in enterocyte differentiation might provide mechanical stability to nascent, growing microvilli. Overexpression experiments in HeLa cells, which generally do not make microvilli, also revealed that MISP can drive the formation of aberrant actin bundles, and these structures in turn recruit fimbrin but not villin or espin. How MISP binds to and bundles F-actin and recruits fimbrin remains unknown. In our analysis, we failed to identify recognizable actin binding and bundling motifs in the MISP primary sequence, although previous studies

point to actin binding potential as being distributed throughout the molecule (Kumeta et al., 2014), which is consistent with the functional requirements of a bundler. Considering the cooperative effects of MISP and fimbrin on rootlet length and stability, it is tempting to speculate that these factors bind to different sites on F-actin. In contrast to MISP, the multiple actin binding domains of fimbrin are well characterized (Klein et al., 2004) and their binding sites on F-actin in 2D arrays have been mapped using cryo-EM (Volkmann et al., 2001). Based on those structural studies, we speculate that MISP binds outside the canonical inter-monomer cleft that is targeted not only by fimbrin but also cofilin (Tanaka et al., 2018), myosin (Mentes et al., 2018), and even live imaging probes such as Lifeact (Belyy et al., 2020). Future cryo-EM studies aimed toward elucidating the structural details of the MISP binding site on F-actin will be needed to understand the nature of MISP/fimbrin cooperativity. Independent of a detailed actin binding and bundling mechanism, the hierarchical targeting of MISP and fimbrin suggests an order of action for these two bundlers during microvillar assembly. We propose that MISP localization to rootlets leads to the arrival of fimbrin at the apical surface in differentiating enterocytes. Examining this possibility during microvilli biogenesis will require high temporal resolution live imaging as we recently described (Gaeta et al., 2021).

The highly restricted targeting of MISP to the rootlet is unique among epithelial actin bundlers, though previous studies revealed that fimbrin accumulates at higher levels at core bundle rootlets in the terminal web, relative to the distal end (Grimm-Günter et al., 2009). In MISP KD cells, we noted that the membrane-wrapped segment of the core bundle elongated in parallel with the shortening of rootlets induced by loss of MISP. This finding suggested a previously unrecognized interplay between mechanisms that control

the length of membrane-wrapped protruding microvilli and the activity of actin bundlers that dictate the length of rootlets. Thus, we hypothesized that factors that simultaneously bind to plasma membrane and F-actin would be well positioned to prevent MISP binding along the more distal membrane-wrapped segment of the core bundle. A common feature of actin-based protrusions is tethering of the cytoskeleton to the enveloping membrane by ERM (ezrin, radixin, moesin) proteins (Revenu et al., 2004). In the BB, ezrin is the most abundant ERM (McConnell et al., 2011). Interestingly, a previous study showed that ezrin holds the potential to limit MISP accumulation at the cell cortex (Kschonsak & Hoffmann, 2018). Paradoxically, that same work also reported that MISP binds directly to active ezrin, leaving open questions about the nature and mechanism of the functional interaction between these two proteins. Based on super-resolution imaging, our results unambiguously show that MISP and ezrin occupy spatially distinct domains along individual core bundles, with active and inactive ezrin (Hanono et al., 2006) occupying the membrane wrapped domain and MISP residing on the rootlet, which is free of membrane wrapping. Thus, our data suggest that if MISP and active ezrin do physically interact, the resulting complex does not bind to the microvillar core bundle (Kschonsak & Hoffmann, 2018).

Remarkably, we found that inactivation of ezrin using a small molecule inhibitor led to the release of ezrin from the plasma membrane and immediate ectopic redistribution of MISP from the rootlets up to more distal regions of the core bundle. Ezrin and MISP redistribution also led to a drastic increase in microvillar length, which might reflect loss of the mechanical constraint that the membrane normally imposes on the distal barbed ends, the preferred site of actin monomer incorporation. Alternatively, MISP recruitment

to more distal regions of the bundle might directly promote stabilization and slow the robust treadmilling and turnover that normally occur in this system (Meenderink et al., 2019; Tyska & Mooseker, 2002). Taken together, these data argue for a mutual exclusivity model where opposite ends of core bundles are decorated by either ezrin or MISP and the balance between these populations ultimately dictates the extent of membrane coverage.

The fact that ezrin excludes MISP from binding along the membrane-wrapped segment of the microvillus may also offer additional insight on where MISP resides in a core bundle. Assuming that membrane-associated ezrin only binds to F-actin superficially exposed on the surface of the core bundle, MISP's inability to occupy distal regions might suggest that this bundler also binds superficially. Although speculative, such superficial binding has been demonstrated for TRIOBP-4, a bundler that targets specifically to the rootlets of hair cell stereocilia (Kitajiri et al., 2010). MISP and TRIOBP do not share motifs or domain organization, but secondary structure analysis in Phyre2 predicted that MISP sequence is largely disordered as has been reported for TRIOBP-4 (Bao et al., 2013). Thus, it remains possible that MISP bundles filaments using a similar mechanism. It is also worth noting that other well-characterized actin bundlers in microvilli – villin and espin – are uniformly found along the length of the core bundle and they do not exhibit mutually exclusive localization with ezrin.

Collectively, the discoveries reported here point to an unconventional mechanism for bundling F-actin in the core bundles that support epithelial microvilli. These findings strengthen our molecular understanding of the biologically robust formation of evolutionary conserved microvillus-rich apical specializations. The emergence of MISP

as a linear actin bundler also offers a molecular explanation for the remarkable finding that triple villin-espin-fimbrin KO mice are still capable of assembling BB microvilli (Revenu et al., 2012). Because MISP is also implicated in promoting mitotic progression (Maier et al., 2013; Zhu et al., 2013), future studies might focus on examining the role of MISP in coupling oriented cell division with differentiation in transporting epithelial cells.

CHAPTER IV

MISP PREFERENTIALLY BINDS NEAR THE POINTED ENDS OF AGED ACTIN FILAMENTS

Summary

Actin bundling proteins crosslink filaments into polarized higher-order structures such as those shaping the membrane protrusions of filopodia, microvilli and stereocilia. In the case of microvilli, MISP is an actin bundler that exhibits a selective decoration of the basal rootlets, where the pointed ends of filaments converge. Yet, whether MISP sorts to these segments of polarized bundles of microvilli independent of extrinsic factors remains an open question. Using *in vitro* TIRF microscopy assays, we found that MISP harbors intrinsic properties for its sorting towards the pointed ends of aged filaments in the ADP nucleotide composition. Moreover, although MISP assembles two-filament bundles in parallel and antiparallel configurations, the ability of MISP to assemble polarized parallel bundles persists in multi-filament arrays. These discoveries highlight nucleotide sensing as a mechanism to sort bundling proteins in polarized actin-based protrusions, which may provide distinct structural properties along continuous linear actin bundles.

Introduction

Actin filament assemblies provide structural support for a variety of cell surface features, which enable interactions with the external environment in different biological contexts. Two general architectures include actin meshworks and bundles; meshworks generate large mechanical forces, such as those needed for leading edge protrusion during cell motility, whereas bundles generate localized forces that can power the extension of membrane protrusions (Blanchoin et al., 2014; T. M. Svitkina, 2020). Examples of the latter case include filopodia, which extend from crawling cells to promote surface attachment and control steering. Other well-studied protrusions that are supported by actin bundles include microvilli, which extend from the apex of solute-transporting epithelial cells (Crawley, Mooseker, et al., 2014b; Delacour et al., 2016); and morphologically related stereocilia, which comprise the mechanosensory hair bundle that resides at the functional surface of cochlear and vestibular hair cells (Schwander et al., 2010). In all three of these cases, individual protrusions are supported by a core consisting of multiple actin filaments, ranging from ~25 for microvilli and up to 100s for stereocilia (Mooseker & Tilney, 1975; Ohta et al., 2012; Tilney & DeRosier, 1986). Multiple actin filaments are needed because individual actin filaments exhibit a flexural rigidity that is too low to support plasma membrane deformation alone (Atilgan et al., 2006). By bundling multiple filaments together with cell-type specific factors, cells can create more rigid structures that promote and maintain membrane protrusion without buckling.

A defining feature of protrusion core bundles is the polarized alignment of constituent actin filaments. In all cases, actin filament barbed ends, the kinetically favored site of new monomer addition, are oriented out into the distal tips of protrusions; whereas

the kinetically slower pointed ends, extend down into the cytoplasm. Because of the resulting structural and biochemical differences in the two ends, the critical concentration for assembly at the barbed end is much lower than the pointed end (0.1 vs. 0.6 μM, respectively) (Pollard, 1986). Moreover, the eventual hydrolysis of ATP in newly incorporated monomers at the barbed end creates a gradient of nucleotide states consisting of ATP-, ADP-Pi-, and ADP-bound actin subunits (Pollard, 2016). Such filament nucleotide composition further provides distinctive structural and physical properties along the filament including greater flexibility at the older end of the filament (McCullough et al., 2008; Reynolds et al., 2022).

The differential kinetic properties at the two ends also fuel dynamic behaviors such as treadmilling, where new actin monomers incorporate at the barbed end, flux through the polymer, and exit from the pointed ends (Wegner, 1976). Treadmilling filaments and networks also generate mechanical force at their growing barbed ends, which can be harnessed to power subcellular and cellular scale activities ranging from the motion of vesicles and endomembranes to the leading-edge protrusion that powers cell motility (Wang, 1985). Treadmilling activity has also been observed in core bundles that support some protrusions. For instance, filopodia are supported by core bundles that exhibit robust treadmilling (Mallavarapu & Mitchison, 1999), and nascent (newly formed) microvilli on the surface of differentiating epithelial cells also demonstrate treadmilling, which powers gliding motility across the apical cell surface (Loomis et al., 2003; Meenderink et al., 2019; Tyska & Mooseker, 2002). How the behaviors of individual filaments in a treadmilling parallel actin bundle are synchronized or coordinated remains unclear, although *in vitro* studies implicate factors with multivalent filament binding

potential, such as VASP at barbed ends of core bundles in filopodia (Winkelman et al., 2014).

In addition to creating a kinetic scenario that supports treadmilling, the gradient of nucleotide states along the length of an actively growing actin filament might also impact where regulatory and network building proteins are able to bind. One classic example of this type of “sorting” is found in studies of cofilin, a ubiquitously expressed filament severing protein that only binds to “older” ADP-actin (Blanchoin & Pollard, 1999). Undesired cofilin-driven severing of other filament nucleotide states can be counterbalanced by coronin-1B, which displays a binding preference for ATP/ADP-Pi-actin (Cai et al., 2007; Gandhi et al., 2009). Another well-studied factor is the Arp2/3 complex, a pointed end binder that crosslinks newly polymerizing filaments to the sides of pre-existing filaments in the ATP/ADP-Pi composition (Mahaffy & Pollard, 2006). Such biased targeting and function of all these factors observed in biochemical and single molecule studies are now acknowledged in complex actin networks including the polarized branched actin networks that build filopodial protrusions. How the intrinsic features of actin are harnessed to promote the organization and composition of protrusions lacking branched networks like microvilli or stereocilia remains unexplored.

Interestingly, the bundling proteins that comprise microvillar cores - fimbrin, espin, villin, and MISP - also sort into different segments along the length of the structure (Grimm-Günter et al., 2009; Morales et al., 2022). While espin and villin localize along the full length of the core bundle, as expected for canonical bundlers (Bartles et al., 1998; Bretscher & Weber, 1979), fimbrin seems to prefer the more basal half (Grimm-Günter et al., 2009). Unlike these bundlers, MISP exclusively decorates the rootlets, which are

presumably enriched in ADP-actin. Although the selective localization of MISP is partially dependent on ezrin's membrane-actin crosslinking activity (Morales et al., 2022), whether the intrinsic polarity of actin filaments in core bundles contributes to the sorting of MISP or other bundlers remains an open question.

In this study, we report that the actin bundling protein MISP exhibits intrinsic properties for binding near the pointed ends of actin filaments. Using *in vitro* reconstitution assays coupled with Total Internal Fluorescence (TIRF) microscopy, we found that MISP preferentially binds to the pointed ends of aged actin filaments with long dwell times. In agreement with these findings, we found that MISP preferentially "senses" ADP-actin over other filament nucleotide compositions independent of other factors. Although not exclusively, bunding assays also reveal that MISP can assemble multiple actin filaments into a parallel bundle configuration, a feature that is presumably conferred by its pointed end binding ability. Overall, these intrinsic binding modalities suggest that MISP may organize growing filaments in a parallel fashion at early stages of microvillar assembly; and further provide a mechanistic understanding of its specificity to rootlets.

Results

MISP binding to ADP F-actin is stronger than that of ADP-Pi and AMP-PNP

We previously found that the actin-binding protein MISP selectively decorates the membrane-free rootlets of microvilli, a restriction that is partially exerted by ezrin's membrane-actin crosslinking activity (Morales et al., 2022). Whether the instinct polarity of core actin bundles also contributes to MISP specific targeting to rootlets remained an open question we sought to answer.

As core actin bundles supporting microvilli undergo treadmilling (Loomis et al., 2003; Meenderink et al., 2019; Tyska & Mooseker, 2002), rootlets are expected to be predominantly enriched with ADP-bound actin. To test this, we immunostained sections of mouse small intestinal tissue displaying fully differentiated microvilli with antibodies targeting cofilin, an actin binding protein that preferentially targets ADP F-actin, thus serving as a marker for this nucleotide state of filaments (Blanchoin & Pollard, 1999; Suarez et al., 2011). Notably, we found that cofilin is highly enriched at the rootlets of microvilli, which resembled MISP localization (Figure 4-1 A-B). These results suggest that filaments comprising the rootlets of microvilli are predominantly composed of ADP F-actin, further suggesting that the filament nucleotide composition may contribute to MISP's selective targeting to rootlets.

To directly test if MISP displays a preferential binding for ADP F-actin over other nucleotide states, we turned to *in vitro* reconstitution assays with purified proteins using Total Internal Reflection Fluorescence (TIRF) microscopy. We generated biotin-rhodamine-labeled F-actin in three nucleotide states (ADP, ADP-Pi, or ATP-like). ADP F-actin and ADP-Pi F-actin were generated using phalloidin as previously described

(Zimmermann et al., 2015). To mimic the ATP state, we used AMP-PNP as a nucleotide analog (Figure 4-2 A-C; top row). Although phalloidin incorporation in all three F-actin populations may arguably mask MISP's binding sites, we previously showed that phalloidin labeling does not disrupt MISP's binding and/or function on filaments (Morales et al., 2022). Furthermore, we purified the MBP-EGFP tagged version of MISP (herein referred to as 'MISP') as described in our previous study (Morales et al., 2022). If MISP displays a preferential affinity for ADP F-actin, this must be reflected in its association and/or dissociation rates. Thus, we sought to determine if MISP's dissociation from filaments was dependent on nucleotide composition. To mimic single molecule events, we flowed in MISP at low concentrations on immobilized filaments in each nucleotide state. Notably, the lifetime of MISP molecules that remained bound to filaments (i.e., dwell time) was ~1.5 and ~1.8 times longer on ADP F-actin compared to ADP-Pi or AMP-PNP F-actin, respectively (10.72 s [95% CI = 10.15 – 11.33]; 6.78 s [95% CI = 6.13 – 7.50]; 5.83 s [95% CI = 5.53 – 6.14]) (Figure 4-2 A-F; Figure 4-1 F). Consistently, the number of dwell time events longer than 60 seconds was higher in the ADP condition relative to ADP-Pi and AMP-PNP (Figure 4-1 G). Although the reported MISP dwell times reflected a slow dissociation from ADP F-actin, they may be underestimated as we did not consider events lasting longer than our imaging timeframe. We next sought to determine if MISP's association to filaments depends on the nucleotide composition. To test this, we monitored MISP's fluorescence intensity decorating immobilized actin filaments over time. We found that the apparent association rates of MISP to filaments slightly increased from ADP F-actin to ADP-Pi and AMP-PNP F-actin by a factor of ~1.1 and ~1.2, respectively (0.30 $\mu M^{-1}.s^{-1}$ vs 0.34 $\mu M^{-1}.s^{-1}$ vs 0.36 $\mu M^{-1}.s^{-1}$) (Figures 4-1 C-E), suggesting

that MISP's association rate likely does not contribute to its preferential occupancy on ADP F-actin. Overall, these findings suggest that nucleotide-sensing may be an alternative mechanism for MISP's specific targeting to actin rootlets in microvilli.

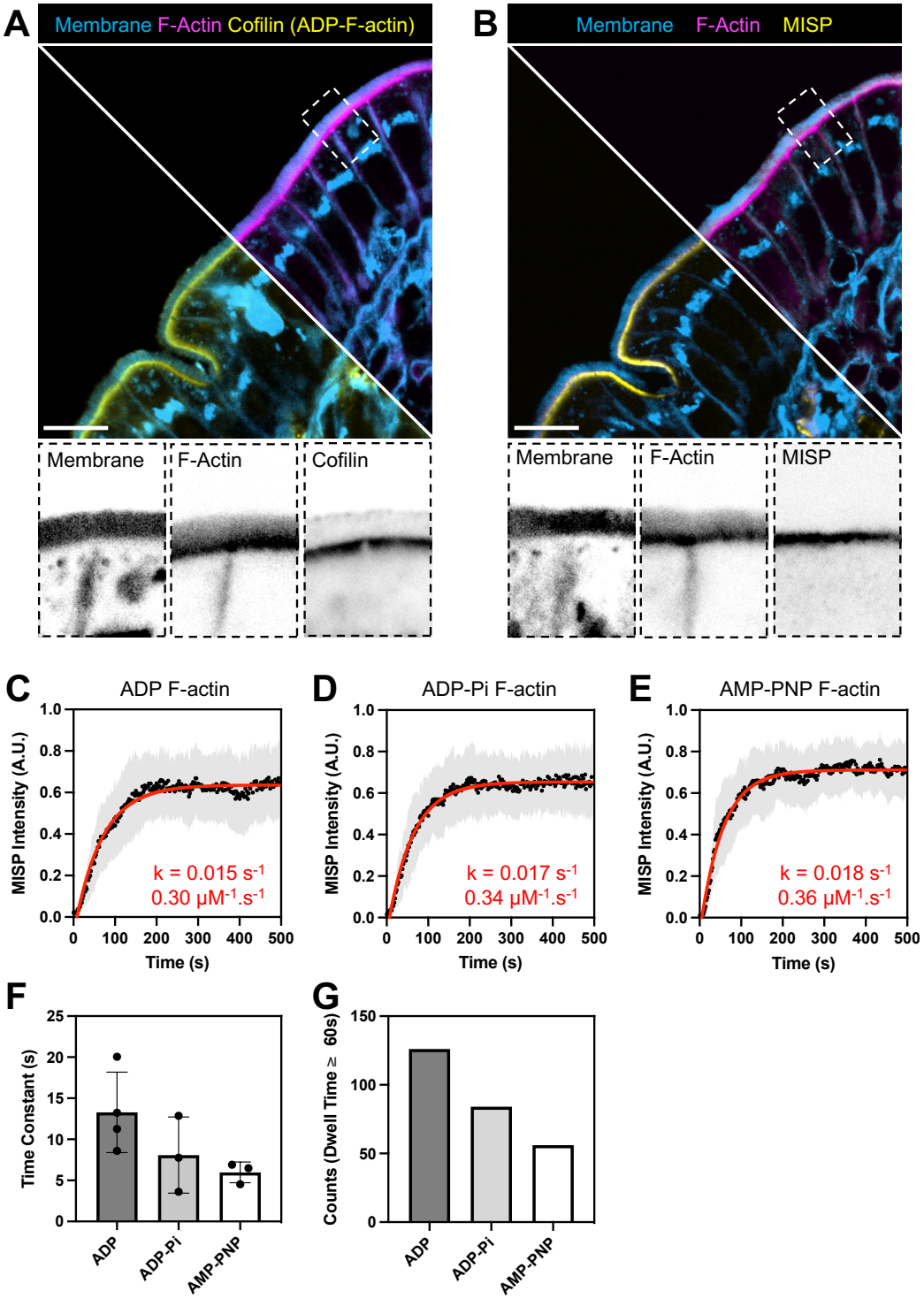

Figure 4-1. MISP preferentially binds to aged actin filaments *in vivo* and *in vitro*
(A-B) Confocal images of frozen small intestinal sections stained for membrane with WGA (blue), F-actin with phalloidin (magenta), cofilin (yellow; panel A), and MISP (yellow; panel B). Each panel shows a split two-color merge. Bottom rows show inverted single channels for each marker from in A and B. Scale bar = 10 μm.
(C-E) Fluorescence intensity of EGFP-MISP (50 nM) on immobilized F-actin (50 nM) in each indicated nucleotide state as a function of time. Non-linear exponential fittings shown in red were used to determine the apparent association rates for each condition. All data in each condition are representative of three independent experiments.
(F) Time constants of EGFP-MISP for each replicate used in Figure 4-2 D-F.
(G) Number of EGFP-MISP binding events lasting longer than 60 seconds in each nucleotide state of actin.

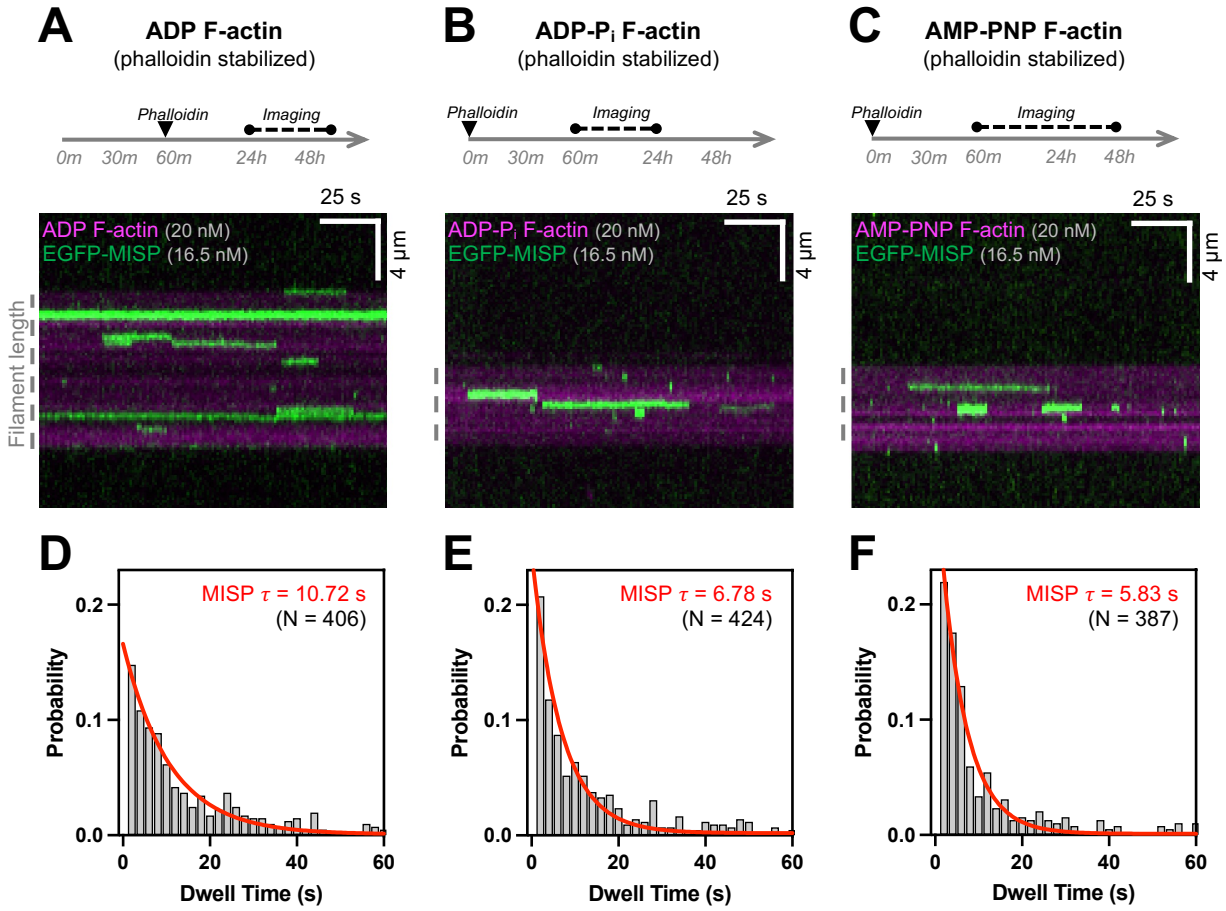

Figure 4-2. MISP preferentially binds to ADP-bound actin filaments
(A-C) Top row: Experimental setup showing the preparation and imaging of F-actin in each nucleotide state: ADP (A), ADP-Pi (B), AMP-PNP (C). In all conditions, actin polymerization begins at t = 0; Bottom row: TIRF microscopy kymographs representative of dwell times of EGFP-MISP (green) on each indicated nucleotide state of rhodamine F-actin (magenta). Dashed gray line next to each panel denotes the length of filament.

(D-F) Probability distribution of all MISP's dwell times in ADP F-actin (D), ADP-Pi F-actin **(E)** and AMP-PNP F-actin (F). Bin size= 2 s. Non-linear one-phase exponential decay fittings for each distribution are shown in red. The X axis (i.e., dwell time) was purposefully ended at 60 s to display comparisons between fitting curves at early time points. All data in each condition are representative of at least three independent experiments.

MISP preferentially binds near the pointed ends of actin filaments

Given that filaments comprising microvillar core bundles extend their pointed ends down into the rootlets, we next sought to determine if MISP had a preferential binding to the filament ends relative to filament sides independent of the nucleotide state. To determine this, we conducted similar experiments as described above by flowing in MISP at low concentrations reflecting single binding events on aged filaments; the reactions were incubated for at least 30 minutes to reach equilibrium (Figure 4-3 A). Interestingly, we found that the number of end-binding events was higher compared to the side-binding events (266 vs. 193) (Figure 4-3 B-C). This suggests that MISP may also hold the ability to preferentially bind near the ends of filaments.

To unambiguously test this, we set up reconstitution assays with polymerizing actin filaments, which displayed fast-growing barbed ends relative to pointed ends, thus revealing filament polarity. We subsequently flowed in low concentrations of MISP molecules (Figure 4-4 A). Notably, we observed MISP puncta preferentially binding near the pointed ends and their vicinity with long dwell times (> 70 s) (Figure 4-4 B-E). The accumulation of MISP to segments in proximity to pointed ends is presumably the result of its observed preferential binding to ADP F-actin as this nucleotide composition is expected to populate these ends following ATP hydrolysis and Pi release after ~5 minutes of filament polymerization (i.e., > 2 μm) (Carlier & Pantaloni, 1986). Consistent with this,

we observed fewer binding events at distal segments, likely enriched in ATP/ADP-Pi F-actin (Figure 4-4 E). Interestingly, we also found that MISP's dwell time near the pointed ends was longer compared to filament sides (269.2 ± 155 s vs. 57.62 ± 92.34 s) (Figure 4-4 F). These findings suggest that MISP may target additional binding sites near the pointed ends, which may be favored by its observed preferential binding to ADP actin.

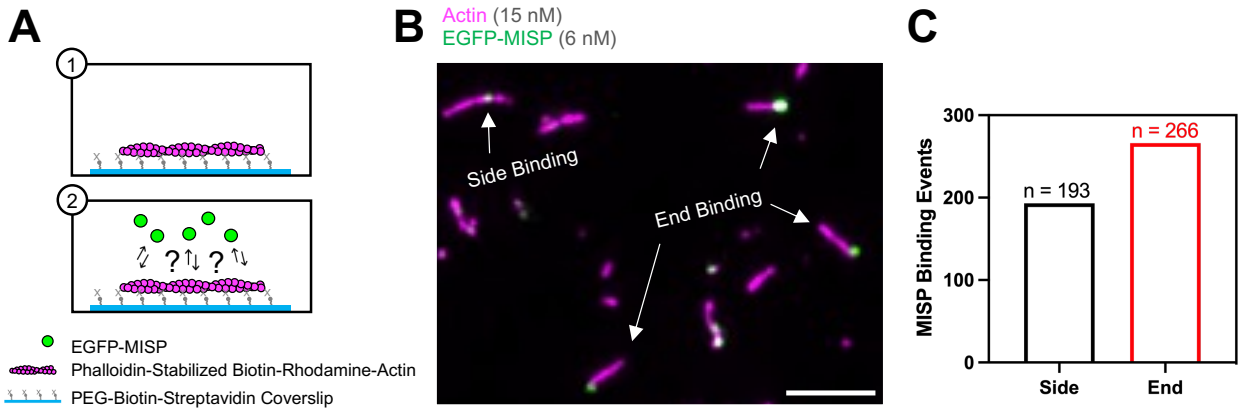

Figure 4-3. MISP preferentially binds to the ends of stabilized ADP-actin filaments
(A) Cartoon schematic of the experimental setup (1-2).
(B) TIRF microscopy image of phalloidin-stabilized biotin-rhodamine-actin filaments (magenta), and EGFP-MISP molecules (green). Scale bar = 5 μm.
(C) Quantification of EGFP-MISP's filament end and side binding events on stabilized actin filaments from B.

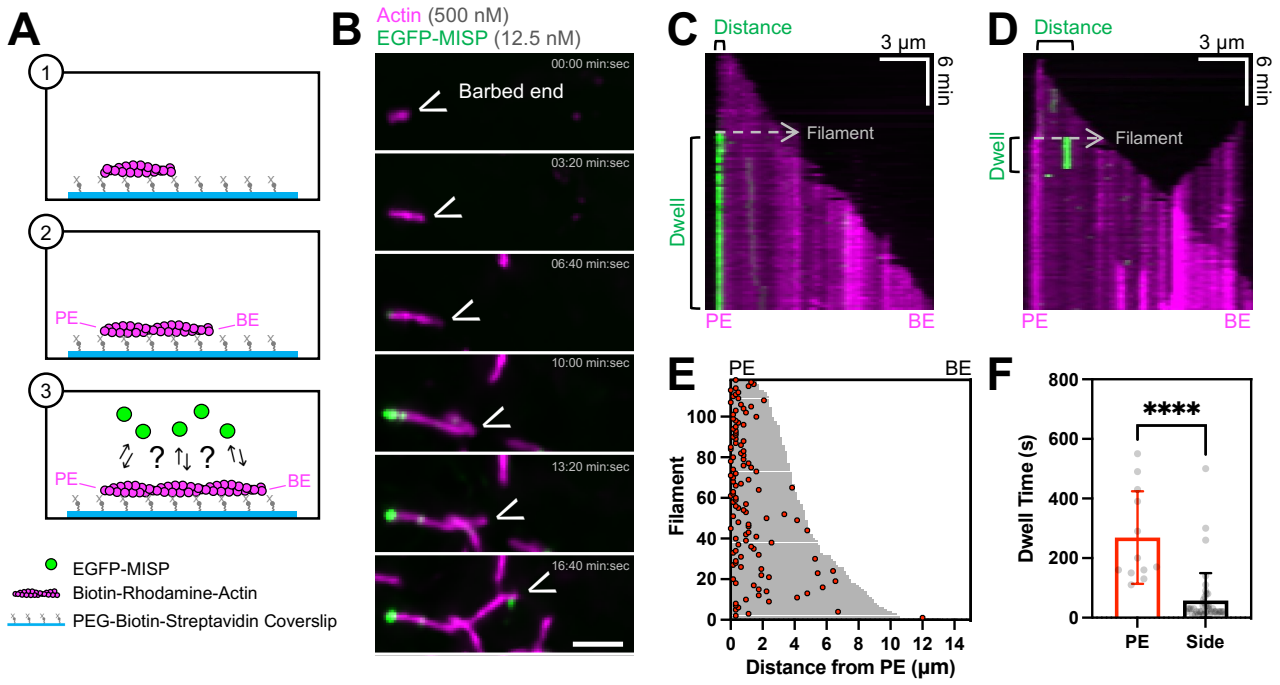

Figure 4-4. MISP preferentially binds near the pointed ends of actin filaments
(A) Cartoon schematic of the experimental setup (1-2) and possible outcomes (3).
(B) TIRF microscopy montage of a tethered polymerizing rhodamine F-actin (magenta) and EGFP-MISP molecules (green). Scale bar = 3 µm.
(C-D) TIRF microscopy kymographs representative of EGFP-MISP's binding events (green) on F-actin (magenta), near their pointed end (C), and at their side (D).
(E) Distribution of EGFP-MISP's binding events on actin filaments of known polarity. Each filament length is plotted as a horizontal bar in gray, and the distance of each binding event from the pointed ends ('PE') is plotted as a red dot.
(F) Mean dwell time of MISP's binding events near the pointed ends ('PE') or at the filament side ('Side'). Each dot represents a single event. Bar plots and error bars denote mean ± SD. p value was calculated using the unpaired t test (****$p < 0.0001$). All data are representative of three independent experiments.

MISP preferentially captures filaments from the pointed ends

Although freely diffusing MISP targets the pointed ends of filaments, MISP seems to be anchored to pre-existing actin networks before core bundles assemble in intestinal epithelial cells (Morales et al., 2022). Thus, we next sought to determine if MISP still binds to the pointed ends of newly polymerizing filaments from a confined configuration. To

mimic this, we tethered MISP molecules on the coverslip using anti-MISP antibodies and flowed in short seeds of polymerizing actin filaments (Figure 4-5 A). We found that immobilized MISP maintains its preferential binding near the pointed ends as evidenced by a fast elongation from the opposite barbed end over several minutes (Figure 4-5 B-C). To simplify our quantification, we classified the number of binding events as “pointed end”, “barbed end”, and “filament side”, which revealed that pointed end binding events prevailed over the others (71 vs. 34 vs 29) (Figure 4-5 D). These results further support that MISP preferentially binds near the pointed ends of actin filaments.

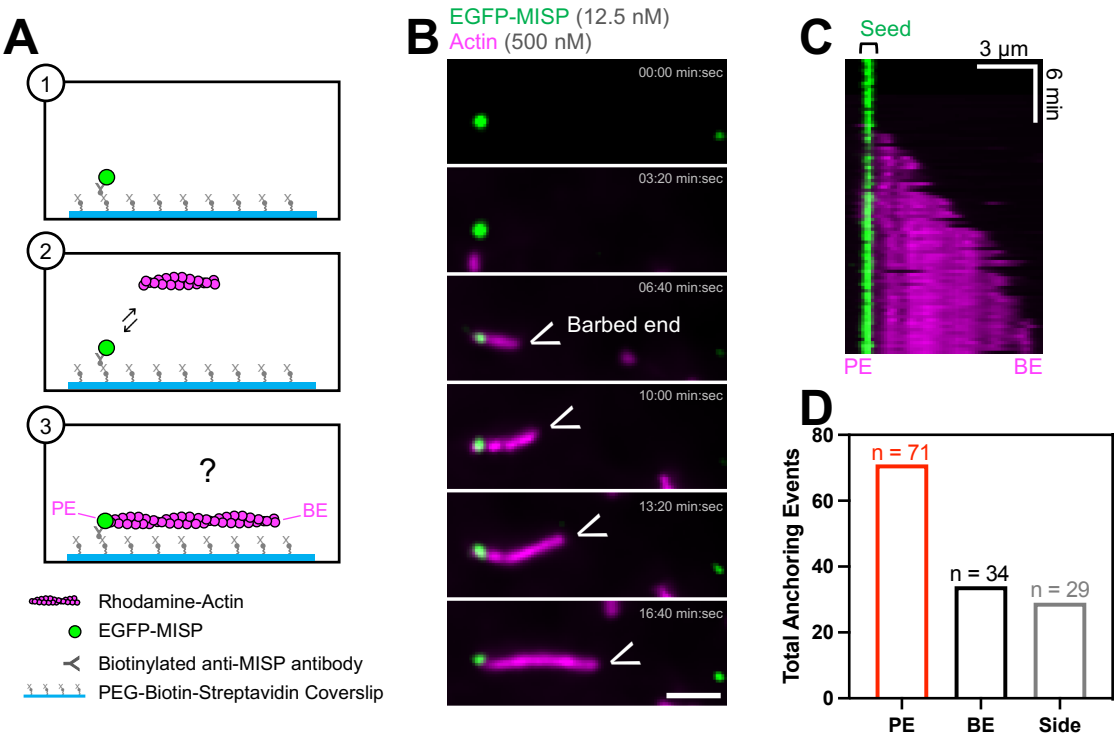

Figure 4-5. MISP preferentially captures actin filaments from the pointed ends
(A) Cartoon schematic of the experimental setup (1-2) and expected outcome (3).
(B) TIRF microscopy montage of immobilized EGFP-MISP molecules (green) anchoring a polymerizing rhodamine F-actin (magenta) from the pointed end. Scale bar = 3 µm.
(C) Kymograph of movie corresponding to the montage in (B).
(D) Quantification of EGFP-MISP-driven anchoring events from the pointed ends (‘PE’), barbed ends (‘BE’), and side (‘Side’) of actin filaments. All data are representative of three independent experiments.

MISP bundles actin filaments in a parallel and antiparallel manner

Thus far, we have characterized MISP's binding properties on single actin filaments. Considering that MISP functions as a crosslinker of multiple filaments in cells (Kumeta et al., 2014; Morales et al., 2022), we next investigated whether MISP's preferential binding near the pointed ends and ADP F-actin has implications on its bundling function. One tentative hypothesis is that MISP may harness its ability to bind near the slow-growing ends of filaments to create a bundle of uniform polarity. To determine if MISP is sufficient to create parallel bundles, we set up TIRF assays using untethered and pre-assembled polymerizing actin. Visualizing two-filament bundling events, we found that MISP bundles filaments in a parallel and antiparallel fashion with no preferential bundling in either orientation (Figure 4-6 A-C). We also found that MISP intensity was higher in two-filament bundles compared to single filaments (Figure 4-6 B, D), suggesting a stronger affinity for two-filament arrays, likely reflecting MISP's multiple actin binding sites (Kumeta et al., 2014). A close inspection of two-filament parallel bundling events also revealed that MISP signal was lower on newly polymerizing pairs of filaments (Figure 4-6 B; top row, green channel), presumably due to its preferential affinity for aged filaments (Figure 4-2 C). Occasionally, we also observed MISP/actin bundles of more than four filaments landing on the field of view (Figure 4-7 A-C). As the number of filaments in a bundle increases, we expected MISP may solely give rise to antiparallel bundles, which we observed (Figure 4-7 B). Nevertheless, we also noticed that some of these thick bundles grew all their barbed ends exclusively in one direction (Figure 4-7 C), indicating that MISP is still capable of bundling more than two filaments in a parallel fashion. We failed to recapitulate these parallel bundling events *de novo* on the surface of the coverslips, presumably

because the spatial confinement in 2D limited MISP/actin to freely diffuse and adopt an optimal spatial configuration. A close inspection across multiple fields of view revealed various actin structures in a broom-like shape consisting of more than 20 filaments with a strong MISP signal at one end, suggesting that these structures may also reflect parallel bundling events. Overall, these results suggest that MISP holds the capacity to create antiparallel and parallel bundles of multiple filaments; the polarized parallel arrays were presumably the result of MISP's ability to preferentially associate to pointed ends of newly polymerizing filaments.

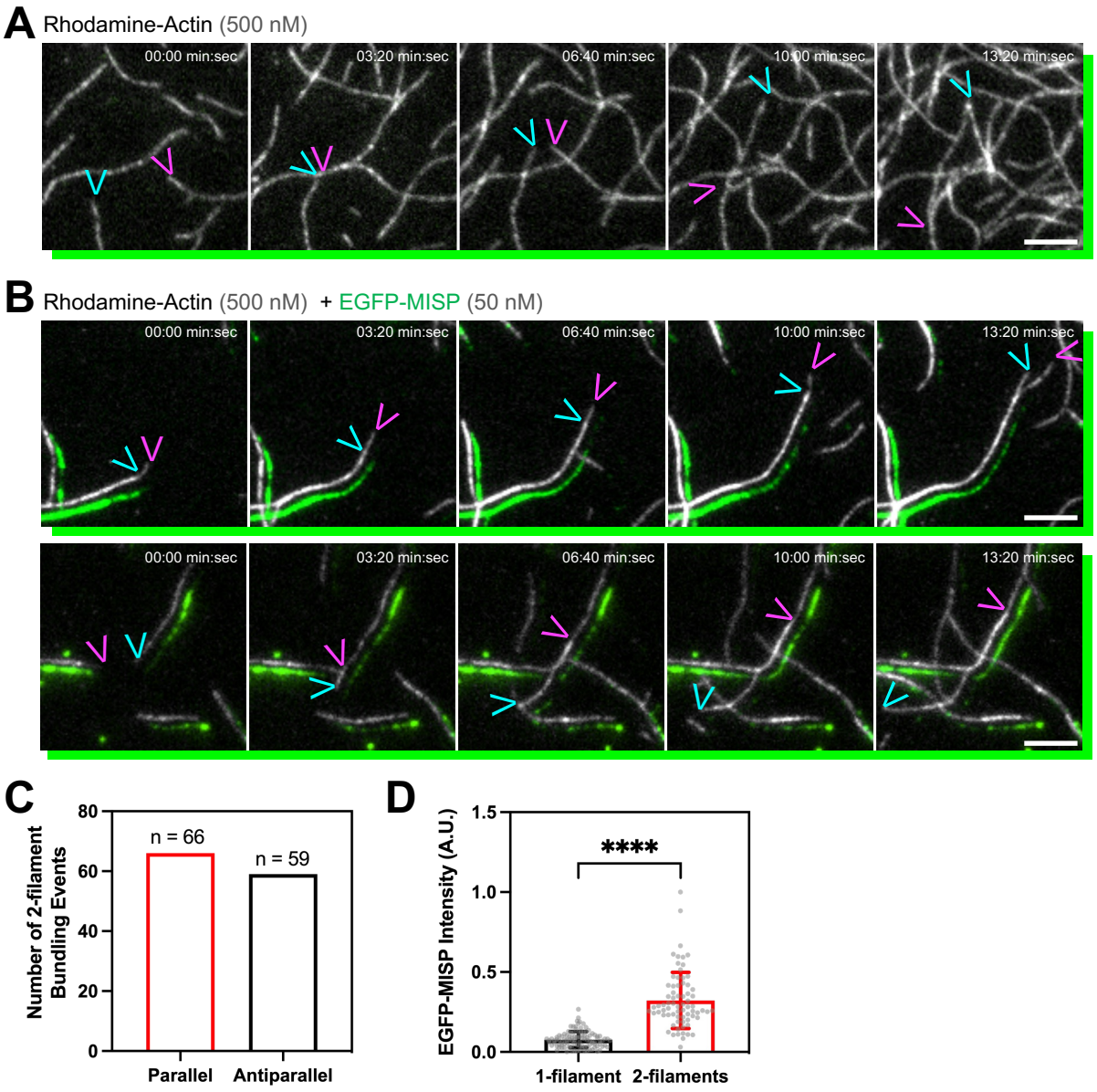

Figure 4-6. MISP bundles actin filaments in a parallel and antiparallel manner
(A-B) TIRF microscopy montages of rhodamine F-actin (gray), and EGFP-MISP (green). (A) Control experiment without EGFP-MISP. (B) 2-filament bundling event driven by EGFP-MISP in a parallel (top row) and antiparallel (bottom row) manner. Green channels in A and B were slightly shifted to the lower right side of image to better visualize the overlap between F-actin and MISP. Scale bar = 5 μm.
(C) Quantification of 2-filament parallel and antiparallel bundling events from movies as shown in (B). All data are representative of at least three independent experiments.
(D) Mean intensity of EGFP-MISP on 1-filaments versus 2-filaments from movies as shown in (B). Bar plots and error bars denote mean ± SD. p value was calculated using the unpaired t test (****p < 0.0001).

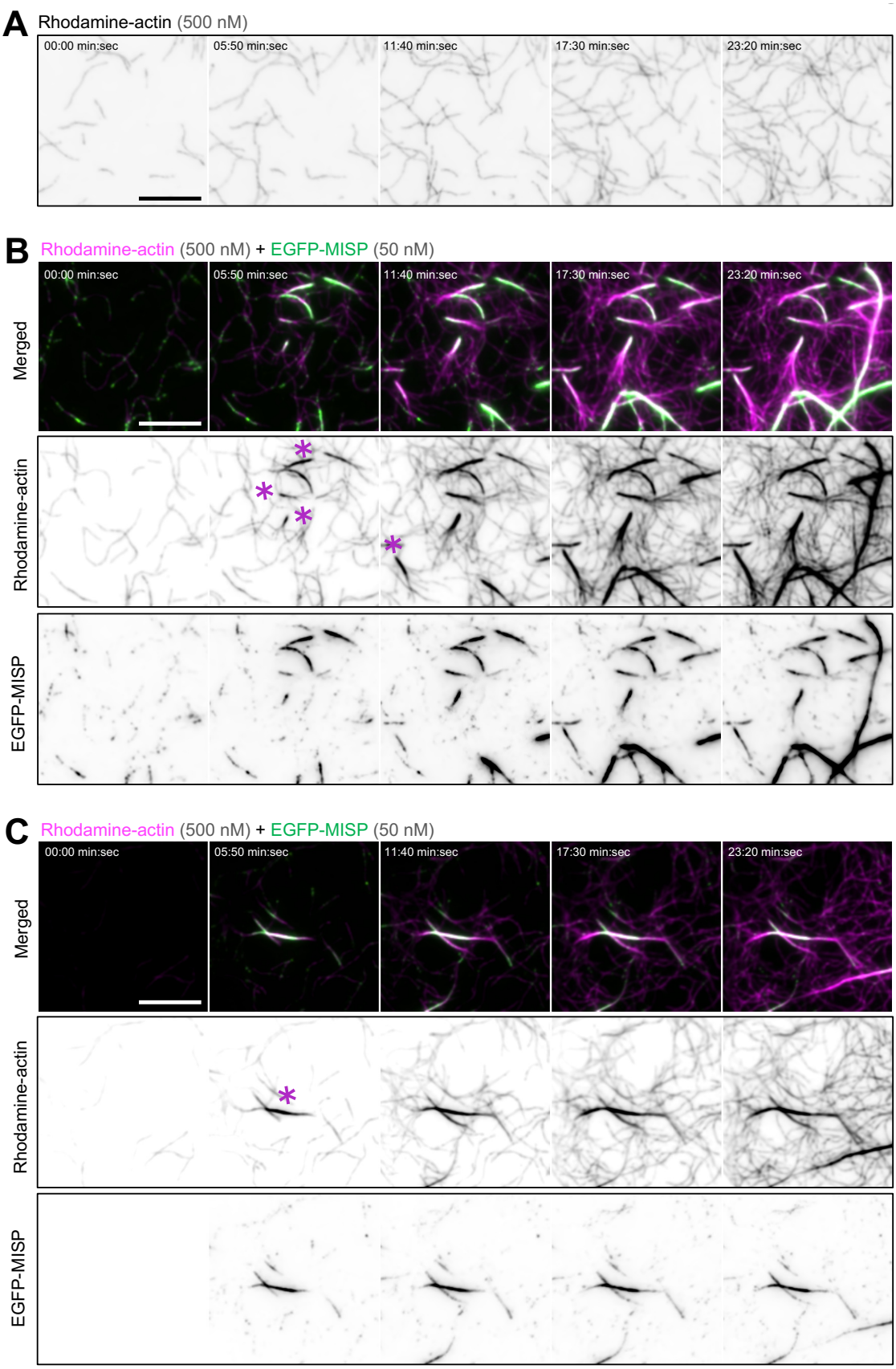
A
Rhodamine-actin (500 nM)
00:00 min:sec
05:50 min:sec
11:40 min:sec
17:30 min:sec
23:20 min:sec
B
Rhodamine-actin (500 nM) + EGFP-MISP (50 nM)
Merged
Rhodamine-actin
EGFP-MISP
C
Rhodamine-actin (500 nM) + EGFP-MISP (50 nM)
Merged
Rhodamine-actin
EGFP-MISP

Figure 4-7. MISP assembles multi-filament parallel and antiparallel bundles
(A-C) TIRF microscopy montages of biotin-rhodamine F-actin (magenta), and EGFP-MISP (green). (A) Control experiment without EGFP-MISP. (B) Multi-filament parallel bundling events driven by EGFP-MISP. (C) Multi-filament antiparallel bundling events driven by EGFP-MISP. Scale bar = 10 μm.

Discussion

Using *in vitro* reconstitution assays coupled with TIRF microscopy, we showed that the microvillar protein MISP directly binds to single actin filaments employing two modalities: end binding (i.e., near pointed ends) and side binding (i.e., ADP F-actin) (Figure 4-2; Figure 4-4, 4-5). These binding mechanisms agree with MISP's selective localization to microvillar rootlets (Morales et al., 2022), which are predominantly comprised of aged filaments and their pointed ends (Hirokawa et al., 1982; Loomis et al., 2003; Meenderink et al., 2019; Tyska & Mooseker, 2002). Live-imaging bundling assays further showed that MISP holds the potential to create multi-filament arrays of antiparallel and parallel bundles, the latter conformation presumably orchestrated by its pointed end- and side-binding ability. These findings highlight the role of MISP as a bundler that may contribute to establishing the polarity of core bundles early in microvillar assembly.

Dwell time assays on three F-actin nucleotide states (ADP, ADP-Pi, and AMP-PNP) revealed that MISP can discriminate among all these filament conformations exhibiting slow dissociation rates from ADP F-actin (Figure 4-2), which likely confers stronger affinity for this nucleotide state as no major differences in association rates were observed (Figure 4-1 C-E). This is consistent with cell and tissue immunostaining showing MISP's selective localization to microvillar core rootlets (Morales et al., 2022), which are expected to be enriched in ADP F-actin as core bundles undergo treadmilling during

microvilli assembly (Loomis et al., 2003; Meenderink et al., 2019; Tyska & Mooseker, 2002). While it is uncertain whether treadmilling persists in fully matured native intestinal microvilli, the selective labeling of their rootlets by cofilin suggests that these ends may remain enriched in ADP F-actin. (Figure 4-1 A). The fact that MISP and cofilin share a similar localization to rootlets further suggests that their preferential binding to ADP F-actin is not mutually exclusive, but rather may coexist at those ends. Recent ultrastructural studies showed that ADP-bound filaments display a flexibility that may expose multiple binding sites in addition to those triggered by phosphate release alone (Oosterheert et al., 2022; Reynolds et al., 2022), which may further prime the association of multiple nucleotide-sensing factors.

Why would a microvillar factor preferentially “sense” ADP F-actin? MISP localization at rootlets is required for microvilli assembly and maintenance (Morales et al., 2022). Such restriction of MISP to rootlets is partially exerted by the membrane-cytoskeleton crosslinking activity of ezrin (Morales et al., 2022). Thus, nucleotide-sensing may represent an alternative mechanism for restraining MISP targeting and function solely at rootlet ends. Whether the nucleotide composition of filaments controls the selective binding of ezrin or other factors to the membrane-wrapped segment of core bundles remains unknown. However, previous *in vitro* reconstitution assays indicate that myosin-6, a membrane-cytoskeleton crosslinker, exhibits preferential binding to aged filaments (Zimmermann et al., 2015), which may contribute to its membrane tethering function near microvillar rootlets (Hegan et al., 2012).

Moreover, bundling proteins can generate specific spatial configurations on multi-filament bundles that may create a sorting mechanism to favor or restrict the binding of

other factors (Winkelman et al., 2016). In treadmilling microvilli, MISP selective bundling of ADP-bound actin filaments may confer the rootlet ends with unique properties that favor the recruitment of other rootlet-enriched factors. One such factor is fimbrin, a bundling protein that displays preferential binding to MISP-bundled filaments (Grimm-Günter et al., 2009; Morales et al., 2022). Both MISP and fimbrin are the only microvillar bundling proteins that cooperate to elongate and stabilize the rootlets, presumably reflecting their specific targeting to these ends (Morales et al., 2022). Although speculative, the nucleotide composition of microvillar core actin bundles may segregate factors to specific regions that may ultimately define the boundaries of membrane-wrapped versus unwrapped segments of core bundles.

Actin dynamics assays further revealed that MISP preferentially binds near the pointed ends of filaments displaying long dwell times at these ends relative to the filament side (Figure 4-3 E-F). Although our experimental setup prevented us from studying whether MISP regulates actin dynamics at those ends, previous overexpression experiments show that MISP promotes rootlet elongation (Morales et al., 2022). This raises the possibility that MISP may favor monomer incorporation at these ends, presumably by removing cappers such as Tmod3 from microvillar pointed ends. Consistent with this, recent studies indicate that the actin bundler espin displays anti-capping activity at the barbed ends, which likely reflects its ability to create long microvillar protrusions when overexpressed (Loomis et al., 2003; Zheng et al., 2022). Our findings provide insights that may explain how actin bundling proteins promote the elongation of actin-based protrusions in cells.

Why would an F-actin bundler exhibit both end and side binding? Having both filament pointed end and side binding potential may be convenient for crosslinking and orienting newly polymerizing filaments into a polarized core bundle. In the case of filopodia, core bundles supporting protrusions have their basal pointed ends crosslinked to filament sides by the Arp2/3 complex, serving as an anchoring platform for orienting filaments during protrusion growth (Svitkina & Borisy, 1999). Given that microvilli assemble in an Arp2/3-independent fashion (Grega-Larson et al., 2015), it remains unclear how their core bundle polarity is established. Our bundling assays indicate that MISP assembles both parallel and antiparallel F-actin bundles (Figure 4-6), which is consistent with MISP localization to the unipolar core bundles of microvilli and the mixed polarity bundles of stress fibers (Kumeta et al., 2014; Morales et al., 2022). Yet, MISP holds the capacity to assemble multi-filament parallel bundles consisting of more than two filaments (Figure 4-7), suggesting that MISP may be sufficient to create higher-order actin bundles of uniform polarity under certain conditions. Although such conditions are still undefined, coordinated coupling of filament elongation and crosslinking have been recently invoked to favor the resulting organization of polarized parallel bundles (Sherer & Courtemanche, 2022). Fimbrin can assemble parallel bundles *in vitro* (Glenney et al., 1981), but its recruitment to microvillar rootlets seems to be MISP-dependent (Morales et al., 2022). Espin is another microvillar bundler capable of creating bundles with uniform polarity in cells (Loomis et al., 2006), although its late accumulation during microvilli differentiation is at odds with orchestrating bundle polarity (Bartles et al., 1998). Thus, as an early microvillar factor with the ability to preferentially bind and crosslink filaments near

their pointed ends, MISP may be a candidate for establishing the polarity of core bundles early in microvillar assembly.

If MISP were not sufficient to assemble core bundles of uniform polarity, it may still contribute to organizing filament polarity with other early barbed end-specific proteins. One such factor is Epidermal Growth Factor Receptor Pathway Substrate 8 (EPS8), a tip-specific microvillar protein that also holds bundling potential *in vitro* (Croce et al., 2004; Gaeta et al., 2021; Hertzog et al., 2010). Like MISP, EPS8 is an early factor that strongly localizes at the apical region of immature enterocytes within intestinal crypts (Gaeta et al., 2021; Morales et al., 2022). Given their end-specific targeting and bundling functions, it is tempting to speculate that EPS8 and MISP may orchestrate the polarity of nascent core bundles from their barbed and pointed ends, respectively. Future cell and single-molecule temporal visualization studies will be required to determine whether these factors are sufficient to assemble newly polymerizing filaments into parallel actin bundles (Gaeta et al., 2021).

Previous studies have found that bundling proteins can self-segregate within the same actin networks, which may further promote the sorting of other actin-binding factors by competition or by the differential filament interspacing they create (Christensen et al., 2017; Winkelman et al., 2016). Our findings revealed a previously unrecognized nucleotide-sensing feature of bundling proteins that may drive their sorting along actively treadmilling filaments. This intrinsic segregation of bundlers further provides a mechanistic explanation for the observed differential protein composition along the length of polarized protrusions. Whether the nucleotide composition of filaments in core bundle

protrusions ultimately dictates the ultrastructural features of fully mature protrusions will be an interesting venue for future research.

CHAPTER V

CONCLUSIONS AND FUTURE DIRECTIONS

Conclusions[1]

The work presented here identifies MISP as a fourth actin bundling protein in brush border microvilli (Chapter III) in addition to the previously documented bundlers villin, fimbrin, and espin (Bartles et al., 1998; Bretscher & Weber, 1979, 1980b). Having multiple factors with apparent redundant functions highlights the remarkable evolutionary robustness of epithelial microvilli to maximize the surface area for nutrient absorption and reabsorption in hollow organs of the body.

Yet, MISP functions as an unconventional bundler by selectively targeting and maintaining the membrane-free rootlet ends of microvilli, thus promoting brush border assembly (Chapter III). At least two mechanisms are responsible for MISP restriction to the rootlet ends: an extrinsic mechanism driven by the membrane-cytoskeleton crosslinker ezrin (Chapter III); and an intrinsic mechanism driven solely by the preferential binding of MISP to the pointed ends of aged actin filaments (Chapter IV). These confinement mechanisms for rootlet maintenance further highlight the role of these ends as anchors that mechanically stabilize the membrane-encapsulated protruding core bundle. As bundling proteins can sort other actin-binding factors depending on the inter-filament spacings they arrange (Winkelman et al., 2016), rootlet-specific bundlers such

[1] *Some paragraphs from this section were published in: Morales, E. A., Arnaiz, C., Krystofiak, E. S., Zanic, M., & Tyska, M. J. (2022). Mitotic Spindle Positioning (MISP) is an actin bundler that selectively stabilizes the rootlets of epithelial microvilli. Cell reports, 39(3), 110692.*

as MISP may further create specific “micro-niches” at the rootlets that are suitable for other factors to associate. Moreover, MISP is an early microvillar factor that exhibits both actin-bundling activity and preferential binding to the pointed ends (Chapter III, IV). These complementary functions are well suited for a factor to establish the polarity of filaments that make up the core bundle of microvilli, yet whether MISP meets such demand remains an open question for future investigations.

The primary limitations of the current work are technical. In the intestinal tract, the brush border microvilli assemble on the surface of nascent enterocytes during differentiation as these cells migrate out of stem cell-containing crypts on to the villus. Recapitulating the biochemical and morphological transition that these cells undergo in a laboratory is a major challenge for researchers. In this work, our findings in Chapter III are based largely on data derived from epithelial cell culture models, namely the W4 (Baas et al., 2004) and CACO-2_{BBE} cell lines (Peterson et al., 1993; Peterson & Mooseker, 1993), which are both limited in the extent to which they reflect the mechanistic details and nuances of the native process. Although not employed in the current work, intestinal organoid cultures promise the experimental accessibility afforded by cell culture models while more faithfully recapitulating the phenotypic details of differentiated intestinal epithelial cells *in vivo* (Date & Sato, 2015). Our findings in Chapter IV were based on a two-component minimal reconstitution assay. Although these findings provide a mechanistic explanation for our observations in cell culture models, how other actin-binding factors influence MISP binding and bundling of actin remains elusive. As many actin-binding proteins are now commercially available, we may be able to incorporate

some factors of interest in our reconstitution assays. We will propose future studies to address some of these limitations in the following sections.

Overall, by investigating the targeting and functional mechanisms of MISP across various biological scales ranging from cell culture models to minimal reconstituted systems, we have gained a deep mechanistic understanding of MISP function as an actin-binding factor. Our findings have evoked exciting new questions, some of which aim to further explore preliminary observations, and others aim to determine the functional relevance of MISP *in vivo*.

Mechanisms of MISP-driven elongation and maintenance of rootlets

How does MISP contribute to rootlet elongation?

Does MISP antagonize with end-capping proteins at microvillar rootlets? Actin bundling proteins have been traditionally viewed as factors that passively crosslink adjacent actin filaments. However, actin bundling proteins can also promote other functions such as nucleation, elongation and severing of actin structures (Glenney Jr. et al., 1981; Loomis et al., 2003; Revenu et al., 2007). In Chapter III, we found that MISP overexpression in intestinal epithelial cells creates long microvillar rootlets, while its overexpression in non-epithelial cells generates actin cables (Morales et al., 2022). Another bundler displaying a similar phenotype when overexpressed is espin, which generates long microvilli in kidney epithelial cells, and aberrant cytosolic bundles in neuronal cells (Loomis et al., 2003, 2006). Recent biochemical studies revealed that espin

holds anti-capping activity in addition to its well-known bundling function (Zheng et al., 2022). Specifically, espin competes with capping protein, a barbed end-specific capper, to drive polymerization from barbed ends (Zheng et al., 2022). These findings suggest that in addition to their well-known filament crosslinking role, bundling proteins may serve other functions such as competing with end-specific factors to promote the elongation of polarized core bundles.

How MISP promotes rootlet elongation remains an open question. However, our findings that MISP preferentially binds to the pointed ends are suggestive of an anti-capping activity at the rootlet ends. The only known pointed end capping protein in microvilli is tropomodulin-3 (Tmod3), which is endogenously enriched in the brush border of native intestinal tissue and CACO-2_{BBE} cells (Uhlén et al., 2015; K. L. Weber et al., 2007) (Figure 5-1 A). Our preliminary overexpression studies show that Tmod3 also localizes to the microvillar rootlets of W4 cells (Figure 5-1 B), which resembles MISP selective targeting to these ends (Morales et al., 2022). Using W4 cells as a biological system, we could determine whether MISP promotes rootlet elongation at the expense of outcompeting Tmod3 from rootlets. These experiments could be done by overexpressing either protein with a fluorescent tag and staining for the endogenous version of the other factor using SIM microscopy. Previous overexpression studies in myofibrils indicate that tropomoduline promotes the shortening of actin filaments, presumably as a result of its pointed end capping activity (Littlefield et al., 2001). Thus, we anticipate that Tmod3 overexpression in W4 cells will reduce MISP intensity levels accompanied by shorter rootles. Similarly, we predict that MISP overexpression will reduce Tmod3 intensity levels accompanied by the characteristic long rootlets that MISP generates. These predicted

changes could provide evidence for a possible competition between MISP and Tmod3 for the pointed ends, which might ultimately be responsible for regulating the growth of rootlets.

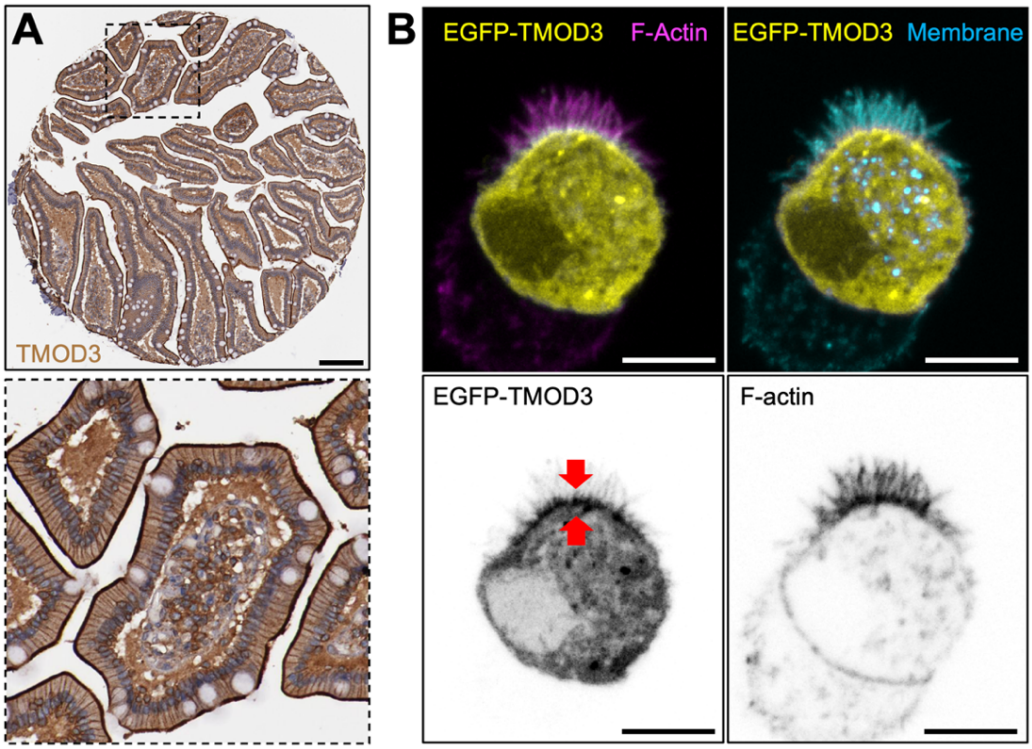

Figure 5-1. Tmod3 enriches at the rootlets of microvilli
(A) H&E staining of human small intestine stained for Tmod3 (brown) extracted from the Human Protein Atlas (Uhlén et al., 2015). The dashed box corresponds to the zoomed area. Scale bar = 200 μm.
(B) Laser-scanning confocal microscopy image of a W4 cell overexpressing EGFP-Tmod3 (yellow), stained for F-actin with phalloidin (magenta), and membrane with WGA (cyan). The top panels show two-color images; the bottom panels show inverted single channels. Red arrows indicate Tmod3 enrichment to rootlets. Scale bar = 7 μm.

Is MISP an anti-capping protein specific to the pointed ends? End-specific factors binding to either the barbed ends or the pointed ends are expected to module the kinetics at those ends. These factors may either favor the incorporation of actin monomers,

serving as anti-cappers such as Ena/VASP (Krause et al., 2003); or block the addition of monomers, functioning as cappers such as Tmod3 (Fischer et al., 2003). Thus, an alternative experimental approach to test if MISP functions as an anti-capping protein at the pointed ends is to directly visualize its effect on monomer incorporation at the pointed ends in the presence of Tmod3.

In our *in vitro* reconstitution assays, the polymerization conditions favored only the incorporation of monomers at the barbed ends, while maintaining the growth from the pointed ends unchanged. One limitation of studying actin dynamics at the pointed ends is their slow rate of polymerization compared to the barbed ends, which grow ~10 times faster (Kuhn & Pollard, 2005). For instance, under conditions favoring polymerization at both ends, by the time the pointed ends grow ~1 μm, the barbed ends will grow ~10 μm, which overcrowds the field of view and impairs tracking polymerization dynamics at the pointed ends. One way to overcome this limitation is to block polymerization from the barbed ends using Cytochalasin D, which binds to the barbed ends at a 1:1 molar ratio (Goddette & Frieden, 1985). Alternatively, the barbed ends can be conjugated with commercially available barbed-end cappers such as Gelsolin (Cytoskeleton, Inc.). Using any of these strategies, which have been used in previous biochemical and single molecules studies (Shekhar, 2017), we could be able to investigate actin dynamics at the pointed ends.

Once polymerization from the barbed ends is blocked, we may be able to test the effect of MISP on the actin dynamics at the pointed ends. One way to test this could be by saturating stabilized filaments (conjugated with either Cytochalasin D or Gelsolin) with a nonfluorescent version of Tmod3 (OriGene), which will result in filaments with both ends

capped. We could subsequently flow in monomeric actin above the critical concentration for pointed end elongation (> 0.6 μM). This control experiment should result in no filament polymerization from either end (Figure 5-2; control). To test if MISP holds anti-capping activity, we could flow in MISP at saturating concentrations before the incorporation of actin monomers. A subsequent elongation from the pointed end (i.e., slow rate) will be indicative of an anti-capping activity driven by MISP (Figure 5-2; test). Given that these assays consist of multiple steps, it is important to always incorporate Cytochalasin D / Gelsolin in all reactions in order to minimize barbed end polymerization, especially when soluble actin is being added. The proposed reconstitutions assays should provide direct evidence to determine whether MISP functions as an anti-capping protein, which could further provide a mechanism by which it promotes core bundle elongation.

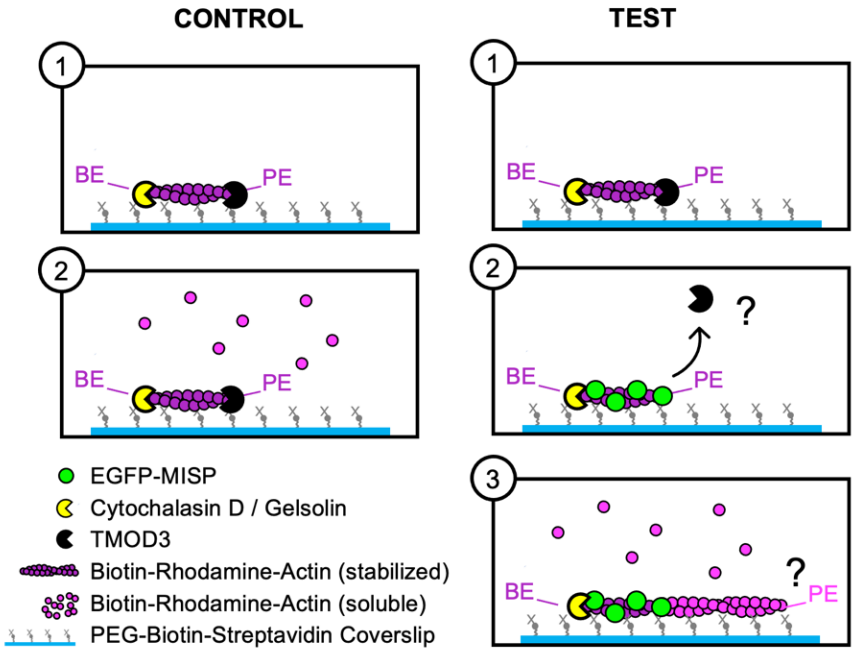

Figure 5-2. Proposed assays to test MISP anti-capping activity at the pointed ends
The left column shows control conditions with phalloidin-stabilized filaments capped at the barbed ends with Cytochalasin D/ Gelsolin; and at the pointed ends with Tmod3. No polymerization is expected under these conditions. The right column shows similar conditions as before, but MISP is incorporated at saturating concentrations to determine if it can displace Tmod3 from the pointed ends and allow actin polymerization.

How does MISP contribute to rootlet maintenance?

To date, cofilin is the only actin binding protein with a strong affinity for ADP F-actin over other nucleotide states (Blanchoin & Pollard, 1999). Such preferential binding of cofilin triggers the severing and depolymerization of these aged filaments, which promotes the turnover of actin filaments in cells (Lappalainen & Drubin, 1997). Our *in vitro* reconstitution assays indicate that MISP also displays a selective targeting to ADP-bound filaments. However, unlike cofilin, MISP stabilizes the rootlets and reduces the turnover of microvillar core bundles (Morales et al., 2022). Intriguingly, despite their antagonistic function, cofilin and MISP coexist at microvillar rootlets (Figure 4-1). We speculated that MISP may be protecting filaments from cofilin-driven severing and depolymerization. To test this, we set up an *in vitro* reconstitution approach by immobilizing aged actin filaments (i.e., ADP F-actin) on a coverslip as described in Chapter IV. We next coated these filaments with EGFP-MISP molecules at high concentrations, and subsequently incorporated cofilin (Cytoskeleton, Inc). Following this procedure, our preliminary results suggest that MISP may reduce the rate of actin depolymerization, and delay the severing of actin filaments (Figure 5-3). Although MISP seems to protect filaments from depolymerization, the concentration of cofilin used in this preliminary experiment severed filament at a higher rate, which prevented us from quantifying multiple events. Considering that the severing activity of cofilin of filaments is concentration dependent (Carlier et al., 1997), it could be necessary to titrate various concentrations to determine optimal conditions compatible with the image acquisition timeframe. Once optimal conditions are established, we could be able to quantify the severing rates of actin filaments with or without MISP decoration.

Another way to address this hypothesis and further complement our *in vitro* experiments is to conduct cellular assays. In cells, cofilin activity is controlled by two factors: LIMK, which phosphorylates cofilin to its inactive state; and SSH, which dephosphorylates cofilin into its active state. Small molecule inhibitors targeting either LIMK or SSH have been widely used to increase or decrease the pool of active cofilin in cells, respectively (Lee et al., 2017; Ross-Macdonald et al., 2008). Using the LIMK inhibitor to increase the pool of active cofilin in W4 cells, preliminary data from our lab have found that cells display shorter microvilli, presumably leading to the disassembly of microvilli. As cofilin is highly enriched at microvillar rootlets, one possibility is that a high pool of active cofilin may sever these ends, leading to the collapse of the brush border. Is MISP protecting the rootlets from cofilin-driven severing and rootlet disassembly? We could address this question using live-cell imaging assays and perturbations with small-molecule inhibitors. We propose to use the LIMK inhibitor to increase the pool of active cofilin in W4 cells expressing EGFP-MISP and mCherry-UtrCH (an actin marker). We could then monitor actin rootlet dynamics (i.e., severing, bending, disassembly) over time in cells overexpressing MISP and cells with normal MISP levels. It would also be interesting the determine whether cofilin-driven microvillar collapse can be delayed or prevented in cells displaying long rootlets, as those found when MISP is highly abundant. These experiments can be further complemented with fixed samples using SIM to accurately measure changes in core actin dimensions, not limited to length but also thickness (related to the number of filaments), and straightness (related to the stiffness of core bundles). The latter parameter is particularly interesting as the rootlets of microvilli exhibit a bending conformation in W4 cells, presumably as a result of cofilin binding

(McCullough et al., 2008). We anticipate that LIMKi3-driven overactivation of cofilin will result in shorter and more curved rootlets. We also predict that MISP levels will be reduced as a result of increased cofilin, which could be quantified in both conditions using antibodies targeting the total MISP content.

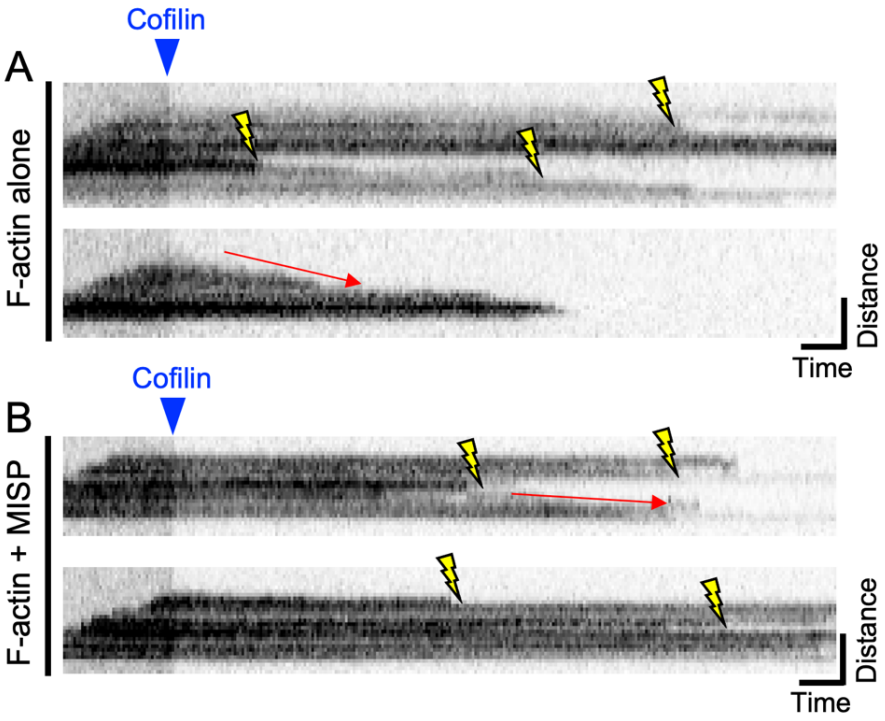

Figure 5-3. Preliminary assays showing MISP-driven filament protection from severing and depolymerization
TIRF microscopy kymographs showing polymerizing actin filaments (black) with no MISP decoration **(A)** or with MISP decoration (100 nM) **(B)**, exposed to cofilin (250 nM). Red arrows show depolymerization events. Yellow symbols show severing events. Note the slower depolymerization rates and late severing events in conditions where filaments were saturated with MISP. A nonfluorescent purified MISP was used in these assays.

Mechanisms of parallel actin bundling by MISP

Is MISP confinement required to assemble actin bundles of uniform polarity?

The specific binding to the pointed ends of actin filaments posits MISP as a factor that may orchestrate the assembly of microvillar core actin bundles in a polarized manner. Although not exclusively, our *in vitro* reconstitutions assays show that MISP holds the capacity to assemble parallel actin bundles containing multiple actin filaments. What additional conditions does MISP need to exclusively assemble parallel bundles of actin? One limitation of our *in vitro* reconstitution bundling assays is that both MISP and polymerizing actin filaments were freely diffusing in solution, which likely decreases MISP's encounters with pointed ends. Given that MISP is unstable as a soluble protein, MISP may remain confined to pre-existing networks to promote microvillar assembly (Kumeta et al., 2014; Morales et al., 2022). In our preliminary *in vitro* reconstitution assays, we observed that MISP promotes the formation of aster-like actin networks (Figure 5-4 A), which suggests that MISP can bundle actin filaments from the ends, presumably the pointed ends. Consistent with these observations, we also found examples of single MISP punctum anchoring multiple filaments from their slow-growing pointed ends (Figure 5-4 B). Thus, we speculate that the confinement of MISP or pointed ends to reduced areas could be a prerequisite for bundling filaments in a polarized manner. We could be able to mimic such confinement using two *in vitro* reconstitution strategies with TIRF microscopy.

The first strategy consists in immobilizing EGFP-MISP molecules in antibody-coated microbeads (~5 μm; Bangs Laboratories, Inc), and triggering actin polymerization

in TIRF flow channels preloaded with beads. In this way, one could increase the probability of pointed end capturing events as filaments will be very short. In fact, bundling of short filaments as opposed to long filaments has been recently found to influence the resulting organization of polarized bundles (Sherer & Courtemanche, 2022). We predict that actin filaments will grow out of the microsphere. Although the rate of actin polymerization can inform us which end will be growing outwards, we could also determine the polarity of filaments flowing in fascin (Cytoskeleton, Inc.), which exclusively bundles actin in a parallel manner (Breitsprecher et al., 2011; Jansen et al., 2011), thus leaving antiparallel filaments free. Similar confinement strategies of actin binding proteins have been used to determine their sorting and evaluate their contribution to the assembly of actin networks in reconstitution assay (Winkelman et al., 2016).

The second strategy consists in confining actin filaments so that all their pointed ends will be exposed outwards. This could be conducted by immobilizing phalloidin-stabilized actin filaments of ~10 µm on the surface microsphere beads from their barbed ends using gelsolin (Cytoskeleton, Inc.). These will generate freely diffusing pointed ends confined in a smaller area. Subsequently, EGFP-MISP molecules can be flowed in at low concentrations to determine if MISP can selectively bundle filaments from their pointed ends. This hypothesis is consistent with the existence of other factors that organize the barbed ends of filaments, such as EPS8, a barbed end-specific factor in microvilli that can bundle filaments (Disanza et al., 2006; Hertzog et al., 2010). Ena/VASP is another filopodia factor that selectively bundles filaments at the barbed ends while promoting their elongation (Winkelman et al., 2014).

Considering that spontaneous polymerization of actin can mask the reaction in all *in vitro* reconstitution assays, the results can be difficult to interpret. If this is the case, one can incorporate profilin and formin into the reaction (Cytoskeleton, Inc.), which will reduce spontaneous nucleation. Taken together, the proposed experiments may provide mechanistic insights on how core actin bundles acquired their intrinsic polarity that results in microvillar protrusions.

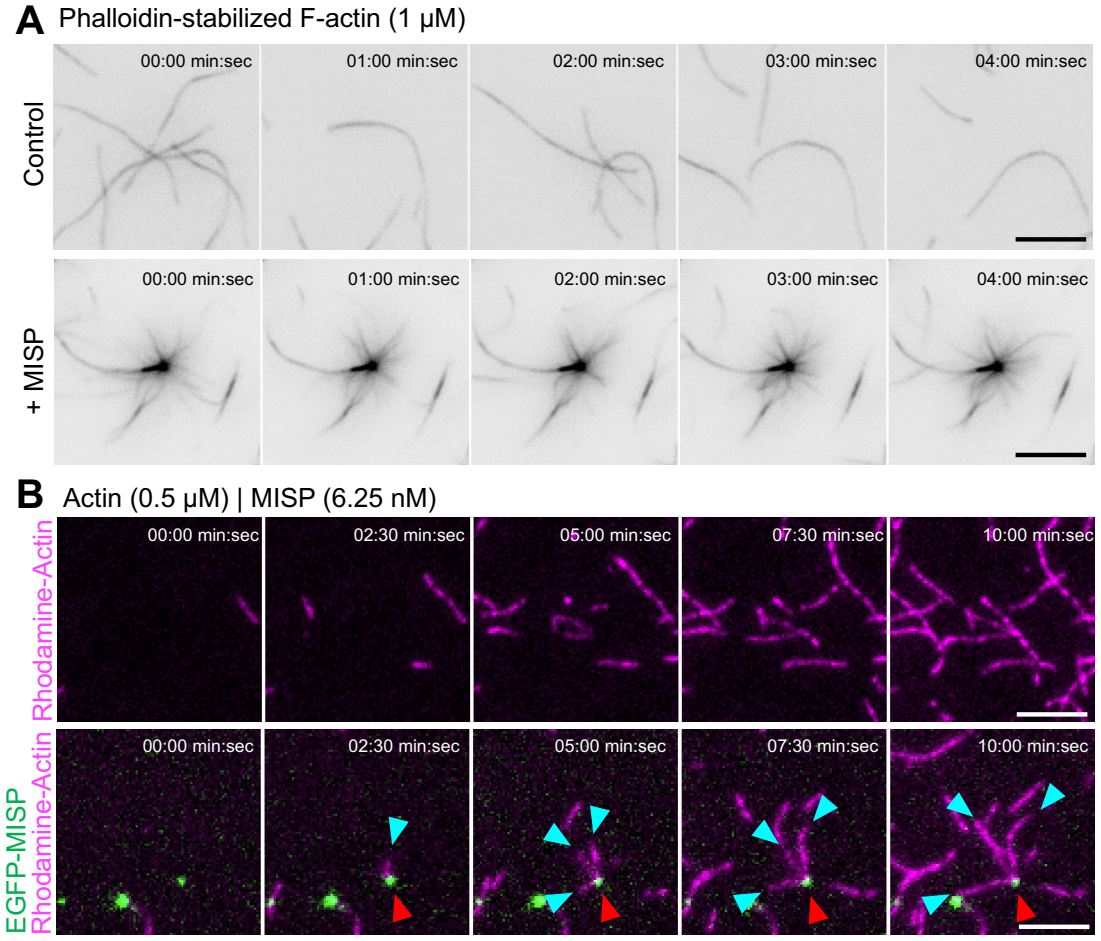

Figure 5-4. Preliminary experiment showing MISP-driven aster-like actin networks
(A) TIRF microscopy movie showing stabilized actin filaments (black) pre-assembled with MISP ('+MISP') or without ('control'). The latter condition shows the formation of an aster-like actin network. Scale bar = 5 μm.
(B) TIRF microscopy movie showing a polymerizing actin filament (magenta) from barbed ends only. The top row shows conditions without MISP. The bottom row shows conditions with MISP (green). Note MISP green punctum anchoring up to three filaments from their pointed ends. Scale bar = 5 μm.

Functional and targeting determinants of MISP to rootlets

What are the structural determinants for MISP targeting to the rootlets?

An actin bundling protein must have at least two actin binding motifs in its amino acid sequence in order to crosslink two adjacent actin filaments into a bundle (Matsudaira, 1991). Although not fully characterized, previous biochemical studies indicate that MISP has at least three actin-binding fragments (AB) spanning across its 679 amino acid sequence (Kumeta et al., 2014) (Figure 5-5 A). In preliminary structure/function experiments, we created two large constructs containing each half of the full-length protein: one construct harboring the first predicted fragment (MISP-AB^{1}; 1-317 aa); and another half harboring the other two predicted fragments (MISP-AB$^{2-3}$; 318-679 aa) (Figure 5-5 A). Interestingly, when these constructs were overexpressed in W4 cells, they no longer displayed the selective targeting of full-length MISP to the rootlet ends of microvilli; construct MISP-AB^{1} decorated the entire core actin bundle overlapping with phalloidin staining, whereas construct MISP-AB$^{2-3}$ seem to retain its rootlet-specific labeling with a partial decoration of distal segment of the core bundles (Figure 5-5 B-D). These findings suggest that the actin-binding motifs conferring MISP with the specificity for rootlet binding may be positioned between amino acids 318 and 679 (MISP-AB$^{2-3}$).

Using UniProt, we conducted a multiple alignment analysis of sequences corresponding to MISP and other proteins harboring actin binding motifs. We began by aligning MISP with other actin bundling proteins to identify possible similarities with actin binding motifs. Interestingly, we found a short, conserved motif in MISP sequence that is positioned within the predicted AB^{3} (ABM: 552-570 aa), which coincides with sequences

corresponding to the actin binding motifs of espin (Figure 5-6 A). Thus, we propose to generate fluorescently tagged versions of MISP containing the large actin-binding fragment AB^3, and our predicted actin-binding motif (ABM) to determine whether this motif confers the observed targeting specificity to microvillar rootlets. (Figure 5-6 E).

We also found a putative WH2 domain within MISP sequence, which we aligned with WH2 domains of other proteins from multiple species (Figure 5-6 B). Interestingly, a short sequence (391- 420 aa) within the previously described AB^2 (Kumeta et al., 2014) seems to contain identical features corresponding to canonical WH2 domains. Canonically, WH2 domains consist of a short alpha-helix, followed by a linker and four conserved amino acids. While the alpha-helix interacts with the hydrophobic cleft of actin, the conserved four-amino acid sequence interacts with the nucleotide-binding cleft of actin through the hydrophobic residues (Figure 5-6C-D) (Chen et al., 2013; Dominguez, 2016). It is worth noting that although WH2 domains are commonly present in actin nucleators, they can also be present in other proteins such as elongator factor and even bundling proteins across multiple species (Figure 5-6 B) (Dominguez, 2016). In this case, we propose to conduct mutations targeting hydrophobic residues (i.e., I398 or V414) found within the predicted WH2 domain of MISP, as these mutations have been reported to disrupt interactions with actin (Chen et al., 2013) (Figure 5-6 E).

Taken together, we propose to overexpress these proposed constructs in W4 cells and determine whether they target specifically to rootlets (Figure 5-6 E). Considering that various WH2-containing proteins bind near the pointed ends of actin (Dominguez, 2016), we anticipate that our predicted WH2 domain may be responsible for MISP's selective targeting to these ends of actin filaments. In addition to testing rootlet targeting of these

truncates, we also propose to conduct measurements of rootlet elongation that each of these constructs could generate and evaluate possible bundling defects.

In Chapter IV, we found that MISP depicts two distinct binding modalities: filament side (i.e., ADP F-actin) and filament end (i.e., pointed ends). As rootlets are expected to be enriched in both ADP F-actin and pointed ends, a construct sufficient to target microvillar rootlets will not necessarily allow us to discriminate between a pointed end- or side-binding due to the diffraction limitation of our imaging approaches. Thus, if our proposed cell assays above identify a rootlet-specific domain, we could further attempt to purify any of these constructs to determine whether they target to pointed ends or ADP F-actin using similar reconstitution assays as described in Chapter IV. Although the full-length MISP protein is highly insoluble, short fragments of MISP have been previously purified in *E. coli* for biochemical studies (Kumeta et al., 2014).

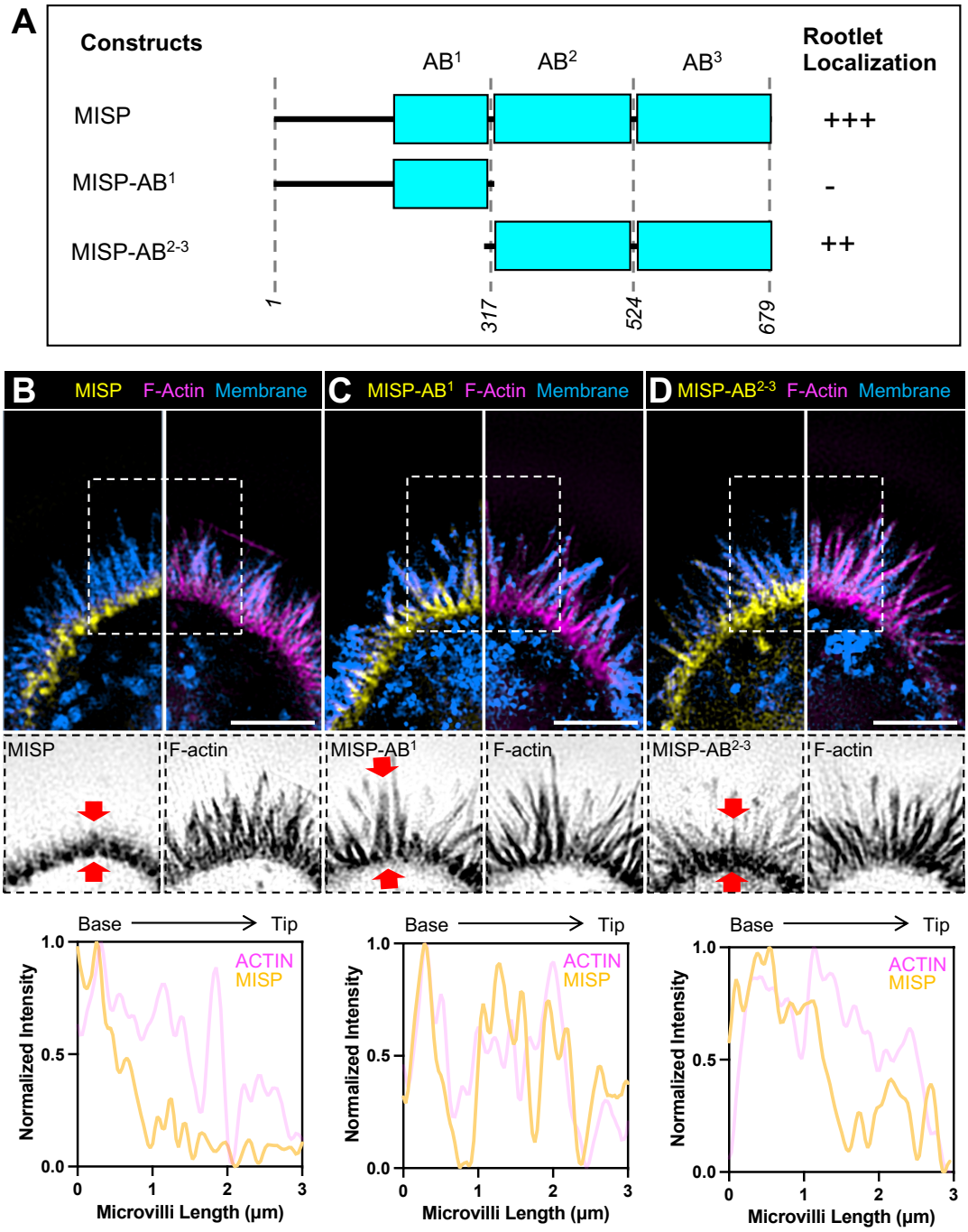

Figure 5-5. Preliminary structure/function studies of MISP in W4 cells

(A) Cartoon schematic showing the previously predicted actin-binding fragments (AB) (Kumeta et al., 2014); and the constructs we generated. '+' and '-' symbols to the right are representative of the observed intensity at the rootlets from the quantifications shown below.

(B-D) SIM images of W4 cells overexpressing EGFP-MISP (1-679 aa) (A); MISP-AB^{1} (1-317 aa) (B); or MISP-AB^{2} (318-679 aa) (C); and stained for F-actin with phalloidin (magenta), and membrane with WGA (blue). Each panel shows two-color merges with

their inverted single channels at the bottom. Scale bar = 3 μm. The bottom row shows a line scan of a single microvillus from base to tip corresponding to each of the conditions above.

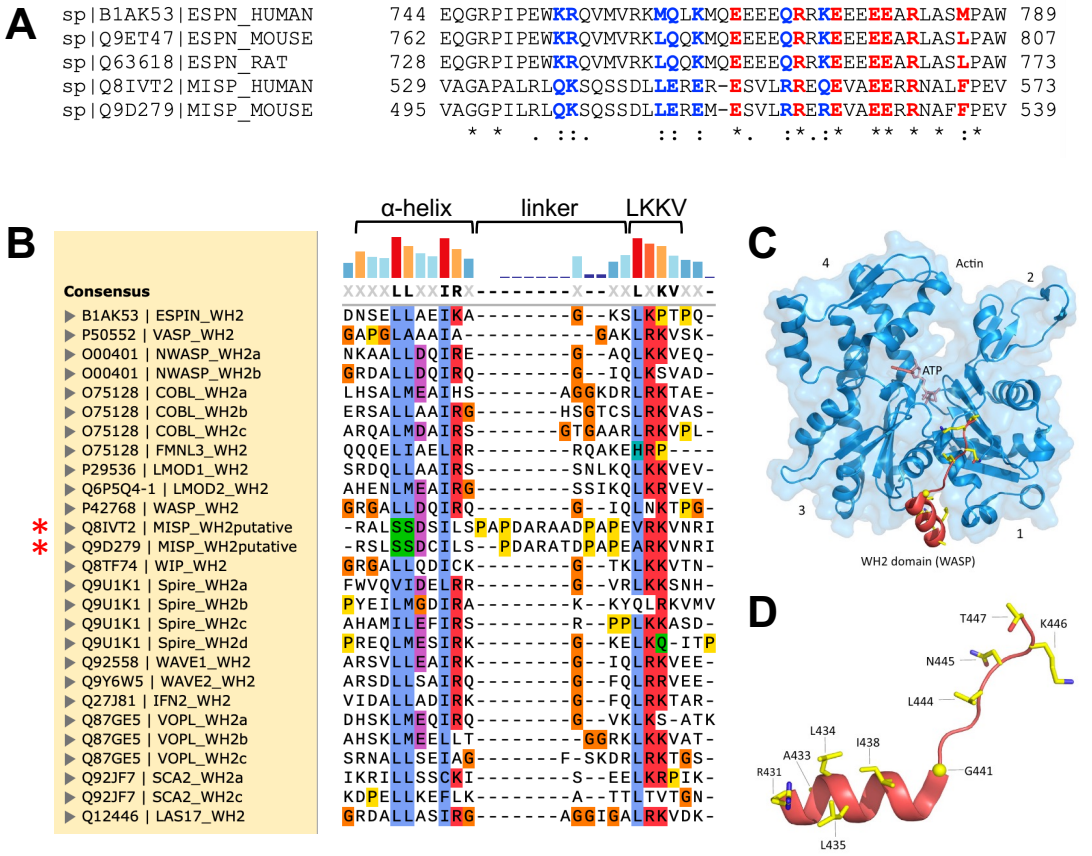

Figure 5-6. Predicted rootlet-specific binding domains within MISP sequence
(A) Multiple alignments of MISP and espin derived from various species. '*' = position of fully conserved residue; ':' = conservation between groups of strongly similar properties; '.' = conservation between groups of weakly similar properties.
(B) Multiple alignments of WH2 domains from proteins derived from various species, including the predicted WH2 region of MISP. UniProt codes for each of the WH2-containing proteins are shown on the left. Bar plots on top of sequences show the average amino acid conservation (>50%). Note that the human and mouse MISP sequences have the canonical amino acid sequence of a WH2 domain, ending with a (V/A)RKV sequence.
(C-D) Ribbon diagram of an actin monomer (blue), and the WH2 domain of WASP (red) forming a complex (C); a canonical WH2 domain of WASP harbors an LNTK sequence (D). Adapted from (Dominguez, 2016).
(E) Schematic representation of proposed EGFP-tagged MISP constructs to determine their contribution to rootlet localization. Cyan boxes represent previously characterized actin binding fragments (Kumeta et al., 2014). Magenta boxes represent our predicted WH2 domain. Yellow boxes represent our predicted actin-binding motif (ABM). The black asterisk represents the proposed mutation to disrupt the function of the predicted WH2 domain.

Do MISP and espin sort to different segments of actin bundles?

Actin bundling proteins have been previously found to segregate to distinct segments of the same bundle as a result of the interspacing between filaments they generate or by having a stronger affinity for the same actin binding sites (Winkelman et al., 2016). In microvilli, fimbrin and MISP share a similar localization to rootlets, and they both cooperate to create hyper-elongated rootlets when overexpressed (Grimm-Günter et al., 2009; Morales et al., 2022). Although other microvillar bundling proteins such as espin have been documented as canonical bundlers that localize along the full length of core bundles (Bartles et al., 1998; Loomis et al., 2003), our preliminary super-resolution studies in W4 cells suggest that espin is less enriched at rootlets relative to MISP (Figure 5-7 A-D). This apparent inconsistency is presumably the result of the short nature of rootlets (~ 400 nm) which may be imperceptible when using confocal imaging approaches

due to diffraction limitation (~ 200 nm). Moreover, our preliminary *in vitro* reconstruction assays show that an unlabeled purified version of espin bundles linear filaments of actin as previously reported (Bartles et al., 1998). Notably, EGFP-MISP preferentially bound the ends of espin-bundled filaments, which contained fewer filaments (Figure 5-7 E-F). This suggests that MISP and espin may sort to distinct domains within the same linear actin bundle, revealing a possible alternative mechanism for MISP confinement to rootlets. To better determine the possible competition between MISP and espin, we propose to create a HALO-Espin recombinant protein in the *E. coli* system, which we could use in a three-component reconstitution assay along with rhodamine-actin and EGFP-MISP. Using this approach, we could visualize whether MISP and espin sort the distinct segments of polymerizing filament as they are bundled by these factors. By visualizing two-filament parallel bundling events, we anticipate that MISP will selectively bundle aged filaments near the pointed ends, while espin will bundle newly polymerizing filaments in proximity to the barbed ends.

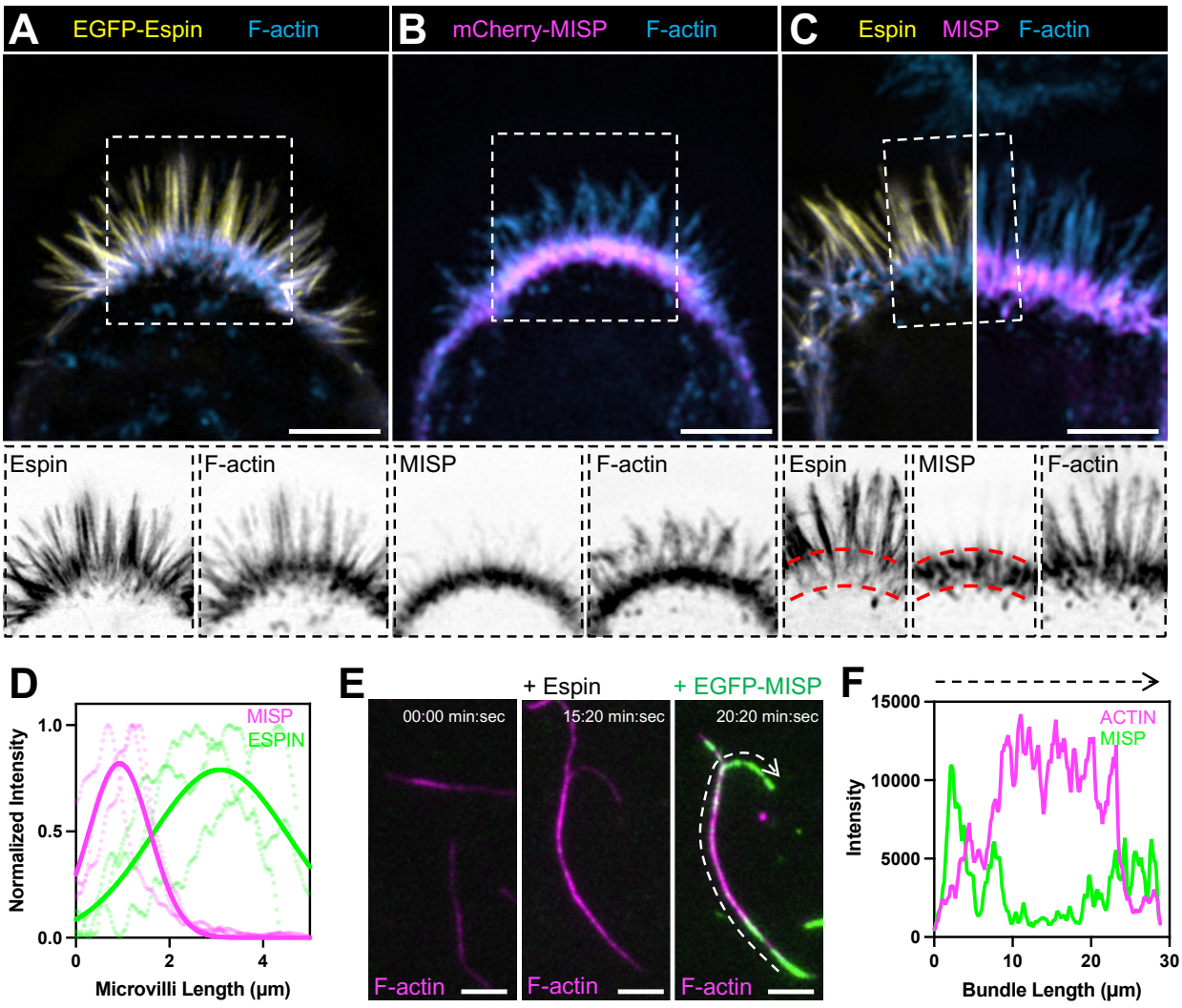

Figure 5-7. Preliminary studies showing MISP exclusion from espin-bundled actin arrays

(A-C) SIM images of W4 cells overexpressing EGFP-Espin (A); mCherry-MISP (B) or EGFP-Espin and mCherry-MISP (C); and stained for F-actin with phalloidin (blue). Each panel shows two-color merges with their inverted single channels at the bottom. Scale bar = 3 μm.

(D) Line scans of MISP (magenta) and espin (green) intensities along the base-tip axis of microvilli from C. Distributions were fit using Gaussian curves.

(E) Montage of *in vitro* reconstitution assays showing EGFP-MISP decoration of espin-bundled actin filaments (magenta). Scale bar = 4 μm.

(F) Line scans of MISP and actin intensities along the bundle delineated in E.

MISP function and localization *in vivo*

Ultrastructure and composition of the brush border in MISP KO mice

Three actin bundling proteins were identified in brush border microvilli: fimbrin, villin, espin (Bartles et al., 1998; Bretscher & Weber, 1979, 1980b). Single KO studies of villin, espin, or fimbrin in mice indicate that the brush border microvilli still assemble in each case (Ferrary et al., 1999; Grimm-Günter et al., 2009; Pinson et al., 1998; Revenu et al., 2012). However, fimbrin KO mice were the only ones displaying a phenotype at the ultrastructural level: short rootlets (Grimm-Günter et al., 2009; Revenu et al., 2012). Interestingly, such short rootlet phenotype aligns well with fimbrin's preferential accumulation to microvillar rootlets, and anchoring of rootlets to the underlying cytokeratin network (Grimm-Günter et al., 2009). Remarkably, a more recent study found that triple fimbrin/villin/espin KO mice are viable, and still assemble microvilli (Revenu et al., 2012). Two decades since the discovery of the last microvillar bundler (Bartles et al., 1998), our findings reveal that MISP is a fourth actin bundling protein in brush border microvilli. What the contribution of MISP in the context of a whole animal model remains an open question.

In collaboration with the core facility at Vanderbilt, we have engineered a MISP KO animal model (Figure 5-8). Preliminary TEM analysis of a KO mouse shows that it exhibits shorter rootlets compared to a wild-type animal (Figure 5-8 A). This is consistent with MISP KD phenotype observed in cell culture models shown in Chapter III (Figure 3-3). Moreover, although the hexagonal packing of microvilli appears to be normal in the MISP KO mouse, the overall microvillar density seems less abundant in this animal relative to the wild type (Figure 5-8 B). It is worth mentioning that these preliminary results are

derived from a single MISP KO mouse, thus further exploration should include more animals to validate these observations with statistical analysis. Considering these apparent abnormal phenotypes, we propose to quantify the overall length of core bundles, as well as the ratios between membrane-wrapped and unwrapped segments. To determine the microvillar density, we could calculate the nearest-neighbor distance, which could provide measurements of the interspacing between protrusions (Pinette et al., 2019).

Another intriguing question is whether actin filaments are equally packed along the full length of the core bundle. We found that MISP creates an inter-filament spacing of ~ 10 nm, which is slightly shorter than the inter-filament spacing exerted by other bundling proteins such as espin or villin (~ 12 nm). Thus, a strong accumulation of MISP to the rootlets may tightly pack filaments at these ends relative to filaments within the membrane-wrapped segment of microvillar protrusions. With this in mind, we propose to examine possible defects in the inter-spacing between filaments not only of membrane-wrapped core bundles, but also between filaments comprising the rootlets.

As MISP is a rootlet-specific protein required to maintain these ends, we also propose to conduct immunostainings to determine if other rootlet-specific proteins are mislocalized (i.e., fimbrin, tropomyosin, non-muscle myosin-2, cofilin). We further propose to evaluate the organization of other networks underlying the brush border such as intermediate filaments (i.e., keratin-8, keratin-19), and microtubules. We anticipate that microtubules may lack organization near the apical region given that MISP was reported to function as a linker between cortical actin and astral microtubules in dividing cells (Zhu et al., 2013).

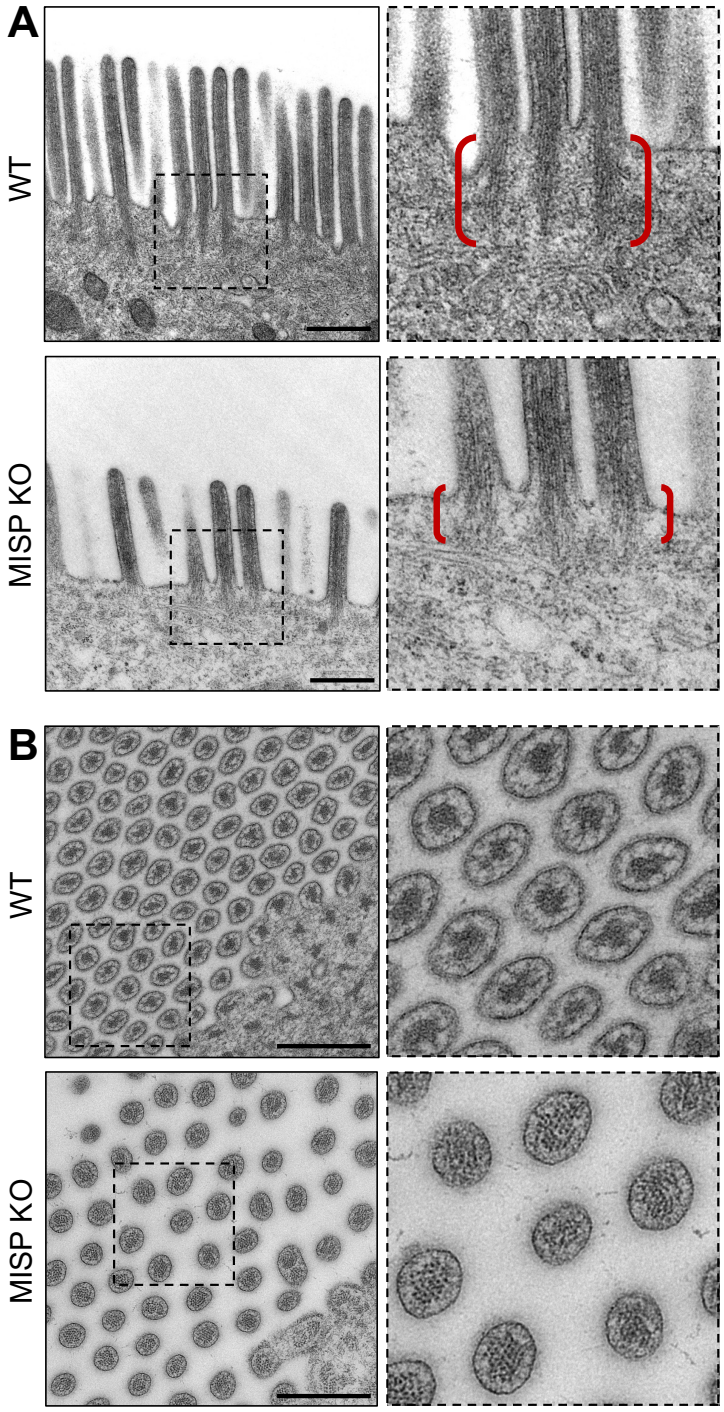

Figure 5-8. Ultrastructure of the brush border microvilli in a MISP KO mouse
(A) TEM image of the apical brush border microvilli of a WT and MISP KO mouse. This section represents a plane parallel to the microvillar axis. Black dash boxes show zooms of areas of interest shown to the right. Scale bar = 400 nm.
(B) TEM image of the apical brush border microvilli of a WT and MISP KO mouse. This section shows a plane perpendicular to the microvillar axis. Black dash boxes show zooms of areas of interest shown to the right. Scale bar = 400 nm.

What is the ultrastructural localization of MISP in native intestinal microvilli?

In actin-based protrusions, canonical bundling proteins localize along the length of core actin bundles. Although the selective localization of MISP to the rootlets of microvilli is unusual for a bundling protein, the antagonism that ezrin exerts on MISP may suggest an unconventional mechanism of bundling. Given that ezrin crosslinks core bundles with the enveloping plasma membrane, MISP binding sites on actin may be localized to the periphery of core bundles. One way to test this hypothesis is by using immunogold labeling in tissue cross-sections of native small intestine. If MISP is a non-canonical bundler that binds around the periphery of core actin bundles, we predict that the gold particles will decorate the periphery around the core with little to no decoration in the center (Figure 5-9). One factor that bundles actin filaments in a similar modality is TRIOBP, which shows a selective targeting to the rootlets of stereocilia in inner hair cells (Kitajiri et al., 2010). Immunogold-TEM images show that TRIOBP functions as a bundler by wrapping around core bundles (Kitajiri et al., 2010).

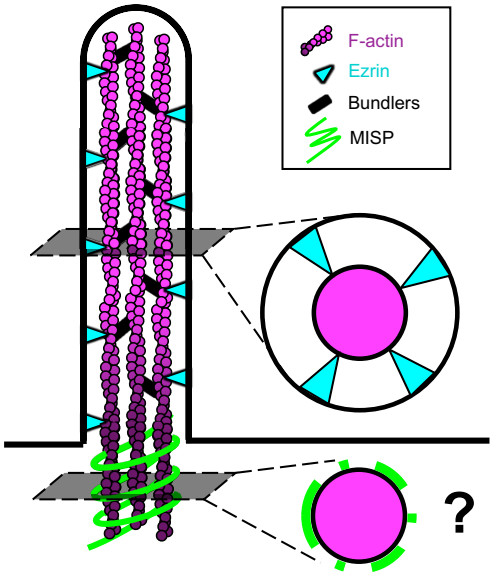

Figure 5-9. Hypothetical ultrastructural localization of MISP in a microvillar rootlet

Does MISP contribute to the establishment of the crypt-villus transition?

In the intestinal epithelium, enterocytes undergo a collective cell migration from the crypt to villus over the course of 3-5 days (van der Flier & Clevers, 2009). The transition from crypt to the basal portion of the villus is facilitated by a pushing force generated by active cell division (Krndija et al., 2019). Interestingly, previous studies indicate that MISP is a cortical factor that promotes mitotic progression, specifically the metaphase-anaphase transition (Maier et al., 2013; Zhu et al., 2013). We found that MISP is uniformly localized along the crypt-villus axis (Morales et al., 2022), even on the surface of immature enterocytes within crypts, which display less brush border microvilli. Such apical localization in actively dividing cells suggests that MISP may be contributing to establishing the crypt-villus transition, presumably because of its role in promoting cell division.

To investigate this, we could use intestinal organoids, which are excellent model systems that recapitulate the composition, structural organization, and dynamics of the intestine (Date & Sato, 2015). Intestinal organoids can be derived from stem cells found in the crypts of mice (i.e., wild type and MISP KO), and grown as spheres in Matrigel, where they will begin growing as spheres resembling the villus domain, and develop outward protrusion resembling crypts later in differentiation (Date & Sato, 2015; Sato et al., 2009). As intestinal organoids can grow such structures in the XY plane over the course of ~5 days (Date & Sato, 2015), they are amenable for imaging. Thus, we could determine whether the establishment of crypt-villus transition is disrupted or delayed in MISP KO organoids compared to wild-type specimens. To determine this, we could measure the apical surface area of cells comprising the crypt (using Lgr5+ as a marker),

and the villus (using villin as a marker) in both specimens. The ratio between these measurements (crypt/villus) would be a good indicator for comparison. One current limitation of using intestinal organoids is the high variability of their shapes. We may be able to overcome this limitation by growing them in micropatterns of known dimensions, which may create more homogenous shapes (Gjorevski et al., 2022), thus facilitating further quantitative analysis. Another benefit of using organoids is that they are amenable to viral transduction, making it possible to express other fluorescent reporters. For instance, we could corroborate that any defect in MISP KO organoids is specific to MISP by reintroducing a fluorescently tagged version.

Finally, we currently lack an understanding of how brush border assembly and cell division are coupled. Given that MISP participates in both processes (Maier et al., 2013; Morales et al., 2022; Zhu et al., 2013), it is tempting to speculate that MISP may play a role in coordinating the cytoskeletal rearrangements required to transition between these two states. This problem opens new venues for future research in our lab, which could be addressed using organoids as models.

Open questions on the cell biology of microvilli[2]

Recent discoveries are now starting to illuminate the detailed molecular mechanisms that enable epithelial cells to generate apical specializations such as the brush border. Our work has elucidated cellular and molecular mechanisms by which the actin bundler MISP selectively targets and functions at the rootlet ends of brush border microvilli. These findings have stimulated other key fundamental questions surrounding microvilli assembly, which remain unanswered and should be targeted in future investigations. For example, how do epithelial cells define the dimensions of a microvillus core bundle? The number of actin filaments in a core bundle dictates protrusion width and is highly stereotyped in brush border microvilli, yet it remains unclear how this parameter is controlled during differentiation. Filament numbers will be impacted by actin monomer concentration, actin bundler stoichiometries, and perhaps even by barbed end binding proteins (e.g. EPS8 or BAIAP2L1) that are well positioned to control how many filaments impinge on the apical membrane. Some tip-specific factors including EPS8 assemble condensates *in vitro* (He et al., 2019; Lin et al., 2021), which might also play a role in controlling filament numbers. This question is also pertinent to understanding the formation of functionally diverse apical protrusions including the stereocilia found on sensory hair cells and the giant microvilli assembled by intestinal tuft cells; in both of these cases, the core bundles contain ~10-fold more actin filaments than we find in microvilli. Another intriguing open question relates to the origin of mechanical force that enables cells to overcome the bending stiffness of the apical membrane during microvillus formation. Although the canonical view is that polymerizing actin filaments are the primary

[2] *Some paragraphs from this section were published in: Morales, E. A., Gaeta, I., & Tyska, M. J. (2023). Building the brush border, one microvillus at a time. Current Opinion in Cell Biology, 80, 102153.*

force generators in this system, microvilli and other structurally similar protrusions contain high levels of force-generating myosin motors. Yet their contribution to growth promoting force remains unexplored. Related to this point, it would be also worth investigating the contribution of external mechanical force in protrusion growth, as fluid shear has been implicated in the growth of placental microvilli (Miura et al., 2015). Finally, as most recent investigations have focused on identifying the protein machinery that is directly involved in core bundle assembly, our understanding of how sites of microvillar growth are specified on the apical membrane during differentiation remains limited. Phosphoinositides such as PI(4,5)P2, PI(4,5)P2, and PI(3,4,5)P3 are strongly implicated in specifying apical vs. basolateral membrane domains (Gassama-Diagne et al., 2006; Martin-Belmonte et al., 2007; Román-Fernández et al., 2018). Whether specific membrane lipid species serve as spatial cues to organize actin polymerization machinery during core bundle growth remains unclear, but this area would also make an appealing target for future studies.

REFERENCES

Ahuja, R., Pinyol, R., Reichenbach, N., Custer, L., Klingensmith, J., Kessels, M. M., & Qualmann, B. (2007). Cordon-Bleu Is an Actin Nucleation Factor and Controls Neuronal Morphology. *Cell*, *131*(2), 337–350. https://doi.org/10.1016/j.cell.2007.08.030

Amann, K. J., & Pollard, T. D. (2001). Direct real-time observation of actin filament branching mediated by Arp2/3 complex using total internal reflection fluorescence microscopy. *Proceedings of the National Academy of Sciences*, *98*(26), 15009–15013. https://doi.org/10.1073/pnas.211556398

Atilgan, E., Wirtz, D., & Sun, S. X. (2006). Mechanics and Dynamics of Actin-Driven Thin Membrane Protrusions. *Biophysical Journal*, *90*(1), 65–76. https://doi.org/10.1529/biophysj.105.071480

Baas, A. F., Kuipers, J., van der Wel, N. N., Batlle, E., Koerten, H. K., Peters, P. J., & Clevers, H. C. (2004). Complete Polarization of Single Intestinal Epithelial Cells upon Activation of LKB1 by STRAD. *Cell*, *116*(3), 457–466. https://doi.org/10.1016/S0092-8674(04)00114-X

Bamburg, J. R. (1999). Proteins of the ADF/Cofilin Family: Essential Regulators of Actin Dynamics. *Annual Review of Cell and Developmental Biology*, *15*(1), 185–230. https://doi.org/10.1146/annurev.cellbio.15.1.185

Bao, J., Bielski, E., Bachhawat, A., Taha, D., Gunther, L. K., Thirumurugan, K., Kitajiri, S., & Sakamoto, T. (2013). R1 Motif Is the Major Actin-Binding Domain of TRIOBP-4. *Biochemistry*, *52*(31), 5256–5264. https://doi.org/10.1021/bi400585h

Barr, F. A., & Gruneberg, U. (2007). Cytokinesis: Placing and Making the Final Cut. *Cell*, *131*(5), 847–860. https://doi.org/10.1016/j.cell.2007.11.011

Barr-Gillespie, P.-G. (2015). Assembly of hair bundles, an amazing problem for cell biology. *Molecular Biology of the Cell*, *26*(15), 2727–2732. https://doi.org/10.1091/mbc.E14-04-0940

Bartles, J. R., Zheng, L., Li, A., Wierda, A., & Chen, B. (1998). Small Espin: A Third Actin-bundling Protein and Potential Forked Protein Ortholog in Brush Border Microvilli. *Journal of Cell Biology*, *143*(1), 107–119. https://doi.org/10.1083/jcb.143.1.107

Beer, A. J., González Delgado, J., Steiniger, F., Qualmann, B., & Kessels, M. M. (2020). The actin nucleator Cobl organises the terminal web of enterocytes. *Scientific Reports*, *10*(1), 11156. https://doi.org/10.1038/s41598-020-66111-9

Belyy, A., Merino, F., Sitsel, O., & Raunser, S. (2020). Structure of the Lifeact–F-actin complex. *PLOS Biology*, *18*(11), e3000925. https://doi.org/10.1371/journal.pbio.3000925

Benesh, A. E., Nambiar, R., McConnell, R. E., Mao, S., Tabb, D. L., & Tyska, M. J. (2010). Differential Localization and Dynamics of Class I Myosins in the Enterocyte Microvillus. *Molecular Biology of the Cell*, *21*(6), 970–978. https://doi.org/10.1091/mbc.e09-07-0638

Berryman, M., Franck, Z., & Bretscher, A. (1993). Ezrin is concentrated in the apical microvilli of a wide variety of epithelial cells whereas moesin is found primarily in endothelial cells. *Journal of Cell Science*, *105*(4), 1025–1043. https://doi.org/10.1242/jcs.105.4.1025

Blanchoin, L., Boujemaa-Paterski, R., Sykes, C., & Plastino, J. (2014). Actin Dynamics, Architecture, and Mechanics in Cell Motility. *Physiological Reviews*, *94*(1), 235–263. https://doi.org/10.1152/physrev.00018.2013

Blanchoin, L., & Pollard, T. D. (1999). Mechanism of Interaction of Acanthamoeba Actophorin (ADF/Cofilin) with Actin Filaments *. *Journal of Biological Chemistry*, *274*(22), 15538–15546. https://doi.org/10.1074/jbc.274.22.15538

Blanchoin, L., & Pollard, T. D. (2002). Hydrolysis of ATP by Polymerized Actin Depends on the Bound Divalent Cation but Not Profilin. *Biochemistry*, *41*(2), 597–602. https://doi.org/10.1021/bi011214b

Breitsprecher, D., & Goode, B. L. (2013). Formins at a glance. *Journal of Cell Science*, *126*(1), 1–7. https://doi.org/10.1242/jcs.107250

Breitsprecher, D., Koestler, S. A., Chizhov, I., Nemethova, M., Mueller, J., Goode, B. L., Small, J. V., Rottner, K., & Faix, J. (2011). Cofilin cooperates with fascin to disassemble filopodial actin filaments. *Journal of Cell Science*, *124*(19), 3305–3318. https://doi.org/10.1242/jcs.086934

Bretscher, A., Reczek, D., & Berryman, M. (1997). Ezrin: A protein requiring conformational activation to link microfilaments to the plasma membrane in the assembly of cell surface structures. *Journal of Cell Science*, *110*(24), 3011–3018. https://doi.org/10.1242/jcs.110.24.3011

Bretscher, A., & Weber, K. (1979). Villin: The major microfilament-associated protein of the intestinal microvillus. *Proceedings of the National Academy of Sciences*, *76*(5), 2321–2325. https://doi.org/10.1073/pnas.76.5.2321

Bretscher, A., & Weber, K. (1980a). Villin is a major protein of the microvillus cystoskeleton which binds both G and F actin in a calcium-dependent manner. *Cell*, *20*(3), 839–847. https://doi.org/10.1016/0092-8674(80)90330-X

Bretscher, A., & Weber, K. (1980b). Fimbrin, a new microfilament-associated protein present in microvilli and other cell surface structures. *Journal of Cell Biology*, *86*(1), 335–340. https://doi.org/10.1083/jcb.86.1.335

Bugyi, B., & Carlier, M.-F. (2010). Control of Actin Filament Treadmilling in Cell Motility. *Annual Review of Biophysics*, *39*(1), 449–470. https://doi.org/10.1146/annurev-biophys-051309-103849

Bugyi, B., & Kellermayer, M. (2020). The discovery of actin: “To see what everyone else has seen, and to think what nobody has thought”*. *Journal of Muscle Research and Cell Motility*, *41*(1), 3–9. https://doi.org/10.1007/s10974-019-09515-z

Bulut, G., Hong, S.-H., Chen, K., Beauchamp, E. M., Rahim, S., Kosturko, G. W., Glasgow, E., Dakshanamurthy, S., Lee, H.-S., Daar, I., Toretsky, J. A., Khanna, C., & Üren, A. (2012). Small molecule inhibitors of ezrin inhibit the invasive phenotype of osteosarcoma cells. *Oncogene*, *31*(3), 269–281. https://doi.org/10.1038/onc.2011.245

Burke, T. A., Christensen, J. R., Barone, E., Suarez, C., Sirotkin, V., & Kovar, D. R. (2014). Homeostatic Actin Cytoskeleton Networks Are Regulated by Assembly Factor Competition for Monomers. *Current Biology*, *24*(5), 579–585. https://doi.org/10.1016/j.cub.2014.01.072

Burridge, K., & Wittchen, E. S. (2013). The tension mounts: Stress fibers as force-generating mechanotransducers. *Journal of Cell Biology*, *200*(1), 9–19. https://doi.org/10.1083/jcb.201210090

Cai, L., Makhov, A. M., & Bear, J. E. (2007). F-actin binding is essential for coronin 1B function in vivo. *Journal of Cell Science*, *120*(10), 1779–1790. https://doi.org/10.1242/jcs.007641

Carlier, M. F., & Pantaloni, D. (1986). Direct evidence for ADP-inorganic phosphate-F-actin as the major intermediate in ATP-actin polymerization. Rate of dissociation of inorganic phosphate from actin filaments. *Biochemistry*, *25*(24), 7789–7792. https://doi.org/10.1021/bi00372a001

Carlier, M.-F., Laurent, V., Santolini, J., Melki, R., Didry, D., Xia, G.-X., Hong, Y., Chua, N.-H., & Pantaloni, D. (1997). Actin Depolymerizing Factor (ADF/Cofilin) Enhances the Rate of Filament Turnover: Implication in Actin-based Motility. *Journal of Cell Biology*, *136*(6), 1307–1322. https://doi.org/10.1083/jcb.136.6.1307

Casaletto, J. B., Saotome, I., Curto, M., & McClatchey, A. I. (2011). Ezrin-mediated apical integrity is required for intestinal homeostasis. *Proceedings of the National Academy of Sciences*, *108*(29), 11924–11929. https://doi.org/10.1073/pnas.1103418108

Chan, C., Beltzner, C. C., & Pollard, T. D. (2009). Cofilin Dissociates Arp2/3 Complex and Branches from Actin Filaments. *Current Biology*, *19*(7), 537–545. https://doi.org/10.1016/j.cub.2009.02.060

Chen, H., Bernstein, B., & Bamburg, J. (2000). Regulating actin-filament dynamics in vivo. *Trends in Biochemical Sciences*, *25*(1), 19–23. https://doi.org/10.1016/S0968-0004(99)01511-X

Chen, X., Ni, F., Tian, X., Kondrashkina, E., Wang, Q., & Ma, J. (2013). Structural Basis of Actin Filament Nucleation by Tandem W Domains. *Cell Reports*, *3*(6), 1910–1920. https://doi.org/10.1016/j.celrep.2013.04.028

Chen, Z.-Y., Hasson, T., Zhang, D.-S., Schwender, B. J., Derfler, B. H., Mooseker, M. S., & Corey, D. P. (2001). Myosin-VIIb, a Novel Unconventional Myosin, Is a Constituent of Microvilli in Transporting Epithelia. *Genomics*, *72*(3), 285–296. https://doi.org/10.1006/geno.2000.6456

Chesarone, M. A., & Goode, B. L. (2009). Actin nucleation and elongation factors: Mechanisms and interplay. *Current Opinion in Cell Biology*, *21*(1), 28–37. https://doi.org/10.1016/j.ceb.2008.12.001

Chhabra, E. S., & Higgs, H. N. (2007). The many faces of actin: Matching assembly factors with cellular structures. *Nature Cell Biology*, *9*(10), 1110–1121. https://doi.org/10.1038/ncb1007-1110

Chinowsky, C. R., Pinette, J. A., Meenderink, L. M., Lau, K. S., & Tyska, M. J. (2020). Nonmuscle myosin-2 contractility-dependent actin turnover limits the length of epithelial microvilli. *Molecular Biology of the Cell*, *31*(25), 2803–2815. https://doi.org/10.1091/mbc.E20-09-0582

Chou, S.-W., Hwang, P., Gomez, G., Fernando, C. A., West, M. C., Pollock, L. M., Lin-Jones, J., Burnside, B., & Jr, B. M. M. (2011). Fascin 2b Is a Component of Stereocilia that Lengthens Actin-Based Protrusions. *PLOS ONE*, *6*(4), e14807. https://doi.org/10.1371/journal.pone.0014807

Christensen, J. R., Hocky, G. M., Homa, K. E., Morganthaler, A. N., Hitchcock-DeGregori, S. E., Voth, G. A., & Kovar, D. R. (2017). Competition between Tropomyosin, Fimbrin, and ADF/Cofilin drives their sorting to distinct actin filament networks. *ELife*, *6*, e23152. https://doi.org/10.7554/eLife.23152

Conzelman, K. A., & Mooseker, M. S. (1987). The 110-kD protein-calmodulin complex of the intestinal microvillus is an actin-activated MgATPase. *Journal of Cell Biology*, *105*(1), 313–324. https://doi.org/10.1083/jcb.105.1.313

Cooper, J. A., Buhle, E. L. Jr., Walker, S. B., Tsong, T. Y., & Pollard, T. D. (1983). Kinetic evidence for a monomer activation step in actin polymerization. *Biochemistry*, *22*(9), 2193–2202. https://doi.org/10.1021/bi00278a021

Courtemanche, N., & Pollard, T. D. (2013). Interaction of Profilin with the Barbed End of Actin Filaments. *Biochemistry*, *52*(37), 6456–6466. https://doi.org/10.1021/bi400682n

Cramer, L. P., Siebert, M., & Mitchison, T. J. (1997). Identification of Novel Graded Polarity Actin Filament Bundles in Locomoting Heart Fibroblasts: Implications for the Generation of Motile Force. *Journal of Cell Biology*, *136*(6), 1287–1305. https://doi.org/10.1083/jcb.136.6.1287

Crawley, S. W., Mooseker, M. S., & Tyska, M. J. (2014a). Shaping the intestinal brush border. *Journal of Cell Biology*, *207*(4), 441–451. https://doi.org/10.1083/jcb.201407015

Crawley, S. W., Mooseker, M. S., & Tyska, M. J. (2014b). Shaping the intestinal brush border. *Journal of Cell Biology*, *207*(4), 441–451. https://doi.org/10.1083/jcb.201407015

Crawley, S. W., Shifrin, D. A., Grega-Larson, N. E., McConnell, R. E., Benesh, A. E., Mao, S., Zheng, Y., Zheng, Q. Y., Nam, K. T., Millis, B. A., Kachar, B., & Tyska, M. J. (2014). Intestinal Brush Border Assembly Driven by Protocadherin-Based Intermicrovillar Adhesion. *Cell*, *157*(2), 433–446. https://doi.org/10.1016/j.cell.2014.01.067

Crawley, S. W., Weck, M. L., Grega-Larson, N. E., Shifrin, D. A., & Tyska, M. J. (2016). ANKS4B Is Essential for Intermicrovillar Adhesion Complex Formation. *Developmental Cell*, *36*(2), 190–200. https://doi.org/10.1016/j.devcel.2015.12.022

Croce, A., Cassata, G., Disanza, A., Gagliani, M. C., Tacchetti, C., Malabarba, M. G., Carlier, M.-F., Scita, G., Baumeister, R., & Fiore, P. P. D. (2004). A novel actin barbed-end-capping activity in EPS-8 regulates apical morphogenesis in intestinal cells of Caenorhabditis elegans. *Nature Cell Biology*, *6*(12), 1173–1179. https://doi.org/10.1038/ncb1198

Date, S., & Sato, T. (2015). Mini-Gut Organoids: Reconstitution of the Stem Cell Niche. *Annual Review of Cell and Developmental Biology*, *31*(1), 269–289. https://doi.org/10.1146/annurev-cellbio-100814-125218

Davies, T., Jordan, S. N., Chand, V., Sees, J. A., Laband, K., Carvalho, A. X., Shirasu-Hiza, M., Kovar, D. R., Dumont, J., & Canman, J. C. (2014). High-Resolution Temporal Analysis Reveals a Functional Timeline for the Molecular Regulation of Cytokinesis. *Developmental Cell*, *30*(2), 209–223. https://doi.org/10.1016/j.devcel.2014.05.009

Delacour, D., Salomon, J., Robine, S., & Louvard, D. (2016). Plasticity of the brush border—The yin and yang of intestinal homeostasis. *Nature Reviews Gastroenterology & Hepatology*, *13*(3), 161–174. https://doi.org/10.1038/nrgastro.2016.5

Disanza, A., Mantoani, S., Hertzog, M., Gerboth, S., Frittoli, E., Steffen, A., Berhoerster, K., Kreienkamp, H.-J., Milanesi, F., Fiore, P. P. D., Ciliberto, A., Stradal, T. E. B., & Scita, G. (2006). Regulation of cell shape by Cdc42 is mediated by the synergic actin-bundling activity of the Eps8–IRSp53 complex. *Nature Cell Biology*, *8*(12), 1337–1347. https://doi.org/10.1038/ncb1502

Dominguez, R. (2016). The WH2 Domain and Actin Nucleation: Necessary but Insufficient. *Trends in Biochemical Sciences*, *41*(6), 478–490. https://doi.org/10.1016/j.tibs.2016.03.004

Dominguez, R., & Holmes, K. C. (2011). Actin Structure and Function. *Annual Review of Biophysics*, *40*(1), 169–186. https://doi.org/10.1146/annurev-biophys-042910-155359

Drummond, M. C., Barzik, M., Bird, J. E., Zhang, D.-S., Lechene, C. P., Corey, D. P., Cunningham, L. L., & Friedman, T. B. (2015). Live-cell imaging of actin dynamics reveals mechanisms of stereocilia length regulation in the inner ear. *Nature Communications*, *6*(1), 6873. https://doi.org/10.1038/ncomms7873

Drummond, M. C., Belyantseva, I. A., Friderici, K. H., & Friedman, T. B. (2012). Actin in hair cells and hearing loss. *Hearing Research*, *288*(1–2), 89–99. https://doi.org/10.1016/j.heares.2011.12.003

Dudouet, B., Robine, S., Huet, C., Sahuquillo-Merino, C., Blair, L., Coudrier, E., & Louvard, D. (1987). Changes in villin synthesis and subcellular distribution during intestinal differentiation of HT29-18 clones. *The Journal of Cell Biology*, *105*(1), 359–369. https://doi.org/10.1083/jcb.105.1.359

Ezzell, R. M., Chafel, M. M., & Matsudaira, P. T. (1989). Differential localization of villin and fimbrin during development of the mouse visceral endoderm and intestinal epithelium. *Development (Cambridge, England)*, *106*(2), 407–419.

Faust, J. J., Millis, B. A., & Tyska, M. J. (2019). Profilin-Mediated Actin Allocation Regulates the Growth of Epithelial Microvilli. *Current Biology*, *29*(20), 3457-3465.e3. https://doi.org/10.1016/j.cub.2019.08.051

Ferrary, E., Cohen-Tannoudji, M., Pehau-Arnaudet, G., Lapillonne, A., Athman, R., Ruiz, T., Boulouha, L., Marjou, F. E., Doye, A., Fontaine, J.-J., Antony, C., Babinet, C., Louvard, D., Jaisser, F., & Robine, S. (1999). In Vivo, Villin Is Required for Ca2Ɛ-dependent F-actin Disruption in Intestinal Brush Borders. *The Journal of Cell Biology*, *146*, 11.

Firat-Karalar, E. N., & Welch, M. D. (2011). New mechanisms and functions of actin nucleation. *Current Opinion in Cell Biology*, *23*(1), 4–13. https://doi.org/10.1016/j.ceb.2010.10.007

Fischer, R. S., Fritz-Six, K. L., & Fowler, V. M. (2003). Pointed-end capping by tropomodulin3 negatively regulates endothelial cell motility. *Journal of Cell Biology*, *161*(2), 371–380. https://doi.org/10.1083/jcb.200209057

Fitz, G. N., Weck, M. L., Bodnya, C., Perkins, O. L., & Tyska, M. J. (2023). Protrusion growth driven by myosin-generated force. *Developmental Cell*, *58*(1), 18-33.e6. https://doi.org/10.1016/j.devcel.2022.12.001

Footer, M. J., Kerssemakers, J. W. J., Theriot, J. A., & Dogterom, M. (2007). Direct measurement of force generation by actin filament polymerization using an optical trap. *Proceedings of the National Academy of Sciences*, *104*(7), 2181–2186. https://doi.org/10.1073/pnas.0607052104

Frolenkov, G. I., Belyantseva, I. A., Friedman, T. B., & Griffith, A. J. (2004). Genetic insights into the morphogenesis of inner ear hair cells. *Nature Reviews Genetics*, *5*(7), 489–498. https://doi.org/10.1038/nrg1377

Gaeta, I. M., Meenderink, L. M., Postema, M. M., Cencer, C. S., & Tyska, M. J. (2021). Direct visualization of epithelial microvilli biogenesis. *Current Biology: CB*, *31*(12), 2561-2575.e6. https://doi.org/10.1016/j.cub.2021.04.012

Gandhi, M., Achard, V., Blanchoin, L., & Goode, B. L. (2009). Coronin Switches Roles in Actin Disassembly Depending on the Nucleotide State of Actin. *Molecular Cell*, *34*(3), 364–374. https://doi.org/10.1016/j.molcel.2009.02.029

Gassama-Diagne, A., Yu, W., ter Beest, M., Martin-Belmonte, F., Kierbel, A., Engel, J., & Mostov, K. (2006). Phosphatidylinositol-3,4,5-trisphosphate regulates the formation of the basolateral plasma membrane in epithelial cells. *Nature Cell Biology*, *8*(9), 963–970. https://doi.org/10.1038/ncb1461

Géléoc, G. G. S., & El-Amraoui, A. (2020). Disease mechanisms and gene therapy for Usher syndrome. *Hearing Research*, *394*, 107932. https://doi.org/10.1016/j.heares.2020.107932

Gjorevski, N., Nikolaev, M., Brown, T. E., Mitrofanova, O., Brandenberg, N., DelRio, F. W., Yavitt, F. M., Liberali, P., Anseth, K. S., & Lutolf, M. P. (2022). Tissue geometry drives deterministic organoid patterning. *Science*, *375*(6576), eaaw9021. https://doi.org/10.1126/science.aaw9021

Glenney, J. R., Kaulfus, P., Matsudaira, P., & Weber, K. (1981). F-actin binding and bundling properties of fimbrin, a major cytoskeletal protein of microvillus core filaments. *Journal of Biological Chemistry*, *256*(17), 9283–9288. https://doi.org/10.1016/S0021-9258(19)52543-1

Glenney Jr., J. R., Kaulfus, P., & Weber, K. (1981). F actin assembly modulated by villin: Ca++-dependent nucleation and capping of the barbed end. *Cell*, *24*(2), 471–480. https://doi.org/10.1016/0092-8674(81)90338-X

Goddette, D. W., & Frieden, C. (1985). The binding of cytochalasin D to monomeric actin. *Biochemical and Biophysical Research Communications*, *128*(3), 1087–1092. https://doi.org/10.1016/0006-291X(85)91051-4

Gould, K. L., Cooper, J. A., Bretscher, A., & Hunter, T. (1986). The protein-tyrosine kinase substrate, p81, is homologous to a chicken microvillar core protein. *Journal of Cell Biology*, *102*(2), 660–669. https://doi.org/10.1083/jcb.102.2.660

Grega-Larson, N. E., Crawley, S. W., Erwin, A. L., & Tyska, M. J. (2015). Cordon bleu promotes the assembly of brush border microvilli. *Molecular Biology of the Cell*, *26*(21), 3803–3815. https://doi.org/10.1091/mbc.E15-06-0443

Grimm-Günter, E.-M. S., Revenu, C., Ramos, S., Hurbain, I., Smyth, N., Ferrary, E., Louvard, D., Robine, S., & Rivero, F. (2009). Plastin 1 Binds to Keratin and Is Required for Terminal Web Assembly in the Intestinal Epithelium. *Molecular Biology of the Cell*, *20*(10), 2549–2562. https://doi.org/10.1091/mbc.e08-10-1030

Hampton, C. M., Liu, J., Taylor, D. W., DeRosier, D. J., & Taylor, K. A. (2008). The 3D Structure of Villin as an Unusual F-Actin Crosslinker. *Structure*, *16*(12), 1882–1891. https://doi.org/10.1016/j.str.2008.09.015

Hampton, C. M., Taylor, D. W., & Taylor, K. A. (2007). Novel Structures for α-Actinin:F-Actin Interactions and their Implications for Actin–Membrane Attachment and Tension Sensing in the Cytoskeleton. *Journal of Molecular Biology*, *368*(1), 92–104. https://doi.org/10.1016/j.jmb.2007.01.071

Hanono, A., Garbett, D., Reczek, D., Chambers, D. N., & Bretscher, A. (2006). EPI64 regulates microvillar subdomains and structure. *Journal of Cell Biology*, *175*(5), 803–813. https://doi.org/10.1083/jcb.200604046

Harrison, R. G. (1910). The outgrowth of the nerve fiber as a mode of protoplasmic movement. *Journal of Experimental Zoology*, *9*(4), 787–846. https://doi.org/10.1002/jez.1400090405

He, Y., Li, J., & Zhang, M. (2019). Myosin VII, USH1C, and ANKS4B or USH1G Together Form Condensed Molecular Assembly via Liquid-Liquid Phase Separation. *Cell Reports*, *29*(4), 974-986.e4. https://doi.org/10.1016/j.celrep.2019.09.027

Hegan, P. S., Giral, H., Levi, M., & Mooseker, M. S. (2012). Myosin VI is required for maintenance of brush border structure, composition, and membrane trafficking functions in the intestinal epithelial cell. *Cytoskeleton*, *69*(4), 235–251. https://doi.org/10.1002/cm.21018

Helander, H. F., & Fändriks, L. (2014). Surface area of the digestive tract – revisited. *Scandinavian Journal of Gastroenterology*, *49*(6), 681–689. https://doi.org/10.3109/00365521.2014.898326

Hertzog, M., Milanesi, F., Hazelwood, L., Disanza, A., Liu, H., Perlade, E., Malabarba, M. G., Pasqualato, S., Maiolica, A., Confalonieri, S., Clainche, C. L., Offenhauser, N., Block, J., Rottner, K., Fiore, P. P. D., Carlier, M.-F., Volkmann, N., Hanein, D., & Scita, G. (2010). Molecular Basis for the Dual Function of Eps8 on Actin Dynamics: Bundling and Capping. *PLOS Biology*, *8*(6), e1000387. https://doi.org/10.1371/journal.pbio.1000387

Higgs, H. N. (2005). Formin proteins: A domain-based approach. *Trends in Biochemical Sciences*, *30*(6), 342–353. https://doi.org/10.1016/j.tibs.2005.04.014

Hirano, Y., Ishii, K., Kumeta, M., Furukawa, K., Takeyasu, K., & Horigome, T. (2009). Proteomic and targeted analytical identification of BXDC1 and EBNA1BP2 as dynamic scaffold proteins in the nucleolus. *Genes to Cells*, *14*(2), 155–166. https://doi.org/10.1111/j.1365-2443.2008.01262.x

Hirokawa, N., Cheney, R. E., & Willard, M. (1983). Location of a protein of the fodrin-spectrin-TW260/240 family in the mouse intestinal brush border. *Cell*, *32*(3), 953–965. https://doi.org/10.1016/0092-8674(83)90080-6

Hirokawa, N., & Heuser, J. E. (1981). Quick-freeze, deep-etch visualization of the cytoskeleton beneath surface differentiations of intestinal epithelial cells. *Journal of Cell Biology*, *91*(2), 399–409. https://doi.org/10.1083/jcb.91.2.399

Hirokawa, N., Tilney, L. G., Fujiwara, K., & Heuser, J. E. (1982). Organization of actin, myosin, and intermediate filaments in the brush border of intestinal epithelial cells. *Journal of Cell Biology*, *94*(2), 425–443. https://doi.org/10.1083/jcb.94.2.425

Hiura, K., Maruyama, T., Watanabe, M., Nakano, K., Okamura, T., Sasaki, H., & Sasaki, N. (2023). Mitotic spindle positioning protein (MISP) deficiency exacerbates dextran sulfate sodium (DSS)-induced colitis in mice. *Journal of Veterinary Medical Science*, *85*(2), 167–174. https://doi.org/10.1292/jvms.22-0483

Holmes, K. C., Popp, D., Gebhard, W., & Kabsch, W. (1990). Atomic model of the actin filament. *Nature*, *347*(6288), 44–49. https://doi.org/10.1038/347044a0

Hotulainen, P., & Lappalainen, P. (2006). Stress fibers are generated by two distinct actin assembly mechanisms in motile cells. *Journal of Cell Biology*, *173*(3), 383–394. https://doi.org/10.1083/jcb.200511093

Hou, W., Izadi, M., Nemitz, S., Haag, N., Kessels, M. M., & Qualmann, B. (2015). The Actin Nucleator Cobl Is Controlled by Calcium and Calmodulin. *PLOS Biology*, *13*(9), e1002233. https://doi.org/10.1371/journal.pbio.1002233

Hou, W., Nemitz, S., Schopper, S., Nielsen, M. L., Kessels, M. M., & Qualmann, B. (2018). Arginine Methylation by PRMT2 Controls the Functions of the Actin Nucleator Cobl. *Developmental Cell*, *45*(2), 262-275.e8. https://doi.org/10.1016/j.devcel.2018.03.007

Howe, C. L., & Mooseker, M. S. (1983). Characterization of the 110-kdalton actin-calmodulin-, and membrane-binding protein from microvilli of intestinal epithelial cells. *Journal of Cell Biology*, *97*(4), 974–985. https://doi.org/10.1083/jcb.97.4.974

Huang, X., Zhao, L., Jin, Y., Wang, Z., Li, T., Xu, H., Wang, Q., & Wang, L. (2022). Up-Regulated MISP Is Associated With Poor Prognosis and Immune Infiltration in Pancreatic Ductal Adenocarcinoma. *Frontiers in Oncology*, *12*, 827051. https://doi.org/10.3389/fonc.2022.827051

Husson, C., Renault, L., Didry, D., Pantaloni, D., & Carlier, M.-F. (2011). Cordon-Bleu Uses WH2 Domains as Multifunctional Dynamizers of Actin Filament Assembly. *Molecular Cell*, *43*(3), 464–477. https://doi.org/10.1016/j.molcel.2011.07.010

Ishii, K., Hirano, Y., Araki, N., Oda, T., Kumeta, M., Takeyasu, K., Furukawa, K., & Horigome, T. (2008). Nuclear matrix contains novel WD-repeat and disordered-region-rich proteins. *FEBS Letters*, *582*(23–24), 3515–3519. https://doi.org/10.1016/j.febslet.2008.09.019

Jansen, S., Collins, A., Yang, C., Rebowski, G., Svitkina, T., & Dominguez, R. (2011). Mechanism of Actin Filament Bundling by Fascin. *Journal of Biological Chemistry*, *286*(34), 30087–30096. https://doi.org/10.1074/jbc.M111.251439

Jiao, Y., Walker, M., Trinick, J., Pernier, J., Montaville, P., & Carlier, M.-F. (2014). Mutagenetic and electron microscopy analysis of actin filament severing by Cordon-Bleu, a WH2 domain protein. *Cytoskeleton*, *71*(3), 170–183. https://doi.org/10.1002/cm.21161

Kabsch, W., Mannherz, H. G., Suck, D., Pai, E. F., & Holmes, K. C. (1990). Atomic structure of the actin: DNase I complex. *Nature*, *347*(6288), 37–44. https://doi.org/10.1038/347037a0

Kazmierczak, P., Sakaguchi, H., Tokita, J., Wilson-Kubalek, E. M., Milligan, R. A., Müller, U., & Kachar, B. (2007). Cadherin 23 and protocadherin 15 interact to form tip-link filaments in sensory hair cells. *Nature*, *449*(7158), 87–91. https://doi.org/10.1038/nature06091

Kirschner, M. W. (1980). Implications of treadmilling for the stability and polarity of actin and tubulin polymers in vivo. *Journal of Cell Biology*, *86*(1), 330–334. https://doi.org/10.1083/jcb.86.1.330

Kitajiri, S., Sakamoto, T., Belyantseva, I. A., Goodyear, R. J., Stepanyan, R., Fujiwara, I., Bird, J. E., Riazuddin, S., Riazuddin, S., Ahmed, Z. M., Hinshaw, J. E., Sellers, J., Bartles, J. R., Hammer, J. A., Richardson, G. P., Griffith, A. J., Frolenkov, G. I., & Friedman, T. B. (2010). Actin-Bundling Protein TRIOBP Forms Resilient Rootlets of Hair Cell Stereocilia Essential for Hearing. *Cell*, *141*(5), 786–798. https://doi.org/10.1016/j.cell.2010.03.049

Kitazawa, T., Shuman, H., & Somlyo, A. P. (1982). Calcium and magnesium binding to thin and thick filaments in skinned muscle fibres: Electron probe analysis. *Journal of Muscle Research and Cell Motility*, *3*(4), 437–454. https://doi.org/10.1007/BF00712093

Klein, M. G., Shi, W., Ramagopal, U., Tseng, Y., Wirtz, D., Kovar, D. R., Staiger, C. J., & Almo, S. C. (2004). Structure of the Actin Crosslinking Core of Fimbrin. *Structure*, *12*(6), 999–1013. https://doi.org/10.1016/j.str.2004.04.010

Korn, E. D., Carlier, M.-F., & Pantaloni, D. (1987). Actin Polymerization and ATP Hydrolysis. *Science*, *238*(4827), 638–644. https://doi.org/10.1126/science.3672117

Kovar, D. R., & Pollard, T. D. (2004). Insertional assembly of actin filament barbed ends in association with formins produces piconewton forces. *Proceedings of the National Academy of Sciences*, *101*(41), 14725–14730. https://doi.org/10.1073/pnas.0405902101

Krause, M., Dent, E. W., Bear, J. E., Loureiro, J. J., & Gertler, F. B. (2003). Ena/VASP Proteins: Regulators of the Actin Cytoskeleton and Cell Migration. *Annual Review of Cell and Developmental Biology*, *19*(1), 541–564. https://doi.org/10.1146/annurev.cellbio.19.050103.103356

Krey, J. F., Krystofiak, E. S., Dumont, R. A., Vijayakumar, S., Choi, D., Rivero, F., Kachar, B., Jones, S. M., & Barr-Gillespie, P. G. (2016). Plastin 1 widens stereocilia by transforming actin filament packing from hexagonal to liquid. *Journal of Cell Biology*, *215*(4), 467–482. https://doi.org/10.1083/jcb.201606036

Krndija, D., El Marjou, F., Guirao, B., Richon, S., Leroy, O., Bellaiche, Y., Hannezo, E., & Matic Vignjevic, D. (2019). Active cell migration is critical for steady-state epithelial turnover in the gut. *Science*, *365*(6454), 705–710. https://doi.org/10.1126/science.aau3429

Kschonsak, Y. T., & Hoffmann, I. (2018). Activated Ezrin controls MISP levels to ensure correct NuMA polarization and spindle orientation. *Journal of Cell Science*, jcs.214544. https://doi.org/10.1242/jcs.214544

Kučera, O., Siahaan, V., Janda, D., Dijkstra, S. H., Pilátová, E., Zatecka, E., Diez, S., Braun, M., & Lansky, Z. (2021). Anillin propels myosin-independent constriction of actin rings. *Nature Communications*, *12*(1), 4595. https://doi.org/10.1038/s41467-021-24474-1

Kudryashova, E., Ankita, Ulrichs, H., Shekhar, S., & Kudryashov, D. S. (2022). Pointed-end processive elongation of actin filaments by Vibrio effectors VopF and VopL. *Science Advances*, *8*(46), eadc9239. https://doi.org/10.1126/sciadv.adc9239

Kuhn, J. R., & Pollard, T. D. (2005). Real-Time Measurements of Actin Filament Polymerization by Total Internal Reflection Fluorescence Microscopy. *Biophysical Journal*, *88*(2), 1387–1402. https://doi.org/10.1529/biophysj.104.047399

Kumeta, M., Gilmore, J. L., Umeshima, H., Ishikawa, M., Kitajiri, S., Horigome, T., Kengaku, M., & Takeyasu, K. (2014). Caprice/MISP is a novel F-actin bundling protein critical for actin-based cytoskeletal reorganizations. *Genes to Cells*, *19*(4), 338–349. https://doi.org/10.1111/gtc.12131

Lange, K. (2011). Fundamental role of microvilli in the main functions of differentiated cells: Outline of an universal regulating and signaling system at the cell periphery. *Journal of Cellular Physiology*, *226*(4), 896–927. https://doi.org/10.1002/jcp.22302

Lappalainen, P., & Drubin, D. G. (1997). Cofilin promotes rapid actin filament turnover in vivo. *Nature*, *388*(6637), 78–82. https://doi.org/10.1038/40418

Lee, S. Y., Kim, W., Lee, Y. G., Kang, H. J., Lee, S.-H., Park, S. Y., Min, J.-K., Lee, S.-R., & Chung, S. J. (2017). Identification of sennoside A as a novel inhibitor of the slingshot (SSH) family proteins related to cancer metastasis. *Pharmacological Research*, *119*, 422–430. https://doi.org/10.1016/j.phrs.2017.03.003

Li, J., He, Y., Lu, Q., & Zhang, M. (2016). Mechanistic Basis of Organization of the Harmonin/USH1C-Mediated Brush Border Microvilli Tip-Link Complex. *Developmental Cell*, *36*(2), 179–189. https://doi.org/10.1016/j.devcel.2015.12.020

Li, J., He, Y., Weck, M. L., Lu, Q., Tyska, M. J., & Zhang, M. (2017). Structure of Myo7b/USH1C complex suggests a general PDZ domain binding mode by MyTH4-FERM myosins. *Proceedings of the National Academy of Sciences*, *114*(19), E3776–E3785. https://doi.org/10.1073/pnas.1702251114

Li, Y., Christensen, J. R., Homa, K. E., Hocky, G. M., Fok, A., Sees, J. A., Voth, G. A., & Kovar, D. R. (2016). The F-actin bundler α-actinin Ain1 is tailored for ring assembly and constriction during cytokinesis in fission yeast. *Molecular Biology of the Cell*, *27*(11), 1821–1833. https://doi.org/10.1091/mbc.e16-01-0010

Lin, L., Shi, Y., Wang, M., Wang, C., Lu, Q., Zhu, J., & Zhang, R. (2021). Phase separation-mediated condensation of Whirlin-Myo15-Eps8 stereocilia tip complex. *Cell Reports*, *34*(8), 108770. https://doi.org/10.1016/j.celrep.2021.108770

Littlefield, R., Almenar-Queralt, A., & Fowler, V. M. (2001). Actin dynamics at pointed ends regulates thin filament length in striated muscle. *Nature Cell Biology*, *3*(6), 544–551. https://doi.org/10.1038/35078517

Liu, X.-P., Koehler, K. R., Mikosz, A. M., Hashino, E., & Holt, J. R. (2016). Functional development of mechanosensitive hair cells in stem cell-derived organoids parallels native vestibular hair cells. *Nature Communications*, *7*(1), 11508. https://doi.org/10.1038/ncomms11508

Loomis, P. A., Kelly, A. E., Zheng, L., Changyaleket, B., Sekerková, G., Mugnaini, E., Ferreira, A., Mullins, R. D., & Bartles, J. R. (2006). Targeted wild-type and jerker espins reveal a novel, WH2-domain-dependent way to make actin bundles in cells. *Journal of Cell Science*, *119*(8), 1655–1665. https://doi.org/10.1242/jcs.02869

Loomis, P. A., Zheng, L., Sekerková, G., Changyaleket, B., Mugnaini, E., & Bartles, J. R. (2003). Espin cross-links cause the elongation of microvillus-type parallel actin bundles in vivo. *Journal of Cell Biology*, *163*(5), 1045–1055. https://doi.org/10.1083/jcb.200309093

Maarof, N. D., Kumeta, M., & Yoshimura, S. H. (2021). Modulation of actin-binding and -bundling activities of MISP/Caprice by multiple phosphorylation. *Biochemical and Biophysical Research Communications*, *561*, 128–135. https://doi.org/10.1016/j.bbrc.2021.05.041

Mahaffy, R. E., & Pollard, T. D. (2006). Kinetics of the Formation and Dissociation of Actin Filament Branches Mediated by Arp2/3 Complex. *Biophysical Journal*, *91*(9), 3519–3528. https://doi.org/10.1529/biophysj.106.080937

Maier, B., Kirsch, M., Anderhub, S., Zentgraf, H., & Krämer, A. (2013). The novel actin/focal adhesion-associated protein MISP is involved in mitotic spindle positioning in human cells. *Cell Cycle*, *12*(9), 1457–1471. https://doi.org/10.4161/cc.24602

Mallavarapu, A., & Mitchison, T. (1999). Regulated Actin Cytoskeleton Assembly at Filopodium Tips Controls Their Extension and Retraction. *Journal of Cell Biology*, *146*(5), 1097–1106. https://doi.org/10.1083/jcb.146.5.1097

Manor, U., Disanza, A., Grati, M., Andrade, L., Lin, H., Di Fiore, P. P., Scita, G., & Kachar, B. (2011). Regulation of Stereocilia Length by Myosin XVa and Whirlin Depends on the Actin-Regulatory Protein Eps8. *Current Biology*, *21*(2), 167–172. https://doi.org/10.1016/j.cub.2010.12.046

Manor, U., & Kachar, B. (2008). Dynamic length regulation of sensory stereocilia. *Seminars in Cell & Developmental Biology*, *19*(6), 502–510. https://doi.org/10.1016/j.semcdb.2008.07.006

Martin-Belmonte, F., Gassama, A., Datta, A., Yu, W., Rescher, U., Gerke, V., & Mostov, K. (2007). PTEN-Mediated Apical Segregation of Phosphoinositides Controls Epithelial Morphogenesis through Cdc42. *Cell*, *128*(2), 383–397. https://doi.org/10.1016/j.cell.2006.11.051

Matsudaira, P. (1991). Modular organization of actin crosslinking proteins. *Trends in Biochemical Sciences*, *16*, 87–92. https://doi.org/10.1016/0968-0004(91)90039-X

Matsudaira, P. (1994). Actin crosslinking proteins at the leading edge. *Seminars in Cell Biology*, *5*(3), 165–174. https://doi.org/10.1006/scel.1994.1021

Matsudaira, P., Mandelkow, E., Renner, W., Hesterberg, L. K., & Weber, K. (1983). Role of fimbrin and villin in determining the interfilament distances of actin bundles. *Nature*, *301*(5897), 209–214. https://doi.org/10.1038/301209a0

Mattila, P. K., & Lappalainen, P. (2008). Filopodia: Molecular architecture and cellular functions. *Nature Reviews Molecular Cell Biology*, *9*(6), 446–454. https://doi.org/10.1038/nrm2406

McConnell, R. E., Benesh, A. E., Mao, S., Tabb, D. L., & Tyska, M. J. (2011). Proteomic analysis of the enterocyte brush border. *American Journal of Physiology-Gastrointestinal and Liver Physiology*, *300*(5), G914–G926. https://doi.org/10.1152/ajpgi.00005.2011

McCullagh, M., Saunders, M. G., & Voth, G. A. (2014). Unraveling the Mystery of ATP Hydrolysis in Actin Filaments. *Journal of the American Chemical Society*, *136*(37), 13053–13058. https://doi.org/10.1021/ja507169f

McCullough, B. R., Blanchoin, L., Martiel, J.-L., & De La Cruz, E. M. (2008). Cofilin Increases the Bending Flexibility of Actin Filaments: Implications for Severing and Cell Mechanics. *Journal of Molecular Biology*, *381*(3), 550–558. https://doi.org/10.1016/j.jmb.2008.05.055

McGrath, J., Roy, P., & Perrin, B. J. (2017). Stereocilia morphogenesis and maintenance through regulation of actin stability. *Seminars in Cell & Developmental Biology*, *65*, 88–95. https://doi.org/10.1016/j.semcdb.2016.08.017

Meenderink, L. M., Gaeta, I. M., Postema, M. M., Cencer, C. S., Chinowsky, C. R., Krystofiak, E. S., Millis, B. A., & Tyska, M. J. (2019). Actin Dynamics Drive Microvillar Motility and Clustering during Brush Border Assembly. *Developmental Cell*, *50*(5), 545-556.e4. https://doi.org/10.1016/j.devcel.2019.07.008

Mellor, H. (2010). The role of formins in filopodia formation. *Biochimica et Biophysica Acta (BBA) - Molecular Cell Research*, *1803*(2), 191–200. https://doi.org/10.1016/j.bbamcr.2008.12.018

Mentes, A., Huehn, A., Liu, X., Zwolak, A., Dominguez, R., Shuman, H., Ostap, E. M., & Sindelar, C. V. (2018). High-resolution cryo-EM structures of actin-bound myosin states reveal the mechanism of myosin force sensing. *Proceedings of the National Academy of Sciences*, *115*(6), 1292–1297. https://doi.org/10.1073/pnas.1718316115

Miura, S., Sato, K., Kato-Negishi, M., Teshima, T., & Takeuchi, S. (2015). Fluid shear triggers microvilli formation via mechanosensitive activation of TRPV6. *Nature Communications*, *6*(1), 8871. https://doi.org/10.1038/ncomms9871

Mogilner, A., & Rubinstein, B. (2005). The Physics of Filopodial Protrusion. *Biophysical Journal*, *89*(2), 782–795. https://doi.org/10.1529/biophysj.104.056515

Mooseker, M. S., C. S. Keller, T., & Hirokawa, N. (1983). Regulation of Cytoskeletal Structure and Contractility in the Brush Border. In R. Porter & G. M. Collins (Eds.), *Novartis Foundation Symposia* (pp. 195–215). John Wiley & Sons, Ltd. https://doi.org/10.1002/9780470720769.ch12

Mooseker, M. S., Pollard, T. D., & Wharton, K. A. (1982). Nucleated polymerization of actin from the membrane-associated ends of microvillar filaments in the intestinal brush border. *Journal of Cell Biology*, *95*(1), 223–233. https://doi.org/10.1083/jcb.95.1.223

Mooseker, M. S., & Tilney, L. G. (1975). Organization of an actin filament-membrane complex. Filament polarity and membrane attachment in the microvilli of intestinal epithelial cells. *Journal of Cell Biology*, *67*(3), 725–743. https://doi.org/10.1083/jcb.67.3.725

Morales, E. A., Arnaiz, C., Krystofiak, E. S., Zanic, M., & Tyska, M. J. (2022). Mitotic Spindle Positioning (MISP) is an actin bundler that selectively stabilizes the rootlets of epithelial microvilli. *Cell Reports*, *39*(3), 110692. https://doi.org/10.1016/j.celrep.2022.110692

Morales, E. A., Gaeta, I., & Tyska, M. J. (2023). Building the brush border, one microvillus at a time. *Current Opinion in Cell Biology*, *80*, 102153. https://doi.org/10.1016/j.ceb.2023.102153

Mullins, R. D., Heuser, J. A., & Pollard, T. D. (1998). The interaction of Arp2/3 complex with actin: Nucleation, high affinity pointed end capping, and formation of branching networks of filaments. *Proceedings of the National Academy of Sciences*, *95*(11), 6181–6186. https://doi.org/10.1073/pnas.95.11.6181

Nambiar, R., McConnell, R. E., & Tyska, M. J. (2010). Myosin motor function: The ins and outs of actin-based membrane protrusions. *Cellular and Molecular Life Sciences*, *67*(8), 1239–1254. https://doi.org/10.1007/s00018-009-0254-5

Narayanan, P., Chatterton, P., Ikeda, A., Ikeda, S., Corey, D. P., Ervasti, J. M., & Perrin, B. J. (2015). Length regulation of mechanosensitive stereocilia depends on very slow actin dynamics and filament-severing proteins. *Nature Communications*, *6*(1), 6855. https://doi.org/10.1038/ncomms7855

Nishimura, Y., Shi, S., Zhang, F., Liu, R., Takagi, Y., Bershadsky, A. D., Viasnoff, V., & Sellers, J. R. (2021). The formin inhibitor SMIFH2 inhibits members of the myosin superfamily. *Journal of Cell Science*, *134*(8), jcs253708. https://doi.org/10.1242/jcs.253708

Oda, T., Iwasa, M., Aihara, T., Maéda, Y., & Narita, A. (2009). The nature of the globular- to fibrous-actin transition. *Nature*, *457*(7228), 441–445. https://doi.org/10.1038/nature07685

Ohta, K., Higashi, R., Sawaguchi, A., & Nakamura, K. (2012). Helical arrangement of filaments in microvillar actin bundles. *Journal of Structural Biology*, *177*(2), 513–519. https://doi.org/10.1016/j.jsb.2011.10.012

Oosterheert, W., Klink, B. U., Belyy, A., Pospich, S., & Raunser, S. (2022). Structural basis of actin filament assembly and aging. *Nature*, *611*(7935), 374–379. https://doi.org/10.1038/s41586-022-05241-8

Orly, G., Naoz, M., & Gov, N. S. (2014). Physical Model for the Geometry of Actin-Based Cellular Protrusions. *Biophysical Journal*, *107*(3), 576–587. https://doi.org/10.1016/j.bpj.2014.05.040

Özel, M. N., Langen, M., Hassan, B. A., & Hiesinger, P. R. (2015). Filopodial dynamics and growth cone stabilization in Drosophila visual circuit development. *ELife*, *4*, e10721. https://doi.org/10.7554/eLife.10721

Palay, S. L., & Karlin, L. J. (1959a). An Electron Microscopic Study of the Intestinal Villus: I. The Fasting Animal. *The Journal of Biophysical and Biochemical Cytology*, *5*(3), 363–371. https://doi.org/10.1083/jcb.5.3.363

Palay, S. L., & Karlin, L. J. (1959b). An Electron Microscopic Study of the Intestinal Villus: II. The Pathway of Fat Absorption. *The Journal of Biophysical and Biochemical Cytology*, *5*(3), 373–384. https://doi.org/10.1083/jcb.5.3.373

Peña, J. F., Alié, A., Richter, D. J., Wang, L., Funayama, N., & Nichols, S. A. (2016). Conserved expression of vertebrate microvillar gene homologs in choanocytes of freshwater sponges. *EvoDevo*, *7*(1), 13. https://doi.org/10.1186/s13227-016-0050-x

Peterson, M. D., Bement, W. M., & Mooseker, M. S. (1993). An in vitro model for the analysis of intestinal brush border assembly. II. Changes in expression and localization

of brush border proteins during cell contact-induced brush border assembly in Caco-2BBe cells. *Journal of Cell Science*, *105 (Pt 2)*, 461–472.

Peterson, M. D., & Mooseker, M. S. (1993). An in vitro model for the analysis of intestinal brush border assembly. I. Ultrastructural analysis of cell contact-induced brush border assembly in Caco-2BBe cells. *Journal of Cell Science*, *105 (Pt 2)*, 445–460.

Pinette, J. A., Mao, S., Millis, B. A., Krystofiak, E. S., Faust, J. J., & Tyska, M. J. (2019). Brush border protocadherin CDHR2 promotes the elongation and maximized packing of microvilli in vivo. *Molecular Biology of the Cell*, *30*(1), 108–118. https://doi.org/10.1091/mbc.E18-09-0558

Pinson, K. I., Dunbar, L., Samuelson, L., & Gumucio, D. L. (1998). Targeted disruption of the mouse villin gene does not impair the morphogenesis of microvilli. *Developmental Dynamics*, *211*(1), 109–121. https://doi.org/10.1002/(SICI)1097-0177(199801)211:1<109::AID-AJA10>3.0.CO;2-7

Pollard, T. D. (1986). Rate constants for the reactions of ATP- and ADP-actin with the ends of actin filaments. *Journal of Cell Biology*, *103*(6), 2747–2754. https://doi.org/10.1083/jcb.103.6.2747

Pollard, T. D. (2016). Actin and Actin-Binding Proteins. *Cold Spring Harbor Perspectives in Biology*, *8*(8), a018226. https://doi.org/10.1101/cshperspect.a018226

Pollard, T. D., Blanchoin, L., & Mullins, R. D. (2000). Molecular Mechanisms Controlling Actin Filament Dynamics in Nonmuscle Cells. *Annual Review of Biophysics and Biomolecular Structure*, *29*(1), 545–576. https://doi.org/10.1146/annurev.biophys.29.1.545

Pollard, T. D., & Borisy, G. G. (2003). Cellular Motility Driven by Assembly and Disassembly of Actin Filaments. *Cell*, *112*(4), 453–465. https://doi.org/10.1016/S0092-8674(03)00120-X

Pollard, T. D., & Cooper, J. A. (1986). ACTIN AND ACTIN-BINDING PROTEINS. A CRITICAL EVALUATION OF MECHANISMS AND FUNCTIONS. *Annual Review of Biochemistry*, *55*(1), 987–1035. https://doi.org/10.1146/annurev.bi.55.070186.005011

Pollard, T. D., & Mooseker, M. S. (1981). Direct measurement of actin polymerization rate constants by electron microscopy of actin filaments nucleated by isolated microvillus cores. *Journal of Cell Biology*, *88*(3), 654–659. https://doi.org/10.1083/jcb.88.3.654

Postema, M. M., Grega-Larson, N. E., Neininger, A. C., & Tyska, M. J. (2018). IRTKS (BAIAP2L1) Elongates Epithelial Microvilli Using EPS8-Dependent and Independent Mechanisms. *Current Biology*, *28*(18), 2876-2888.e4. https://doi.org/10.1016/j.cub.2018.07.022

Pothier, P., & Hugon, J. S. (1980). Characterization of isolated villus and crypt cells from the small intestine of the adult mouse. *Cell and Tissue Research*, *211*(3), 405–418. https://doi.org/10.1007/BF00234396

Revenu, C., Athman, R., Robine, S., & Louvard, D. (2004). The co-workers of actin filaments: From cell structures to signals. *Nature Reviews Molecular Cell Biology*, *5*(8), 635–646. https://doi.org/10.1038/nrm1437

Revenu, C., Courtois, M., Michelot, A., Sykes, C., Louvard, D., & Robine, S. (2007). Villin Severing Activity Enhances Actin-based Motility In Vivo. *Molecular Biology of the Cell*, *18*(3), 827–838. https://doi.org/10.1091/mbc.e06-05-0423

Revenu, C., Ubelmann, F., Hurbain, I., El-Marjou, F., Dingli, F., Loew, D., Delacour, D., Gilet, J., Brot-Laroche, E., Rivero, F., Louvard, D., & Robine, S. (2012). A new role for the architecture of microvillar actin bundles in apical retention of membrane proteins. *Molecular Biology of the Cell*, *23*(2), 324–336. https://doi.org/10.1091/mbc.e11-09-0765

Reymann, A.-C., Boujemaa-Paterski, R., Martiel, J.-L., Guérin, C., Cao, W., Chin, H. F., De La Cruz, E. M., Théry, M., & Blanchoin, L. (2012). Actin Network Architecture Can Determine Myosin Motor Activity. *Science*, *336*(6086), 1310–1314. https://doi.org/10.1126/science.1221708

Reynolds, M. J., Hachicho, C., Carl, A. G., Gong, R., & Alushin, G. M. (2022). Bending forces and nucleotide state jointly regulate F-actin structure. *Nature*, *611*(7935), 380–386. https://doi.org/10.1038/s41586-022-05366-w

Robine, S., Huet, C., Moll, R., Sahuquillo-Merino, C., Coudrier, E., Zweibaum, A., & Louvard, D. (1985). Can villin be used to identify malignant and undifferentiated normal digestive epithelial cells? *Proceedings of the National Academy of Sciences*, *82*(24), 8488–8492. https://doi.org/10.1073/pnas.82.24.8488

Román-Fernández, Á., Roignot, J., Sandilands, E., Nacke, M., Mansour, M. A., McGarry, L., Shanks, E., Mostov, K. E., & Bryant, D. M. (2018). The phospholipid PI(3,4)P2 is an apical identity determinant. *Nature Communications*, *9*(1), 5041. https://doi.org/10.1038/s41467-018-07464-8

Ross-Macdonald, P., de Silva, H., Guo, Q., Xiao, H., Hung, C.-Y., Penhallow, B., Markwalder, J., He, L., Attar, R. M., Lin, T., Seitz, S., Tilford, C., Wardwell-Swanson, J., & Jackson, D. (2008). Identification of a nonkinase target mediating cytotoxicity of novel kinase inhibitors. *Molecular Cancer Therapeutics*, *7*(11), 3490–3498. https://doi.org/10.1158/1535-7163.MCT-08-0826

Rotty, J. D., Wu, C., Haynes, E. M., Suarez, C., Winkelman, J. D., Johnson, H. E., Haugh, J. M., Kovar, D. R., & Bear, J. E. (2015). Profilin-1 Serves as a Gatekeeper for Actin Assembly by Arp2/3-Dependent and -Independent Pathways. *Developmental Cell*, *32*(1), 54–67. https://doi.org/10.1016/j.devcel.2014.10.026

Roy, P., & Perrin, B. J. (2018). The stable actin core of mechanosensory stereocilia features continuous turnover of actin cross-linkers. *Molecular Biology of the Cell*, *29*(15), 1856–1865. https://doi.org/10.1091/mbc.E18-03-0196

Rzadzinska, A. K., Schneider, M. E., Davies, C., Riordan, G. P., & Kachar, B. (2004). An actin molecular treadmill and myosins maintain stereocilia functional architecture and self-renewal. *Journal of Cell Biology*, *164*(6), 887–897. https://doi.org/10.1083/jcb.200310055

Safer, D., Elzinga, M., & Nachmias, V. T. (1991). Thymosin β4 and Fx, an actin-sequestering peptide, are indistinguishable. *Journal of Biological Chemistry*, *266*(7), 4029–4032. https://doi.org/10.1016/S0021-9258(20)64278-8

Sanders, T. A., Llagostera, E., & Barna, M. (2013). Specialized filopodia direct long-range transport of SHH during vertebrate tissue patterning. *Nature*, *497*(7451), 628–632. https://doi.org/10.1038/nature12157

Saotome, I., Curto, M., & McClatchey, A. I. (2004). Ezrin Is Essential for Epithelial Organization and Villus Morphogenesis in the Developing Intestine. *Developmental Cell*, *6*(6), 855–864. https://doi.org/10.1016/j.devcel.2004.05.007

Sato, T., Vries, R. G., Snippert, H. J., van de Wetering, M., Barker, N., Stange, D. E., van Es, J. H., Abo, A., Kujala, P., Peters, P. J., & Clevers, H. (2009). Single Lgr5 stem cells build crypt-villus structures in vitro without a mesenchymal niche. *Nature*, *459*(7244), 262–265. https://doi.org/10.1038/nature07935

Sauvanet, C., Wayt, J., Pelaseyed, T., & Bretscher, A. (2015). Structure, Regulation, and Functional Diversity of Microvilli on the Apical Domain of Epithelial Cells. *Annual Review of Cell and Developmental Biology*, *31*(1), 593–621. https://doi.org/10.1146/annurev-cellbio-100814-125234

Schaus, T. E., Taylor, E. W., & Borisy, G. G. (2007). Self-organization of actin filament orientation in the dendritic-nucleation/array-treadmilling model. *Proceedings of the National Academy of Sciences*, *104*(17), 7086–7091. https://doi.org/10.1073/pnas.0701943104

Schwander, M., Kachar, B., & Müller, U. (2010). The cell biology of hearing. *Journal of Cell Biology*, *190*(1), 9–20. https://doi.org/10.1083/jcb.201001138

Schwintzer, L., Koch, N., Ahuja, R., Grimm, J., Kessels, M. M., & Qualmann, B. (2011). The functions of the actin nucleator Cobl in cellular morphogenesis critically depend on syndapin I. *The EMBO Journal*, *30*(15), 3147–3159. https://doi.org/10.1038/emboj.2011.207

Sebé-Pedrós, A., Burkhardt, P., Sánchez-Pons, N., Fairclough, S. R., Lang, B. F., King, N., & Ruiz-Trillo, I. (2013). Insights into the Origin of Metazoan Filopodia and Microvilli. *Molecular Biology and Evolution*, *30*(9), 2013–2023. https://doi.org/10.1093/molbev/mst110

Sekerková, G., Zheng, L., Mugnaini, E., & Bartles, J. R. (2006). Differential expression of espin isoforms during epithelial morphogenesis, stereociliogenesis and postnatal maturation in the developing inner ear. *Developmental Biology*, *291*(1), 83–95. https://doi.org/10.1016/j.ydbio.2005.12.021

Sept, D., Elcock, A. H., & McCammon, J. A. (1999). Computer simulations of actin polymerization can explain the barbed-pointed end asymmetry. *Journal of Molecular Biology*, *294*(5), 1181–1189. https://doi.org/10.1006/jmbi.1999.3332

Shekhar, S. (2017). Microfluidics-Assisted TIRF Imaging to Study Single Actin Filament Dynamics. *Current Protocols in Cell Biology*, *77*(1), 12.13.1-12.13.24. https://doi.org/10.1002/cpcb.31

Shekhar, S., & Carlier, M.-F. (2017). Enhanced Depolymerization of Actin Filaments by ADF/Cofilin and Monomer Funneling by Capping Protein Cooperate to Accelerate Barbed-End Growth. *Current Biology*, *27*(13), 1990-1998.e5. https://doi.org/10.1016/j.cub.2017.05.036

Sherer, L. A., & Courtemanche, N. (2022). Cooperative bundling by fascin generates actin structures with architectures that depend on filament length. *Frontiers in Cell and Developmental Biology*, *10*, 974047. https://doi.org/10.3389/fcell.2022.974047

Shin, J.-B., Longo-Guess, C. M., Gagnon, L. H., Saylor, K. W., Dumont, R. A., Spinelli, K. J., Pagana, J. M., Wilmarth, P. A., David, L. L., Gillespie, P. G., & Johnson, K. R. (2010). The R109H Variant of Fascin-2, a Developmentally Regulated Actin Crosslinker in Hair-Cell Stereocilia, Underlies Early-Onset Hearing Loss of DBA/2J Mice. *Journal of Neuroscience*, *30*(29), 9683–9694. https://doi.org/10.1523/JNEUROSCI.1541-10.2010

Sjöblom, B., Ylänne, J., & Djinović-Carugo, K. (2008). Novel structural insights into F-actin-binding and novel functions of calponin homology domains. *Current Opinion in Structural Biology*, *18*(6), 702–708. https://doi.org/10.1016/j.sbi.2008.10.003

Steffen, A., Faix, J., Resch, G. P., Linkner, J., Wehland, J., Small, J. V., Rottner, K., & Stradal, T. E. B. (2006). Filopodia Formation in the Absence of Functional WAVE- and Arp2/3-Complexes. *Molecular Biology of the Cell*, *17*(6), 2581–2591. https://doi.org/10.1091/mbc.e05-11-1088

Suarez, C., Carroll, R. T., Burke, T. A., Christensen, J. R., Bestul, A. J., Sees, J. A., James, M. L., Sirotkin, V., & Kovar, D. R. (2015). Profilin Regulates F-Actin Network Homeostasis by Favoring Formin over Arp2/3 Complex. *Developmental Cell*, *32*(1), 43–53. https://doi.org/10.1016/j.devcel.2014.10.027

Suarez, C., Roland, J., Boujemaa-Paterski, R., Kang, H., McCullough, B. R., Reymann, A.-C., Guérin, C., Martiel, J.-L., De La Cruz, E. M., & Blanchoin, L. (2011). Cofilin Tunes the Nucleotide State of Actin Filaments and Severs at Bare and Decorated Segment Boundaries. *Current Biology*, *21*(10), 862–868. https://doi.org/10.1016/j.cub.2011.03.064

Sun, X., & Alushin, G. M. (2022). Cellular force-sensing through actin filaments. *The FEBS Journal*, febs.16568. https://doi.org/10.1111/febs.16568

Svitkina, T. (2018). The Actin Cytoskeleton and Actin-Based Motility. *Cold Spring Harbor Perspectives in Biology*, *10*(1), a018267. https://doi.org/10.1101/cshperspect.a018267

Svitkina, T. M. (2020). Actin Cell Cortex: Structure and Molecular Organization. *Trends in Cell Biology*, *30*(7), 556–565. https://doi.org/10.1016/j.tcb.2020.03.005

Svitkina, T. M., & Borisy, G. G. (1999). Arp2/3 Complex and Actin Depolymerizing Factor/Cofilin in Dendritic Organization and Treadmilling of Actin Filament Array in Lamellipodia. *Journal of Cell Biology*, *145*(5), 1009–1026. https://doi.org/10.1083/jcb.145.5.1009

Svitkina, T. M., Bulanova, E. A., Chaga, O. Y., Vignjevic, D. M., Kojima, S., Vasiliev, J. M., & Borisy, G. G. (2003). Mechanism of filopodia initiation by reorganization of a dendritic network. *Journal of Cell Biology*, *160*(3), 409–421. https://doi.org/10.1083/jcb.200210174

Svitkina, T. M., Verkhovsky, A. B., McQuade, K. M., & Borisy, G. G. (1997). Analysis of the Actin–Myosin II System in Fish Epidermal Keratocytes: Mechanism of Cell Body Translocation. *Journal of Cell Biology*, *139*(2), 397–415. https://doi.org/10.1083/jcb.139.2.397

Tanaka, K., Takeda, S., Mitsuoka, K., Oda, T., Kimura-Sakiyama, C., Maéda, Y., & Narita, A. (2018). Structural basis for cofilin binding and actin filament disassembly. *Nature Communications*, *9*(1), 1860. https://doi.org/10.1038/s41467-018-04290-w

Taylor, R., Bullen, A., Johnson, S. L., Grimm-Günter, E.-M., Rivero, F., Marcotti, W., Forge, A., & Daudet, N. (2015). Absence of plastin 1 causes abnormal maintenance of hair cell stereocilia and a moderate form of hearing loss in mice. *Human Molecular Genetics*, *24*(1), 37–49. https://doi.org/10.1093/hmg/ddu417

Theriot, J. A. (2000). The Polymerization Motor. *Traffic*, *1*(1), 19–28. https://doi.org/10.1034/j.1600-0854.2000.010104.x

Tilney, L. G., & Cardell, R. R. (1970). Factors controlling the reassembly of the microvillus border of the small intestine of the salamander. *Journal of Cell Biology*, *47*(2), 408–422. https://doi.org/10.1083/jcb.47.2.408

Tilney, L. G., & DeRosier, D. J. (1986). Actin filaments, stereocilia, and hair cells of the bird cochlea. IV. How the actin filaments become organized in developing stereocilia and in the cuticular plate. *Developmental Biology*, *116*(1), 119–129. https://doi.org/10.1016/0012-1606(86)90048-5

Tilney, L. G., & Mooseker, M. (1971). Actin in the Brush-Border of Epithelial Cells of the Chicken Intestine. *Proceedings of the National Academy of Sciences*, *68*(10), 2611–2615. https://doi.org/10.1073/pnas.68.10.2611

Tilney, L. G., & Saunders, J. C. (1983). Actin filaments, stereocilia, and hair cells of the bird cochlea. I. Length, number, width, and distribution of stereocilia of each hair cell are related to the position of the hair cell on the cochlea. *Journal of Cell Biology*, *96*(3), 807–821. https://doi.org/10.1083/jcb.96.3.807

Tilney, L. G., Tilney, M. S., & DeRosier, D. J. (1992). Actin Filaments, Stereocilia, and Hair Cells: How Cells Count and Measure. *Annual Review of Cell Biology*, *8*(1), 257–274. https://doi.org/10.1146/annurev.cb.08.110192.001353

Tyska, M. J., Mackey, A. T., Huang, J.-D., Copeland, N. G., Jenkins, N. A., & Mooseker, M. S. (2005). Myosin-1a Is Critical for Normal Brush Border Structure and Composition. *Molecular Biology of the Cell*, *16*(5), 2443–2457. https://doi.org/10.1091/mbc.e04-12-1116

Tyska, M. J., & Mooseker, M. S. (2002). MYO1A (Brush Border Myosin I) Dynamics in the Brush Border of LLC-PK1-CL4 Cells. *Biophysical Journal*, *82*(4), 1869–1883. https://doi.org/10.1016/S0006-3495(02)75537-9

Uhlén, M., Fagerberg, L., Hallström, B. M., Lindskog, C., Oksvold, P., Mardinoglu, A., Sivertsson, Å., Kampf, C., Sjöstedt, E., Asplund, A., Olsson, I., Edlund, K., Lundberg, E., Navani, S., Szigyarto, C. A.-K., Odeberg, J., Djureinovic, D., Takanen, J. O., Hober, S., … Pontén, F. (2015). Tissue-based map of the human proteome. *Science*, *347*(6220), 1260419. https://doi.org/10.1126/science.1260419

van der Flier, L. G., & Clevers, H. (2009). Stem Cells, Self-Renewal, and Differentiation in the Intestinal Epithelium. *Annual Review of Physiology*, *71*(1), 241–260. https://doi.org/10.1146/annurev.physiol.010908.163145

Vignjevic, D., Kojima, S., Aratyn, Y., Danciu, O., Svitkina, T., & Borisy, G. G. (2006). Role of fascin in filopodial protrusion. *Journal of Cell Biology*, *174*(6), 863–875. https://doi.org/10.1083/jcb.200603013

Viswanatha, R., Ohouo, P. Y., Smolka, M. B., & Bretscher, A. (2012). Local phosphocycling mediated by LOK/SLK restricts ezrin function to the apical aspect of epithelial cells. *Journal of Cell Biology*, *199*(6), 969–984. https://doi.org/10.1083/jcb.201207047

Volkmann, N., DeRosier, D., Matsudaira, P., & Hanein, D. (2001). An Atomic Model of Actin Filaments Cross-Linked by Fimbrin and Its Implications for Bundle Assembly and Function. *Journal of Cell Biology*, *153*(5), 947–956. https://doi.org/10.1083/jcb.153.5.947

Wagner, A. R., Luan, Q., Liu, S.-L., & Nolen, B. J. (2013). Dip1 Defines a Class of Arp2/3 Complex Activators that Function without Preformed Actin Filaments. *Current Biology*, *23*(20), 1990–1998. https://doi.org/10.1016/j.cub.2013.08.029

Wang, Y. L. (1985). Exchange of actin subunits at the leading edge of living fibroblasts: Possible role of treadmilling. *The Journal of Cell Biology*, *101*(2), 597–602. https://doi.org/10.1083/jcb.101.2.597

Wayt, J., & Bretscher, A. (2014). Cordon Bleu serves as a platform at the basal region of microvilli, where it regulates microvillar length through its WH2 domains. *Molecular Biology of the Cell*, *25*(18), 2817–2827. https://doi.org/10.1091/mbc.e14-06-1131

Weber, A., Pennise, C. R., Babcock, G. G., & Fowler, V. M. (1994). Tropomodulin caps the pointed ends of actin filaments. *Journal of Cell Biology*, *127*(6), 1627–1635. https://doi.org/10.1083/jcb.127.6.1627

Weber, K. L., Fischer, R. S., & Fowler, V. M. (2007). Tmod3 regulates polarized epithelial cell morphology. *Journal of Cell Science*, *120*(20), 3625–3632. https://doi.org/10.1242/jcs.011445

Weck, M. L., Crawley, S. W., Stone, C. R., & Tyska, M. J. (2016). Myosin-7b Promotes Distal Tip Localization of the Intermicrovillar Adhesion Complex. *Current Biology*, *26*(20), 2717–2728. https://doi.org/10.1016/j.cub.2016.08.014

Weck, M. L., Crawley, S. W., & Tyska, M. J. (2020). A heterologous in-cell assay for investigating intermicrovillar adhesion complex interactions reveals a novel protrusion length-matching mechanism. *Journal of Biological Chemistry*, *295*(48), 16191–16206. https://doi.org/10.1074/jbc.RA120.015929

Wegner, A. (1976). Head to tail polymerization of actin. *Journal of Molecular Biology*, *108*(1), 139–150. https://doi.org/10.1016/S0022-2836(76)80100-3

Welch, M. D., & Mullins, R. D. (2002). Cellular Control of Actin Nucleation. *Annual Review of Cell and Developmental Biology*, *18*(1), 247–288. https://doi.org/10.1146/annurev.cellbio.18.040202.112133

Winkelman, J. D., Bilancia, C. G., Peifer, M., & Kovar, D. R. (2014). Ena/VASP Enabled is a highly processive actin polymerase tailored to self-assemble parallel-bundled F-actin networks with Fascin. *Proceedings of the National Academy of Sciences*, *111*(11), 4121–4126. https://doi.org/10.1073/pnas.1322093111

Winkelman, J. D., Suarez, C., Hocky, G. M., Harker, A. J., Morganthaler, A. N., Christensen, J. R., Voth, G. A., Bartles, J. R., & Kovar, D. R. (2016). Fascin- and α-Actinin-Bundled Networks Contain Intrinsic Structural Features that Drive Protein Sorting. *Current Biology*, *26*(20), 2697–2706. https://doi.org/10.1016/j.cub.2016.07.080

Wioland, H., Guichard, B., Senju, Y., Myram, S., Lappalainen, P., Jégou, A., & Romet-Lemonne, G. (2017). ADF/Cofilin Accelerates Actin Dynamics by Severing Filaments and Promoting Their Depolymerization at Both Ends. *Current Biology*, *27*(13), 1956-1967.e7. https://doi.org/10.1016/j.cub.2017.05.048

Wood, W., & Martin, P. (2002). Structures in focus—Filopodia. *The International Journal of Biochemistry & Cell Biology*, *34*(7), 726–730. https://doi.org/10.1016/S1357-2725(01)00172-8

Xue, Z., & Sokac, A. M. (2016). -Back-to-back mechanisms drive actomyosin ring closure during Drosophila embryo cleavage. *Journal of Cell Biology*, *215*(3), 335–344. https://doi.org/10.1083/jcb.201608025

Yang, C., & Svitkina, T. (2011). Filopodia initiation. *Cell Adhesion & Migration*, *5*(5), 402–408. https://doi.org/10.4161/cam.5.5.16971

Yu, I.-M., Planelles-Herrero, V. J., Sourigues, Y., Moussaoui, D., Sirkia, H., Kikuti, C., Stroebel, D., Titus, M. A., & Houdusse, A. (2017). Myosin 7 and its adaptors link cadherins to actin. *Nature Communications*, *8*(1), 15864. https://doi.org/10.1038/ncomms15864

Zhai, L., Zhao, P., Panebra, A., Guerrerio, A. L., & Khurana, S. (2001). Tyrosine Phosphorylation of Villin Regulates the Organization of the Actin Cytoskeleton. *Journal of Biological Chemistry*, *276*(39), 36163–36167. https://doi.org/10.1074/jbc.C100418200

Zheng, L., Adam, S. A., García-Anoveros, J., Mitchell, B. J., & Bartles, J. R. (2022). Espin overexpression causes stereocilia defects and provides an anti-capping effect on actin polymerization. *Cytoskeleton*, *79*(6–8), 64–74. https://doi.org/10.1002/cm.21719

Zheng, L., Sekerková, G., Vranich, K., Tilney, L. G., Mugnaini, E., & Bartles, J. R. (2000). The Deaf Jerker Mouse Has a Mutation in the Gene Encoding the Espin Actin-Bundling Proteins of Hair Cell Stereocilia and Lacks Espins. *Cell*, *102*(3), 377–385. https://doi.org/10.1016/S0092-8674(00)00042-8

Zhu, H., Li, M., Zhao, R., Li, M., Chai, Y., Zhu, Z., Yang, Y., Li, W., Xie, Z., Li, X., Lei, K., Li, X., & Ou, G. (2022). In situ structure of intestinal apical surface reveals nanobristles on microvilli. *Proceedings of the National Academy of Sciences*, *119*(24), e2122249119. https://doi.org/10.1073/pnas.2122249119

Zhu, M., Settele, F., Kotak, S., Sanchez-Pulido, L., Ehret, L., Ponting, C. P., Gönczy, P., & Hoffmann, I. (2013). MISP is a novel Plk1 substrate required for proper spindle orientation and mitotic progression. *Journal of Cell Biology*, *200*(6), 773–787. https://doi.org/10.1083/jcb.201207050

Zigmond, S. H. (2004). Formin-induced nucleation of actin filaments. *Current Opinion in Cell Biology*, *16*(1), 99–105. https://doi.org/10.1016/j.ceb.2003.10.019

Zimmermann, D., Santos, A., Kovar, D. R., & Rock, R. S. (2015). Actin Age Orchestrates Myosin-5 and Myosin-6 Run Lengths. *Current Biology*, *25*(15), 2057–2062. https://doi.org/10.1016/j.cub.2015.06.033